STUDY OF WAVES IN THE MIDDLE ATMOSPHERE AND ASSOCIATED MOMENTUM FLUX USING INDIAN MST RADAR

Thesis
Submitted to
SAURASHTRA UNIVERSITY
Rajkot

For the Award of the Degree of
DOCTOR OF PHILOSOPHY

in
Physics

By
NIRAJ Y.PANDYA
Guide: Prof. K N Iyer
Head
Department of Physics
Saurashtra University
Rajkot-360 005
(INDIA)
August 2007

Dedicated to

My beloved Family

STATEMENT UNDER O.Ph.D.7 OF SAURASHTRA UNIVERSITY

The contents of this thesis is my own work carried out under the supervision of Prof. K N Iyer and leads to some contribution in Physics supported by necessary references.

Niraj Y Pandya

CERTIFICATE

This is to certify that the present work submitted for the award of Ph.D. degree of Saurashtra University, Rajkot by Mr. Niraj Y Pandya has been the result of about seven years of work under my supervision and is a valuable contribution in the field of ATMOSPHERIC SCIENCE.

Prof. K N Iyer
Research Guide,
Head,
Department of Physics,
Saurashtra University,
Rajkot-360 005
INDIA

Acknowledgement

I would like to express my heartfelt gratitude to my honorable guide Prof. K. N. Iyer for his invaluable guidance during the entire period of my work. His patience encouraging attitude, powerful insight and willingness to discuss various topics in a simple and effective manner has made this period of association with him very pleasant and memorable for me. I consider it fortunate to have worked under him.

I am very much grateful to Dr. H. P. Joshi for his kind support, guidance, encouragement, stimulating discussions and useful suggestions during all stages of this work.

I am very much thankful to Indian Space Research Organization (ISRO), Bangalore for granting me the Research fellowship under its RESPOND programme.

I wish to express sincere thanks to Prof. H. H. Joshi, Dr. G. J. Baldha, Dr. M. J. Joshi, Dr. D. G. Kuberkar , Dr. K. B. Modi, Dr. J. A Bhalodia, for their guidance and the non-teaching staff of Department of physics for their kind cooperation.

I am extremely thankful to Prof. D Narayana Rao, Director of National Atmospheric Research Laboratory providing the atmospheric wind data and all the possible help. The hospitality and technical help provided by all the staff members of NARL is also appreciated.

I am very much thankful to Dr. Yogesh Jani , Dr. Ravi Jadhav, Dr. Malini Aggrawal , Mr. Ritweej Rajeev Rnajan , Mr.Ajayhsin Jadeja ,and Miss Mala Bagiya of our Space Physics Group for their invaluable suggestions and cooperation during the course of the work.

I am also very much thankful to all research students of Ferrites group, Material Science group for their selfless help.

I express my heartiest regards to my parents, parents in law, my brother, bhabhiji, Niece, and my brother in law for their constant encouragement, magnanimous support.

And at last but not the least I am indebted to my wife Nirali and my son Divya, for their, love and hope allowed me to carry on with this task.

Niraj Y Pandya

Preface

The atmosphere is a envelope of gas and suspended particles extending from the Earth's surface out to many hundreds of kilometers , becoming increasingly thinner with distance but always held by the Earth's gravitational pull. The atmosphere is made up of layers surrounding the earth that holds the air we breath, protects us from outer space, and holds moisture (clouds), gases, and tiny particles. The present Thesis aims to study the dynamics of the troposphere and lower stratosphere at a tropical station using Indian MST Radar observations of winds. The major outcome of this Thesis is that wind data collected by the MST radar at Gadanki (13.5^{o} N, 79.2^{o} E) over the period 2001-2005 have been used for the first time to study various characteristics of short period gravity waves in the middle atmosphere.

Chapter -I : is introductory and describes the thermal and chemical structure and dynamics of the middle atmosphere. The region between 10 to 100 km is called the middle atmosphere. In the lower parts of the troposphere is highly prone to turbulence and is of great interest form the point of view of atmospheric dynamics. Instability can generate wave motion which can propagate both horizontally and vertically and the upward propagation of these waves has significance to middle atmosphere phenomena.

Chapter II describes the MST Radar at Gadanki used in the study and its specifications. Data processing and vector wind measurement from the estimated moments using spectrum analysis has been discussed along with the computation of zonal, meridional, and vertical winds. MST Radar uses the scattering and reflection of VHF radio waves from fluctuations in radio refractive index of neutral atmosphere. which in turn depends on variability of humidity, temperature, and induced by turbulence in the middle atmosphere. The Indian MST Radar situated near Tirupati (13.47^{o} N 79.1^{o} E) provides an excellent opportunity to study the lower and middle atmospheric dynamic particularly in the Indian sector.

Chapter III describes the behavior of mean winds and wave like structures observed in many events. Several campaigns have been conducted to study of the gravity waves. Observations are taken with time resolution is 4 minutes and height resolution 150 m over a height range of 4 to 20 km. For the study of the gravity waves the zonal, meridional and vertical component and fluctuations therein are derived from the Doppler spectra.

Chapter IV deals with the study of the variance which is a measure of gravity wave activity. Using the FFT analysis wave characteristics such as period, power spectral density, and vertical wavelength are derived. This chapter also describes the results on momentum flux study, in the troposphere and lower stratosphere. The internal gravity waves as well as other, long period waves play a crucial role in transporting momentum flux from the lower atmosphere, upward into the mesosphere. The waves efficiently transfer energy and momentum between different regions of the atmosphere thereby coupling the different layers and act as an important source of turbulence, when the wave energy is dissipated.

Chapter V Summarises the main results and conclusions.

LIST OF RESEARCH PUBLICATIONS/ PRESENTATIONS :

1. Presented a paper **" Preliminary results of Gravity waves study using Indian MST Radar "**
   N.Y. Pandya , H.P.Joshi , K.N.Iyer
   (XII National Space Science Symposium held during February 25 – 28, 2002 at Bhopal, M.P) DS – 2, AEG -39 Page no. 249.

2. Presented a paper **"Study of short period Gravity waves using wavelet analysis using Indian MST Radar "**
   N.Y. Pandya , H.P.Joshi and K.N.Iyer
   (XIII National Space Science Symposium held during February 17 – 20, 2004 at Kottayam, Kerala) DS-2,ION-16, Page no. 82.

3 . Presented a paper "Studty the Characteristics of Gravity waves using Indian MST Radar:"
   N.Y. Pandya , H.P.Joshi and K.N.Iyer
   7th User Scientists' workshop held at Gadanki Tirupati (A.P) on 5 – 7 March 2004.

4. Presented a paper **"Studty of Characteristics of Gravity waves using Indian MST Radar"** 41st annual convention and meeting on "Inter and Interaplate Seismicity in India present knowledge and future strategy" organized by IGU Hyderabad, during December 29-31, 2004.

5. **Study the short period Gravity waves and associated momentum flux in the tropical middle atmosphere using Indian MST Radar**"
   N.Y. Pandya , H.P.Joshi and K.N.Iyer
   (XIV National Space Science Symposium held during February 9 – 12, 2006 at Visakhapatnam)

6. **" Study of Equatorial Spread F (ESF) using GPS receiver and MST radar"**
   Malini Aggarwal, H.P.Joshi, K.N. Iyer, **N.Y.Pandya**, A.K.Patra and Smitha V. Thampi (Proceedings in National Space Science Symposium 2006, 2IT-29, page no.87 held at Vishakhapatnam, India during February 9-12)

7. **"Study of Equatorial Spread F using L-band scintillation and VHF radar at Gadanki"**
   Malini Aggarwal, H.P.Joshi, K.N. Iyer, , A.K.Patra, **N.Y.Pandya** and Smitha V.Thampi (Proceedings in 8th User Scientists Workshop, NARL, Gadanki, page noo.52 held at NARL,Gadanki, Tirupati , India during 20-21June 2006).

SYMPOSIUM / SCHOOLS/WORKSHOPS ATTENDED

a) **Winter School on National MST Radar facility (NMRF)**, Gadanki,Tirupati (A.P) during 5-9March,2001

b) **XII National Space Science Symposium (NSSS) – 2002** held at Barkattullah University, Bhopal during 25 – 28th ,February 2002

c) **Workshop on Operation, Maintanance and Utilization of electronic Instruments** held at Department of Physics, Saruashtra University Rajkot during 7 to 13 October 2002.

d) **Workshop on Space and Geomatics Applications** held at Rajkot on 19th October, 2002

e) **SERC (Scientific & Engineering Research Council) School** held at Banaras Hindu University, Varanasi during 1 – 20th September,2003

f) **Winter School on National MST Radar facility (NMRF)**, Gadanki,Tirupati (A.P) during 21-30th January,2004

g) **XIII National Space Science Symposium (NSSS) – 2004** held at Mahatma Gandhi University, Kottayam (Kerala) during 17-20th, February 2004.

h) **National workshop on " Prospects of Astronomy Research in Universities** " held at Saurashtra University, Rajkot during 25-27 February, 2004

i) **XVIII Gujarat Science Congress at** Saurashtra University Rajkot on March 13, 2004.

j) **7th User Scientists' workshop** held at Gadanki Tirupati (A.P) on 5 – 7 March 2004.

k) **2nd Astroset workshop on "Block hole Astrophysics"** held at Bhabha atomic Research center (B.A.R.C) during 9th to 16th may 2004,

l **)** **41st annual convention and meeting on "Inter and Interaplate Seismicity in India present knowledge and future strategy"** organized by IGU, Hyderabad, during December 29-31, 2004 and present a poster paper entitled "*Characteristics of gravity waves using Indian MST Radar* "

m) **GPS Occultation work shop held** at Tirupati, Gadanki **March 2005**

n) **One day National Seminar on Recent Advance in Condensed Matter and Space Physics** held at Department of Physics Saurashtra University Rajkot on 21st March, 2006.

CONTENTS

1.1 Introduction:

The Earth is surrounded by a vast, gaseous envelope, extending several hundreds of kilometers from the Earth's surface. The Earth's atmosphere is of great interest to us, not only because it provides a benevolent environment for the sustenance of plant and animal life, but also by virtue of its role in a variety of phenomena that have an impact on human activities and lifestyle. For example, it plays a role in weather and climate, effect of radio communication both in HF as well as VHF bands, as well as in microwave regions of the spectrum. This has become especially important in the present era of satellites, as well as satellite-to-satellites communication. Several atmospheric phenomena, such as lighting and auroras in the Polar regions, evoke not only scientific curiosity but also affect communications and have a practical significance.

The Earth's atmosphere has been studied extensively over a long period of time, at first using ground-based observational techniques, and later with balloons. In space age, 1950 onwards, rockets and satellites have increasingly been put to use for investigations of atmospheric science. Space techniques have provided new insights into our understanding of atmospheric phenomena. Rockets have given us information on the height variation of various atmospheric parameters. Satellites have also given the global distributions of the same and can probe the atmosphere over remote areas as well as oceans, in a manner which is not possible using ground-based techniques. We now have reliable accurate information on the temporal and spatial behavior of the Earth's atmosphere, Its various parameters-density, temperature, winds, clouds, composition (including trace gases), electric and magnetic field parameters, etc as a result of these investigations.

The atmosphere is conventionally divided into layers based on the vertical structure of the temperature field it is shown in Figure 1.1. These layers, the *troposphere, stratosphere*, *mesosphere,* and *thermosphere*, are separated by the *tropopause*, the *stratopause*, and the *mesopause*. In the past, meteorologists often designated the entire region above the tropopause as the "upper atmosphere". Only fairly recently has the term "middle atmosphere" become

popular in referring to the region from the tropopause(10-16 km) to the homopause (at ~110 km.) In this region of the atmosphere eddy processes keep the constituents well mixed and ionization plays only a minor role. However the name “middle atmosphere” has eventually become the standard term for describing the layers of the atmosphere between about 10 to 100 km.

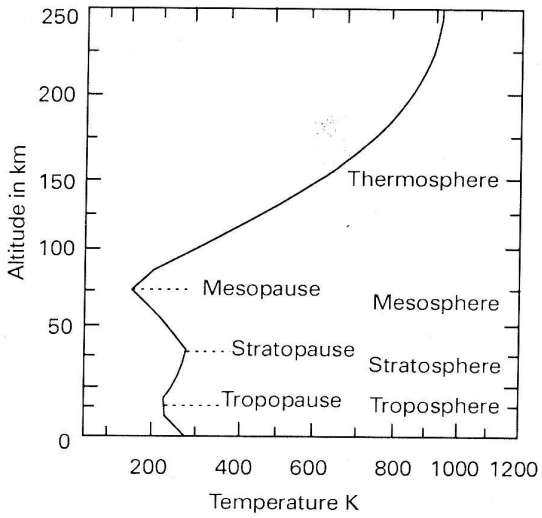

Figure 1.1 Temperature Structure of the Atmosphere (after Chamberlain 1978)

1.2 Composition of the Atmosphere

Table -1.1 lists the eleven most abundant gases by volume found in the Earth's lower atmosphere. Of the gases listed**, nitrogen, oxygen, water vapour, carbon dioxide, methane, nitrous oxide,** and **ozone** are extremely important to the health of the Earth's biosphere. The table indicates that **nitrogen** and **oxygen** are the main components of the atmosphere by volume. Together these two gases make up approximately 99 % of the dry atmosphere. Both of these gases have very important associations with life. Nitrogen is removed from the atmosphere and deposited at the Earth's surface mainly by specialized nitrogen fixing bacteria, and by way of lightning through precipitation. The addition of this nitrogen to the Earth's surface soils and various water bodies’ supplies much

needed nutrition for plant growth. Nitrogen returns to the atmosphere primarily through biomass combustion and denitrification.

Oxygen is exchanged between the atmosphere and living beings through the processes of photosynthesis and respiration. Photosynthesis produces oxygen when carbon dioxide and water are chemically converted into glucose with the help of sunlight. Respiration is the opposite process of photosynthesis. In respiration, oxygen is combined with glucose to chemically release energy for metabolism. The products of this reaction are water and carbon dioxide. Oxygen does absorb extremely short wave, ultra violate and X-ray radiation from the sun at a high level in the atmosphere and this is party responsible for the formation of an electrically conducting layer-the ionosphere. Absorption by oxygen of longer ultra-violet solar radiation splits the two atoms associated in a molecule of oxygen into single atoms. These single atoms may combine with an oxygen molecule to give a molecule of ozone. It is in this way that the ozone in the upper atmosphere is formed.

Water vapour is extremely important in radiative absorption and emission processes in the atmosphere. Its concentration is highly variable. Although always present, in some localities it is difficult to measure, but in the tropics its concentration can be as high as 3 or 4 per cent by volume. Water vapour content of air is a strong function of air temperature .The release of latent heat from condensation of water in the atmosphere is significant in the global energy budget and climate. Relatively small amounts of water vapour can produce great variations in weather. This is largely due to changes in its concentration and in latent heat release, particularly below about 6 km where a high proportion of moisture exists. The major sources of water vapour are evaporation and transpiration from plant life. The main sink is condensation in clouds with resulting precipitation over oceans and land. On average the concentration of atmospheric water vapour decreases with altitude, although this distribution may be reversed from time to time. The highest concentrations of water vapour are found near the equator over the oceans and tropical rain forests. Cold polar

areas and subtropical continental deserts are locations where the volume of water vapour can approach zero percent.

Carbon dioxide has a relatively constant mixing ratio with height in the atmosphere, that is, it is fairly evenly distributed on average. The main sources of carbon dioxide are burning of fossil fuels, human and animal respiration, the oceans and volcanic activity. The main sinks are photosynthesis and the production of carbonates (limestones) in the ocean/land system. The rate of removal of carbon dioxide, a greenhouse gas, is observed to be less than the generation (from fossil fuel burning) because the concentration of carbon dioxide in the atmosphere has been rising steadily during and since the early part of this century. About 99% of the earth's carbon dioxide is dissolved in the oceans. Because solubility is temperature dependent the gas therefore enters or leaves the oceans. It is estimated that the annual amount of carbon dioxide entering or leaving the air by all mechanisms is about one tenth of the total carbon dioxide content of the atmosphere.

The concentration of **ozone** is highly variable in space (latitude and altitude for example) and time. Most of the ozone is generated and destroyed by photochemical reactions in the layer between 20 km and 60 km. Ozone tends to accumulate in the lower stratosphere at altitudes between 15 and 25 km. Small amounts of ozone are also produced by electrical discharges and in photochemical smog over cities. At the surface, ozone is destroyed rapidly by reacting with plants and dissolving in water, whereas in the stratosphere the lifetime is on the order of months. Ozone has characteristic pronounced absorption at UV, IR and microwave wavelengths. The absorption of UV radiation makes human life possible on the earth's surface. Anthropogenically induced depletion of the earth's ozone layer has become a very serious issue following detailed observational and theoretical studies which have focused primarily on the Antarctic "ozone hole".

In addition to the three major radiatively active trace species, there are a large number of trace species present in sufficient concentrations to play significant roles in the chemistry of the middle atmosphere. Of special significance for meteorological studies are the so-called “long-lived “trace species such as nitrous oxide (N_2O), methane (CH_4), and the chlorofluromethanes (CF_2Cl_2) etc. They are well mixed in the vertical direction in the troposphere and are destroyed in the stratosphere by oxidation or photo dissociation. Thus, they all have vertical profiles in which mixing ratios decay with altitude in the middle atmosphere.

Table 1.1

Gas Name	Chemical Formula	Percent Volume
Nitrogen	N_2	78.08
Oxygen	O_2	20.95
Water	H_2O	0 to 4
Argon	Ar	0.93
Carbon Dioxide	CO_2	0.0360
Neon	Ne	0.0018
Helium	He	0.0005
Methane	CH_4	0.00017
Hydrogen	H_2	0.00005
Nitrous Oxide	N_2O	0.00003
Ozone	O_3	0.000004

(http://www.physicalgeography.net/fundamentals/7a.html)

1.3 Solar Radiation spectrum

Solar radiation is becoming increasingly appreciated because of its influence on living matter and the feasibility of its application for useful purposes. It is a perpetual source of natural energy that, along with other forms of renewable energy, has a great potential for a wide variety of applications because it is abundant and accessible. It controls the entire structure and the energetic of the earth's atmosphere and has a dominant influence on the chemical and dynamical processes taking place in it. However, different parts of the solar electromagnetic spectrum play different roles, have different influences and at different levels in the atmosphere. Figure 1.2 illustrates the distribution of energy in the solar electromagnetic spectrum received at the top of the atmosphere. The solar flux is variable on a large variety of time scales and the degree of variability is wavelength dependent, the year period associated with the sunspot cycle being the most dominant feature. Reliable quantitative estimate of the eleven year, 22 year and longer period variation in the solar constant is not yet possible. For most of the studies in the middle and upper atmosphere this flux is treated as constant.

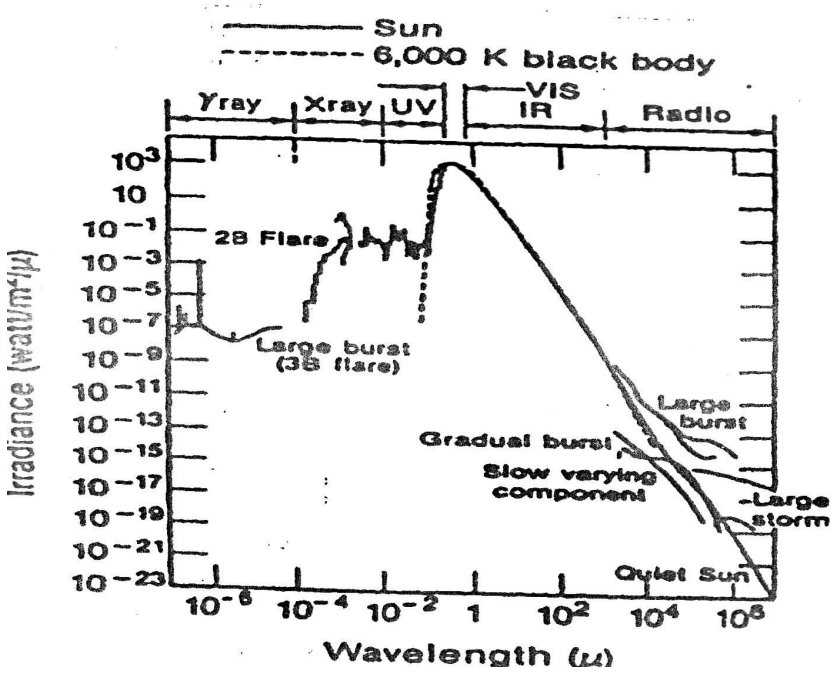

Figure 1.2 Solar Electromagnetic Spectrum (after Nicolson 1982)

The energetic radiation at shorter wavelength in the UV, EUV, and x-rays are emitted from different regions of the sun, e.g. the chromosphere and the corona where the temperatures are higher and deviate from the black body radiation curve corresponding to photospheric temperature.These radiations exhibit significant short term and long term variation. Even though this part of solar of solar spectrum constitutes less than 1% of the total solar flux, it has great significance for atmospheric phenomena. The most important variations are those related to the eleven year period. These are given in Table 1.2. These changes in solar flux do have an impact on the structure and energetic of the of the middle atmosphere. (e.g. Brasseur et al., 1978, Hood 1978).

Table 1.2

Variability of the solar radiation flux from solar minimum to solar maximum

Spectral Region	Variability
Visible and infrared $\lambda > 4000\ A^o$	Extremely small. Negligible for most purpose
Ultraviolet to near visible $3000\ A^o < \lambda < 4000\ A^o$	Very small, fraction of a percent.
Ultraviolet $2000\ A^o < \lambda < 3000\ A^o$	1-2% from solar minimum to solar maximum
Ultraviolet $1000\ A^o < \lambda < 2000\ A^o$	A few percent to about 10 percent from solar minimum to solar maximum
Lyman-alpha ($1216\ A^o$)	Factor of 2 from solar minimum to solar maximum.
EUV and X-rays $\lambda < 1000\ A^o$	Highly variable. Orders of magnitude variations from solar minimum to solar maximum to flare conditions, especially in the X-ray region.

1.4 Absorption of Solar Radiation in the Atmosphere

The sun is the ultimate source of energy for all the processes taking place in the Earth's atmosphere. The solar electromagnetic spectrum consists of the visible (4000-7000 Å), IR radiation (> 7000 Å), UV (2000-4000 Å), extreme UV (< 2000Å), x-ray and gamma-ray radiations. These different radiations are absorbed at different levels in the atmosphere), X-ray and gamma-ray radiations. These different radiations are absorbed at different levels in the atmosphere giving rise to heating of the different atmospheric regions and, thereby, controlling the temperature structure of the atmosphere. This is also the main source of energy that drives all atmospheric motions. The visible and most of the IR radiation from the Sun reach the Earth's surface without getting absorbed in the atmosphere and are responsible for heating of the Earth's surface-both land and oceans. However, a small part of the visible and IR radiation is absorbed by water vapour and other trace gases in the lower atmosphere (0-10km); the UV radiation is absorbed at higher levels. The more energetic part of the radiation (radiation with a wavelength of less than about 2000A) is absorbed mostly by the molecular oxygen in the atmosphere. Radiation with a wavelength lying between 2000a-3000A is mostly absorbed by ozone in the altitude region of 20-60 km, the so-called stratosphere. When the very high-energy part of the solar UV spectrum (wavelength of less than 1000A) is absorbed in the atmosphere, the gas molecules are ionized (broken up into positively-charged ions and negatively-charged electrons). This gives rise t the ionosphere. Table-1.3 gives a summary of the various features of the absorption of solar radiation in the Earth's atmosphere.

Table-1.3

Absorption of solar radiation in the Earth's Atmosphere

Wavelength Region	Fraction of solar energy	Altitude level at which it is absorbed	Primary absorbing mechanism	Percentage of energy absorbed
< 1000 A^o	3 parts in a million	90Km -200km	Ionization	100%
1000 A^o - 2000 A^o	100 parts in a million	50Km -100km	Photo dissociation of oxygen molecule	100%
H Lyman-Alpha (`1216 A^o)	A few parts per million	60Km -90km	Ionization of nitric oxide and photo dissociation of O_2	100%
2000 A^o - 3100 A^o	1.75 %	30Km -60km	Photo-dissociation of Ozone	More than 95%
3100 A^o –7000 A^o	48%	-	Minor role in ozone photo dissociation	Very little absorption
>7000 A^o	50 %	0 -10 km	Absorption by water vapor	10-15%

1.5 Structure of Atmosphere based on temperature

The atmosphere broadly divided into four regions as shown in figure 1.1 namely Troposphere, Stratosphere, Mesosphere, and Thermosphere.

1.5.1 Troposphere

This is the lower most region from ground to about 15 km. The name has come from Tropos which means turn or change. The primary heat source for this

region is the ground itself and heat is convected by turbulent motion. Therefore, temperature decrease with height in this region due to adiabatic cooling at a rate of 10^{o} K per km. The height at which this decrease of temperature halts is known as the tropopause which is at 15 km over the equator and 10 km over the poles. The temperature at the tropopause over the equator is about 190^{o} K and over the poles 220^{o} K. Thus the upper atmosphere is cooler over the hottest part of the earth and warmer over the coldest part of the earth. Rain, cloud, winds, cyclone etc. take place in the troposphere which is convective zone. The tropopause and the troposphere are known as the lower atmosphere.

1.5.2 Stratosphere

The Stratosphere extends from the tropopause up to its boundary (the Stratopause), 50 km above the Earth's surface. This layer holds 19 percent of the atmosphere's gases and it contains little water vapour. Compared to the troposphere, it is calm in this layer with movements of the gasesslow. In the Stratosphere, a series of photochemical reactions involving O_3 and molecular O_2 occur. Ozone strongly absorbs solar radiation in the regions from ~210 -290nm, where as O_2 absorbs at ≤240 nm. The absorption of light, primarily by O_3 , is a major factor causing the increase in temperature with altitude in the stratosphere. The ozone concentration in the troposphere is, in general, much smaller than that of the stratosphere and the tropopause level can also be defined in terms of a particular ozone concentration, this is, in general in good agreement with the thermal tropopause level.

1.5.3 Mesosphere

The mesosphere is the next layer above the stratopause and extends to its upper boundary (the Mesopause), at 80 km above the ground. The gases in the mesosphere are too thin to absorb much of the sun's heat, although the air is still thick enough to slow down meteorites hurtling into the atmosphere, where they burn up, leaving fiery trails in the night sky.
The temperatures in the mesosphere drop to -120℃ at the mesopause. The

regions of the stratosphere and the mesosphere, along with the stratopause and mesopause, are called the **middle atmosphere.**

1.5.4 Thermosphere

Above the mesopause, EUV ($\lambda \leq 1800^{o}$) radiation is absorbed and in part used for heating which leads to rapid increase of temperature with height from 90 km to about 500 km which is called thermosphere. This layer is known as the upper atmosphere. In the lower thermosphere (below 130 km) heat is transported to mesopause through convection, while in the upper thermosphere heat is transported to lower levels by conduction, leading, to an isothermal region beyond 500 km. this level may be termed as thermopause. In this region large diurnal variation and solar cycle variation of temperature exists. The range of temperature in the isothermal region is from 600 to 3000 K from low to high sunspot years and diurnally, it varies within a factor of 3 from maximum to minimum. In the thermosphere there is a separate layer called, the Ionosphere. It is made of electrically charged gas particles (ionized). The particles get this electric charge by ultraviolet rays of the sun. The ionosphere has the important quality of bouncing radio signals transmitted from the earth. That's why places all over the world can be reached via radio.

1.6 Circulations in the Earth's atmosphere

In the troposphere, temperature decreases from equator to pole owing to the latitudinal gradient in solar heating. This heating gradient induces circulation of air parcels in the meridional (height-latitude) plane. This circulation consists of rising motion in association with convective(transfer of heat by the mass movement of a fluid is called 'Convection') disturbances in the tropics, poleward drift in the upper troposphere, slow sinking in the extratropics and an equatorward drift in the planetary boundary layer.

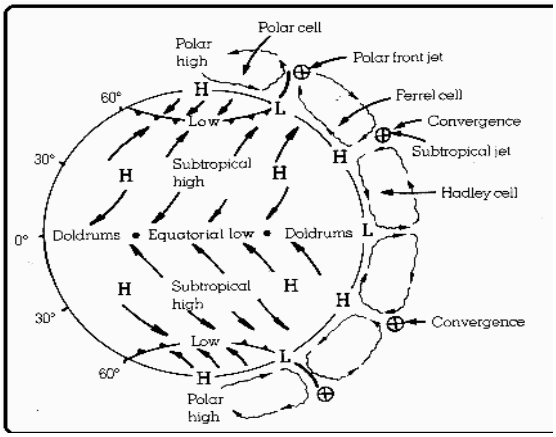

Figure:1.3 Global pattern of wind and pressure
(http//www.uwsp.edu/geo/faculty/ritter/geog101/textbook/circulation /global_scale_circulation.html)

This zonally symmetric circulation is important for transport of water vapour, momentum and heat across latitude circles and is called 'Hadley Circulation' often described as mean zonal circulation and is fuelled by the regions of active convection located over continents of South America, Africa, Indonesia and western Pacific warm pool. The uneven distribution of sea and land mass in different longitudes in the equatorial region produces uneven heating (convection) and results in east-west circulation along the equator. The localized heat sources generate localized circulation cells called 'Walker Circulation' (in the zonal-vertical plane). More active convection is over Indonesia and western Pacific warm pool region, reaching peak during northern winter. This Walker circulation is responsible for upper tropospheric westerlies over the equatorial pacific.

The greatest heating and the consequent expansion of the atmosphere at the equator produce a low-pressure belt called Doldrums. Cooler denser air moves from both north and south of the equator and forces heated equatorial air upwards. These winds southward in the NH and northward in the SH are deflected to the right and left respectively by the coriolis force of earth's rotation and are called NE and SE trade winds. (±25^{o} latitude).

1.7 Convective instability in the troposphere

A negative temperature gradient i.e a decrease in temperature with increase in altitude is in general conducive to the growth of instabilities in the atmosphere, if the lapse rate is greater than what is known as the adiabatic lapse rate (Irbane and Cho 1981) which is given by $L_A = g / C_p$ (9.8^o k /km for a dry atmosphere.) if the lapse rate becomes greater than this value, the atmosphere becomes unstable against convection. (Figure 1.3). Convective instability grows and the medium becomes turbulent. The resulting dissipation of energy heats up the atmosphere to bring the temperature profile back to a stable condition.

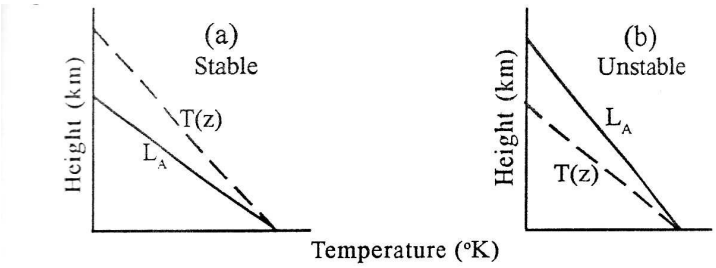

Figure 1.4 Convective instability in the troposphere.
Full line Corresponds to the adiabatic lapse rate.
An observed Temperature profile similar to the dashed line in (a) Corresponds to stable conditions and that in (b) Corresponds to unstable conditions.

Hence in the lower parts of the troposphere, i.e. upto about 10-12 km convective transport dominates over radiation in the energetics. This part of the atmosphere is highly prone to turbulence and is of great interest from the point of view of atmospheric dynamics. Instabilities can generate wave motion which can propagate both horizontally and vertically and the upward propagation of these waves has significance to middle atmospheric phenomena.

1.8 Atmospheric Dynamics: Wave Motions and Oscillation

To have clear understanding on the important role of wave motions in middle atmosphere dynamics, we should know the origin, the propagation characteristics and the interaction of different types of waves. The atmosphere

can sustain a large number of wave phenomena and generally the atmospheric waves are classified broadly into three classes.

Longitudinal waves: Waves whose displacements are in the direction of propagation are called longitudinal waves. e.g.: Acoustic waves.

Vertical transverse waves: Waves that propagate horizontally and have vertical displacements. e.g.: Gravity waves

Horizontal transverse waves: Waves that propagate horizontally with horizontal displacements perpendicular to the propagation direction. e.g.: Rossby waves .Dynamical processes in the middle atmosphere are indicated in he Figure 1.4. They have a wide range of time scales, spatial scales and magnitudes. Another classification of atmospheric waves is according to the time scales of motion. Time scales are having a wide range of 10^0 to 10^8 sec. Correspondingly, the spatial scales of atmospheric motions have a similar wide range.

Component of wind	**Typical period**
Prevailing or steady wind	many years
Quasi biennial oscillation	~ 26 months
Annual oscillation	12 months
Semi-annual oscillation	6 months
Equatorial waves	4-20 days
Tidal winds	24 & 12 hours
Gravity waves	5-100 minutes
Turbulence	1-100 seconds

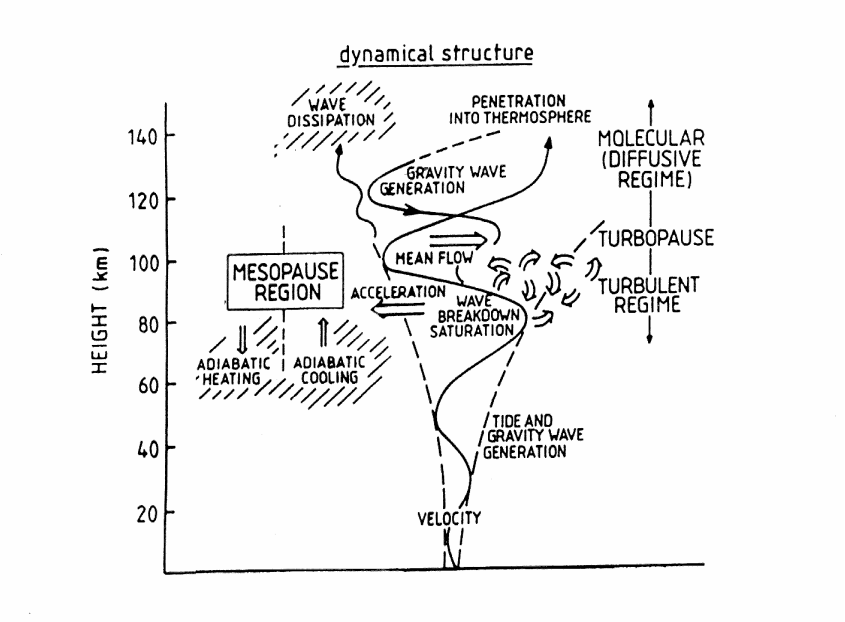

Figure 1.4 Dynamical structure of Atmosphere

1.8.1 Wave motion

A wave may be considered as a perturbation on the steady slowly changing background. A breeze blowing over a river will produce waves that will move in the direction of the wind on the surface of the river, even though the current may be flowing in some other direction. The two main properties of waves are (1) Energy is being propagated from one point to another. (2) Disturbance travels through the medium without giving the medium as a whole any permanent displacement. Waves in atmosphere are oscillatory motions that result from a balance between the inertia of the atmosphere and a restoring force and also they propagate in space. Most weather disturbances are associated with one or more types of atmospheric waves Owing to wave propagation, disturbance in one region can influence the weather in a remote region. To predict weather or to simulate climate, it is necessary to properly account for the influence of wave propagation. Their amplitudes and phases can characterise propagating waves**.** A wave, or any disturbance, can be analysed to regular sinusoidal components, each with its own frequency and wavelength. For a propagating wave, frequency ν depends on the wave number of perturbation and physical properties of the

medium. In these waves, the phase depends on time and one or more space variables also.

1.8.2 Planetary scale waves

These waves derive their name from the observed characteristics that their zonal wavelengths correspond to the earth's circumference or sub multiple of it and they are well organized in zonal and meridional directions in contrast to smaller scale disturbances. These large-scale waves are a dominant part of the spatial and temporal variability in the stratosphere and make contributions in mesospheric heights also. They have significant influence on the wind speeds, temperatures, distribution of ozone and other characteristics of the middle atmospheric structure.

1.8.3 Rossby waves

The most important class of atmospheric waves from the viewpoint of meteorology is the Rossby waves, named after their discoverer C G Rossby in 1949. They are of large enough scales to be influenced by the curvature of earth as well as its rotation. They owe their existence to the variation of Coriolis force with latitude -called β effect. They have horizontal wavelengths ranging from hundreds of kms to the circumference of the earth and vertical scales of tens of kms.

These waves propagate westward relative to the mean zonal flow and the wave speed depends on the zonal and meridional wave numbers. They are dispersive waves and phase speed increase with wavelength. For a typical mid latitude synoptic disturbance, with zonal wavelength ~6000 km and latitudinal width ~3000 km, the Rossby wave speed relative to zonal mean flow was found to be –6 m/s i.e. they are slow moving

Occasionally, strong amplification occurs and the wave has a sudden strong impact on the background wind and temperature. Extreme events can alter the temperature of the polar stratosphere by as much as 40 K in a week. Strongest of these events are known as Sudden Stratospheric Warming

(STRATWARM)**.** These are among the most dramatic examples in the atmosphere of the interaction of the waves with the mean fields. This redistributes Ozone and other chemicals and reverses the direction of the stratospheric jet in high latitudes. Planetary wave amplitudes tend to be larger in the Northenhemisphere than in the Sourthenhemisphere because of the different distributions of continents and orography. As a result SH stratospheric polar temperatures are cooler. Major stratospheric warming have not been observed in the SH.

1.8.4 Lee waves

When airflow approaches an obstacle like mountain, two dominant effects happen. The change in height of the earth's surface will introduce a vorticity (wind rotation) component into the airflow which may be balanced by β effect, if the mountain has sufficient meridional extent. This generates Rossby waves. When air is forced to flow over mountain and then dropped , individual air parcels are displaced from their equilibrium levels and will undergo buoyancy oscillations i.e gravity wave oscillations of smaller wavelength is excited in the lee of the mountain.

If the air is moist enough and the vertical motion associated with these lee waves is strong enough, condensation may occur in the updraft portion of the oscillations giving rise to clouds. Stable stratification, wide mountain and comparatively weak zonal flow provide favorable conditions for the formation of vertically propagating lee waves. As the air rises on the windward side, moisture condenses and get removed from it, the latent heat released during this process causes temperature of air to be higher in the lee of the mountain range than on its wind ward side

1.8.5 Gravity Waves

The wave motions for which gravity and stable stratification are the dominant influences are called gravity waves**.** Their spatial scales are from, a few to hundreds of kilometers and temporal scales from minutes to tens of hours**.**

Major sources of gravity waves are topography, convection, jet streams, unstable shear flows, interaction among gravity waves and of gravity waves with the mean flow. Convection excites gravity waves of wide range of scales. Gravity wave dissipation and change of momentum flux contribute to generation of both QBO and SAO. Turbulence arising from gravity wave dissipation contributes both heating and transport through direct energy dissipation and mixing of constituents of atmosphere.

1.8.6 Equatorial waves

Equatorial waves are subset of planetary scale waves. The response of the atmosphere to the imposed forces are peculiar when the coriolis force vanishes near the equator i.e. equatorial atmosphere will respond in a different way compared to mid-latitudes for the same kind of imposed forces. This unique feature of the equatorial region gives rise to a set of waves which are known as `equatorial waves'. Two most important wave motions of this kind are the `Kevin waves' and `Rossby gravity waves'. Both of them have well ordered properties and they have definitive vertical phase propagation so that they can transport momentum and energy upwards.

Both Kelvin and RG waves are believed to be excited by oscillations in the large-scale convective heating pattern in the equatorial troposphere**.** These waves do not contain much energy as other typical tropospheric disturbances. They being the predominant disturbances of equatorial stratosphere, play crucial role in the general circulation of the stratosphere, through their vertical energy and momentum transport.

Kelvin waves propagate upward through easterly winds and RG waves propagate up through westerly winds until they reach critical levels. The mean zonal wind speed and the location of critical levels vary with time.

1.8.7 Kelvin waves

Kelvin waves are generally defined in relation to shallow water gravity waves which propagate parallel to coastal line and have no component of

velocity normal to coastal boundary. Kelvin wave causes only zonal wind perturbation which decreases away from equator to half value around ± 15° latitude. The zonal wind component of the wave is symmetric about equator. With increasing altitude, shorter periods are found to dominate the Kelvin wave spectrum. Following are the characteristics of Kelvin waves.

Direction of propagation : Eastward;
Period : 10-20 days;
Zonal wave no : 1-2;
Zonal wavelength : 20,000-40,000 km;
Vertical wavelength: 8-10 km; Meridional velocity : 0

Lower-frequency Kelvin waves have larger vertical wave numbers, hence short vertical wavelength**.** These waves take 10-20 days to propagate around the globe, occur in the lower stratosphere but are not able to propagate deep into the middle atmosphere**.** They encounter a critical level when the background wind speed is equal to the phase speed of the wave and can no longer propagate. High frequency Kelvin waves can propagate upto upper mesosphere due to their phase speeds exceeding the background wind speed. Faster phase speeds are associated with larger vertical wavelengths and are less likely to be damped

1.8.8 Rossby Gravity (RG) waves

Matsuno, described theoretically two types of wave motions-one is an eastward and westward moving gravity wave and the other is a westward moving Rossby wave. These two types of waves are distinguished from each other by their different dispersion characteristics and relationships between pressure and velocity fields. He found that for low frequency waves, the amplitudes are confined near the equator. With the increase of zonal wave no., the frequency of this wave is found to decrease and approach the value of Rossby wave. With smaller wave no., the frequency approaches that of gravity wave. The meridional velocity component associated with the wave is symmetric about equator while the zonal component is antisymmetric

Following are the characteristics of RG waves*.*

Direction of propagation	: Westward;
Period	: 4-5 days
Zonal wave no.	: 4
Zonal wavelength	: -10,000 km
Vertical wavelength	: 6 km

In the upper stratosphere and lower mesosphere RG wave of period more than 2 days are found to be absent. The RG waves induce a purely meridional wind at the equator which decreases in amplitude away from the equator to half value around $\pm$ 10 $^\circ$ latitudes. The RG wave induced zonal wind perturbation increases with latitude (from zero at equator) to a maximum around $\pm$ 10 $^\circ$ latitude and then decreases rapidly to very low values near 25 $^\circ$ latitude.

1.8.9 Quasi-Biennial Oscillation (QBO)

Zonally symmetric easterly and westerly wind regimes alternating regularly with a period varying from about 22-34 months (with a mean value of 27 months) is called the Quasi biennial oscillation (QBO). Successive regimes first appear below 40 km but propagate downward at a rate of 1 km per month. The downward propagation occurs without loss of amplitude between 30 and 23 km. but there is rapid attenuation below 23 km. The oscillation is symmetric about the equator with maximum amplitude of about 20 ms $^{-1}$, and a half width of about 12° latitude. Vertically propagating equatorial waves- the Kelvin and MRG waves provide the zonal momentum sources to drive the QBO. The dissipating westerly Kelvin waves impart a westerly acceleration to the background wind through deposition of their westerly momentum, while dissipating MRG waves impart an easterly acceleration through similar interaction. Thus alternate layers of westerly and easterly winds are set up in the altitude region of 20-40 km. Thus this QBO is a dynamically driven oscillation -ie; produced by wave-mean flow interaction.

1.8.10 Semi-Annual Oscillation (SAO)

SAO like QBO is also dynamically driven oscillation**.** This zonal wind oscillation of ~ 6 months period has two maxima of its amplitude- one near the

stratopause and other near mesopause with a minimum at about 65 km. Latitudinally, the stratospheric SAO has a broad maximum at about 8° south of equator. It is believed that the westerly phase of SAO is driven by the process of momentum deposition by the westerly propagating Kelvin waves into the mean flow in the upper stratosphere, while the easterly phase of SAO is driven by the momentum deposition by the extra-tropical planetary waves (Rossby waves) penetrating to the equatorial upper stratosphere.

These extra-tropical planetary waves are much more variable in their strength than Kelvin waves and this feature could explain the larger variability of the easterly phase of SAO. There is a phase variation in the vertical so that the SAO wind variation at the amplitude maximum near the mesopause are nearly 180 deg. out of phase with those at the maximum near the stratopause

1.8.11 Tidal Oscillations

Sun and moon exert periodic external forces upon earth's atmosphere. The sun exerts a strong thermal and a weak gravitational effect whereas moon exerts wholly gravitational force. The steady state responses of the atmosphere to these forces are known as tides. They will have periods that are equal to or sub-multiples of the solar or lunar days. The lunar atmospheric tides which are of gravitational origin are smaller compared with solar atmospheric tides, since the atmosphere is primarily driven by the heating effects of the sun. Most of the solar radiation incident on earth and its atmosphere are absorbed by ground and sea

A significant amount of solar insolation is absorbed by water vapour in the troposphere, ozone in the stratosphere and mesosphere and also by ionised oxygen in the ionosphere and daily variation in heating by these, is the most important source of these tidal excitations**.** The heating generates pressure changes with particular patterns of variations with latitude, longitude and height. If the distribution of the absorbing medium is zonally uniform around the globe, then the solar heating will produce diurnal oscillations that are sun-synchronous, traversing the globe in one solar day. These oscillations represent 'the migrating tides'. Any longitudinal deviation in the absorbing medium will result in

oscillations having zonal wave numbers different from one (asymmetric absorption resulting in zonally asymmetric diurnal heating) which are not capable of migrating with sun and are termed as 'non-migrating tides'. Recent studies have revealed that, non-migrating tides are forced by diurnally varying heat transfer in planetary boundary layer produced by land-sea distribution and also by latent heat released by deep convective clouds in the tropics. Non-migrating tides are predominantly local and hence non-uniform in any latitudinal circle. Usually, each solar tidal mode is identified by the notation S (m, n) where 'm' is the longitudinal wave number and 'n' is related to the latitudinal structure of a tidal mode; 'm'=1 for diurnal tide(24 hr period) and 2 for the semi-diurnal tide (12 hr period). [A mode is specified by its frequency $\omega = m \Omega$]. 'n' can be + ve or – ve. + ve modes correspond to propagating modes and – ve modes to trapped or evanescent modes. 'n' can take values starting from 'm'. For non-migrating tides notation used is (m, s, n) , s is the zonal wave no. (m=s for migrating tides).Of the diurnal and semi-diurnal oscillations, diurnal modes are found to be stronger than semi-diurnal modes at low latitudes (both theoretically and observationally) whereas semi-diurnal modes are stronger than diurnal modes at mid-latitudes. Diurnal amplitude change rapidly with latitude with minimum at equator and maximum at 30°N latitude. Mid-latitude observations revealed that tidal activity is enhanced during summer season whereas at low latitudes, equinoctial enhancement of tidal activity is observed. The diurnal and semi-diurnal tidal oscillations are seen to be interacting non-linearly giving rise to ter-diurnal (8 hr) tidal wind oscillations. The study of dynamics at a variety of scales with periods ranging from minutes to hours, days and years requires continuous monitoring of the atmosphere. Sporadic measurements like that given by balloons and rockets are biased towards long periods, while continuous long-term ground-based monitoring (passive/active techniques) is able to provide local access to large range of periods.

1.9 Observational technique

Most of the present-day information on atmospheric dynamic comes from conventional meteorological measurements. The weather vane, which gives wind direction, has been in use for over a thousand years now and anemometers, which give wind speeds, and have been in use since 1660. Upper-air observations started, have been in use since about a hundred years ago to be subsequently followed by balloons. The balloon-borne radiosonde carries instruments to measure temperature, humidity, etc, the motion of the balloon itself is tracked by ground –based radar to obtain measurements at higher altitudes, and rockets are used. A parachute dropped from the rocket, are used.

In recent years, several new technology have become available for studying winds and waves. These are radars and lidars. A verity of radars, such as the whether radar, HF and VHF backscatter radar, partial –reflection radar, and the MST radar are being used to study the dynamics of different height regions in the atmosphere. A lidar is a laser radar, in which coherent light waves are used instead of radio waves. There are now several lidars in the world, which regularly monitor atmospheric motions.

Satellites have also been extensively used for more than two decades now to study atmospheric motions. Using a suitable camera on board the satellite, cloud pictures are obtained and the motion of these clouds is used to obtain cloud- top wind vectors. This program, initiated in the ‘60s, has been a major thrust in satellite meteorology. Geostationary satellites, such as the Meteosat, INSAT and the GEOS Series, as well as several Earth – orbiting, Sun-synchronous satellites, have been used for global mapping of atmospheric winds. In the meteorological regions. The dynamics of the upper atmosphere have been studied by satellite-born airglow mappers and instruments to measure the movement of ionization.

1.10 Importance of studies of Earth's Atmosphere

The middle atmosphere is the region where largest changes of anthropogenic origin have been observed in the last decades. Discovery of Antarctic ozone hole is the best known of such changes. Under the influence of ozone depletion, partly as a consequence of the increase of CO_2 and H_2O (Green house gases), trends in the temperature both in the stratosphere and mesosphere has been changed faster than that predicted by any model. This could be a major source of perturbation in the wave propagation between troposphere and region above that, which could have an impact on the general circulation and therefore on the climate. Thus monitoring the trends in temperature and winds and thus studying the wave propagation through different regions of the atmosphere is essential for understanding the climate. Atmospheric science is devoted to the determination of quantitative relations between variables that describe the state and motion of the atmosphere. The description involves specifying both what is occurring and how the events vary from place to place and from time to time. We must develop a suitable system of quantities that describe the mass, thermal and motion fields of the atmosphere and we must find ways to utilize the mathematical operations available for determining rates of changes and average properties to study the weather and climate in detail. Climate-change issues have received substantial attention in recent years due to the increasing awareness that human activities may substantially modify the future climate of the Earth. The globally averaged temperature has increased by about 0.6 degrees Celsius over the past hundred years and 1998 was the warmest year recorded on instrumental temperature record covering the last 150 years. These facts and other pieces of evidence suggest that an increased greenhouse effect due to human activities is starting to influence the global climate system. A very important question is thus to assess how a further future increases in greenhouse gases may affect this system. The most effective tools available to answer such questions are global and regional climate models. Co-ordinate measurements of atmospheric parameters like, temperature, wind, trace gases and wave motions are essential

for the detailed study of the different regions of the atmosphere. International programs like CAWSES, CPEA and Indian programs like CAWSES-INDIA, IMDAS etc. are aiming towards these goals.

2.1 Introduction

The term RADAR is an acronym for Radio Detection And Ranging. Radar is basically a means of gathering information about distant objects or targets by sending electromagnetic waves at them and analyzing the echoes. The radar technology was developed in 1935 by Sir Robert A Watson Watt, a Scots physicist. The word radar first used by US Navy in 1940 .It was first developed as a detection device to identify the approach of hostile air crafts and for directing anti aircraft weapons during the Second World War. But nowadays modern radars are used for identification and classification of targets, even to produce an image of the objects. The principle of radar is that a transmitter sends out a radio signal, which will scatter off any thing that it encounters such as land, sea, air craft, ship etc, and a small amount of energy is scattered back to the radio receiver. Location of targets and its related information can be retrieved from the received echo signal with the replica of transmitted signal. After amplification in the receiver signals are processed to get the required information from the unwanted noise components by doing data processing. The radar can be operated in all weather conditions like haze, fog, darkness, rain and snow.

Radar systems are used for the study of atmospheric processes because of their simplicity, reliability and by virtue of the fact that a radar system provides a means of sampling the atmosphere at a rapid rate in a cost effective way. Initially microwave radar systems were used for the study of cloud coverage, precipitation, and storm location, characterization of the intensity of storm clouds and for general day to day meteorological predictions.

A new generation of pulse Doppler radar system has emerged for probing the atmosphere and studying the dynamics of the atmosphere using the backscattered signals from clear air turbulence. The tracer elements for such radar systems are variations in the atmospheric refractive index. Such radars have come to be known popularly as the MST, the ST and the T Radars depending upon the maximum effective height coverage of the radar corresponding to the three regions of the atmosphere viz., Mesosphere, Stratosphere, and Troposphere.

2.2 Basic Radar and Principle

Radar is an electromagnetic system for the detection and location of reflecting objects such as aircraft, ships, spacecraft, vehicles and the natural environment. It consists of a transmitter and a receiver, each connected to a directional antenna. It operates by radiating electromagnetic energy into the space and detecting the echo signal reflected from an object or target. Location of the target and its related information can be obtained by comparing the received echo signal with the replica of the transmitted signal. The block diagram of simplest Radar is shown below.

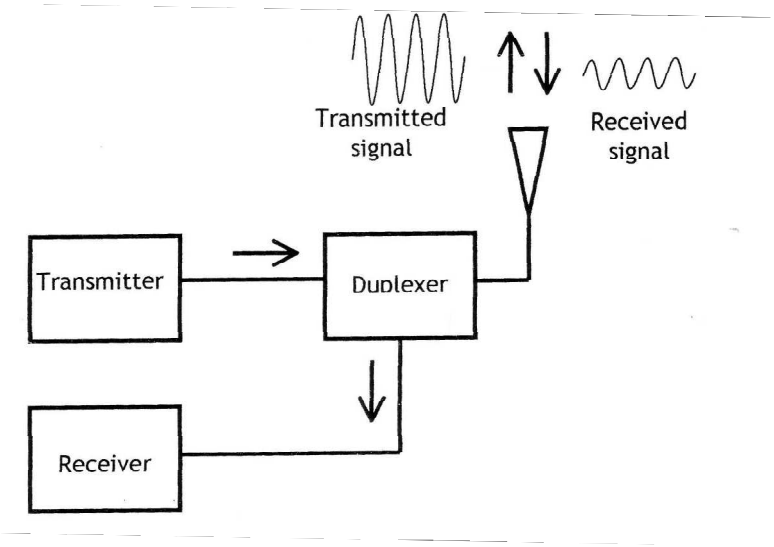

Figure -2.1 Block Diagram of Radar

The transmitter generates a short, rectangular pulse. As soon as a small fraction of the pulse power is fed to the duplexer, this device disconnects the receiver from the antenna and connects the transmitter to it. As soon as the transmitted pulse terminates, the duplexer disconnects the transmitter from the antenna. Transmitter also reconnects the receiver to the antenna, allowing the returning echoes to be correctly processed. The received pulses are amplified and demodulated by the receiver. The pulses from the returning echoes are then fed

to the device on which they are to be displayed. The cycle is completed and the set is once again ready for the transmission of the next pulse.

Radars are basically classified into two categories; Pulsed Radars and CW Radars. Pulsed Radar transmits pulsed energy towards the target and receives the echo signal after time delay T. The radial range is computed using the formula **r = cT/2**. However, the motion of the target cannot be known. A CW Radar radiates EM energy continuously and derives the Doppler frequency (f_d) from the received echo by comparing it with the transmitting frequency. The radial velocity of the target is computed from the formula $\mathbf{V_r = f_d \times \lambda / 2}$. This radar is also referred as Doppler radar. However, in this radar the range of the target cannot be known. Most often these two techniques are combined to derive range and velocity of the target.

2.3 Radar Equation

The radar equation relates the range of radar to the characteristics of the transmitter, receiver, antenna, target and environment. It is useful not just as a means for determining the maximum distance from the radar to the target, but it can serve both as a tool for under standing radar operation and as a basis for radar design. If the power of the radar transmitter is denoted by P_t, and if an isotropic antenna used (one which radiates uniformly in all direction), the power density (watts per unit area) at a distance R from the Radar is equal to the transmitter power divided by the surface area $4\pi R^2$ of an imaginary sphere of radius R, or

$$\text{Power density from isotropic antenna} = P_t / 4\Pi R^2 \qquad (2.1)$$

Gain of antenna is a measure of the increased power radiated in the direction of the target as compared with the power that would have been radiated from all directions from an isotropic antenna. It is defined as the ratio of the maximum radiation intensity from the subject antenna to the radiation intensity of isotropic antenna with the same power input. Radiation intensity is the power

radiated per unit solid angle in a given direction. The power density at the target from an antenna with a transmitting gain G is

$$\text{Power density from directive antenna} = P_t G / 4\Pi R^2 \quad (2.2)$$

The measure of the amount of incident power intercepted by the target and reradiated back in the direction of the radar is denoted as the radar cross section 'σ' and is defined by the relation

$$\text{Power density of echo signal at radar} = P_t G \sigma / (4\Pi R^2)^2 \quad (2.3)$$

The radar cross section σ has units of area. It is a characteristic of the particular target and is measure of its size as seen by the radar. The radar antenna captures a portion of the echo power. If the effective area of the receiving antenna is denoted

A_e, the power P_r received by the radar is

$$P_r = P_t G \sigma A_e / (4\Pi)^2 R^4 \quad (2.4)$$

The maximum radar range R_{max} is the distance beyond which the target cannot be detected. It occurs when the received echo signal power p_r just equals the minimum detectable signal S_{min}. Therefore

$$R_{max} = [P_t G A_e \sigma / (4\Pi)^2]^{¼} \quad (2.5)$$

Equation (2.5) is a fundamental form of the radar equation. Antenna theory gives the relationship between the transmitting gain and the receiving effective area of antenna as

$$G = 4 \Pi A_e / \lambda^2 \quad (2.6)$$

Since radar generally use the same antenna for both transmission and reception. Eq. (2.6) can be substituted in to Eq. (2.5) , first for A_e then for G, to give two other forms of the radar equation

$$R_{max} = [P_t G^2 \lambda^2 \sigma / (4\Pi)^3 S_{min}]^{¼} \quad (2.7)$$

$$R_{max} = [\, P_t \, A_e^{\,2} \sigma / (4\Pi) \, \lambda^2 \, S_{min} \,]^{¼} \qquad (2.8)$$

These three forms (Equation 2.5, 2.7, and 2.8) illustrate the need to be careful interpretation of the radar equation. For example, from equation (2.7) it might be thought that the range of a radar varies $\lambda^{1/2}$, but equation (2.8) indicate a $\lambda^{-1/2}$ relationship, and (2.5) the range to be independent of λ.

2.4 Types of Radar

Radar operating in the extended frequency range from MF to UHF are used to investigate the structure and dynamics of the troposphere, stratosphere, mesosphere and thermosphere/ionosphere. In **Table-2.1** different kinds of radars and their basic technical parameters are summarized. The MF radars, making use of partial reflection from electron density irregularities, are particularly applied to measure electron density profiles of the Ionospheric D-region and lower E-region as well as the horizontal wind velocity in this altitude range, comprising the mesosphere and lower thermosphere. The HF radars and the Ionospheric irregularity scatter radars are used to study total reflections from the ionosphere and scattering from E and F-region plasma irregularities respectively. The meteor radar make use of echoes returned from meteor trail to measure wind velocities in the upper mesosphere and lower thermosphere. Incoherent Scatter radar echoes from the D-region also have long coherence times like MST radar echoes.

Table -2.1

Radar Method	Frequency Range	Wavelength In m	Average Power in KW	Antenna Dimension in	Height Region
MF Radar	MF-HF	150 -50	0.01-1	1-10	M,L
HF Radar	HF	300-20	0.01-5	0.5-1	Th/Io
Coherent Radar	HF-VHF	30-1	0.1-1	5-50	Th/Io
Meteor Radar	HF-VHF	10-6	0.1-10	2-10	M.LT
MST Radar	VHF	6-7	1-100	5-50	M,S,T
Incoherent Scatter Radar	HF-UHF	1.4-0.25	100-300	100-300	M,LT
ST Radar	VHF-SHF	6-0.1	10-500	10-500	S,T

2.5 Indian MST radar

The Indian MST radar is a highly sensitive, pulse coded, coherent VHF phased array radar, operating at 53 MHz with an average power-aperture product of 7 X 10^8 Wm^2. The basic system has been discussed in detail by Jain et al (1995), Rao et al.(1994,95). The system design specification are present in Table2.2 and Figure 2.2 shows functional diagram of the Indian MST radar.

Table-2.2

Specification of the Indian MST Radar

Parameter	:	Specification
Location	:	Gadanki (13.4^0 N, 79.18^0 E)
Frequency	:	53 MHz
Average power aperture product	:	7×10^8 Wm^2
Peak power	:	2.5 MW
Maximum duty ratio	:	2.5%
Number of Yagi antennas	:	1024
Beam width	:	3^0
Number of beams for automatic		
Scan Pulse-	:	7*
Pulse width	:	6 and 32µs coded and 1-32 µs
		Uncoded (in binary step)
Maximum number of range bins	:	256
Number of coherent integrations	:	4 to 512 (in binary steps)
Maximum number of FFT points	:	512
Radar controller	:	PC/AT featuring programmable
		experimental specification file
Computer system	:	32-bit super mini with vector
		Accelerator (Masscomp MC5600)

*Zenith in X and Y polarization ± 10^o off-zenith in E-W and N-S plane, and 14.8^o N looking transverse to B field. This capability has now been enhanced to 18 beam which can be chose from available 82 beams.

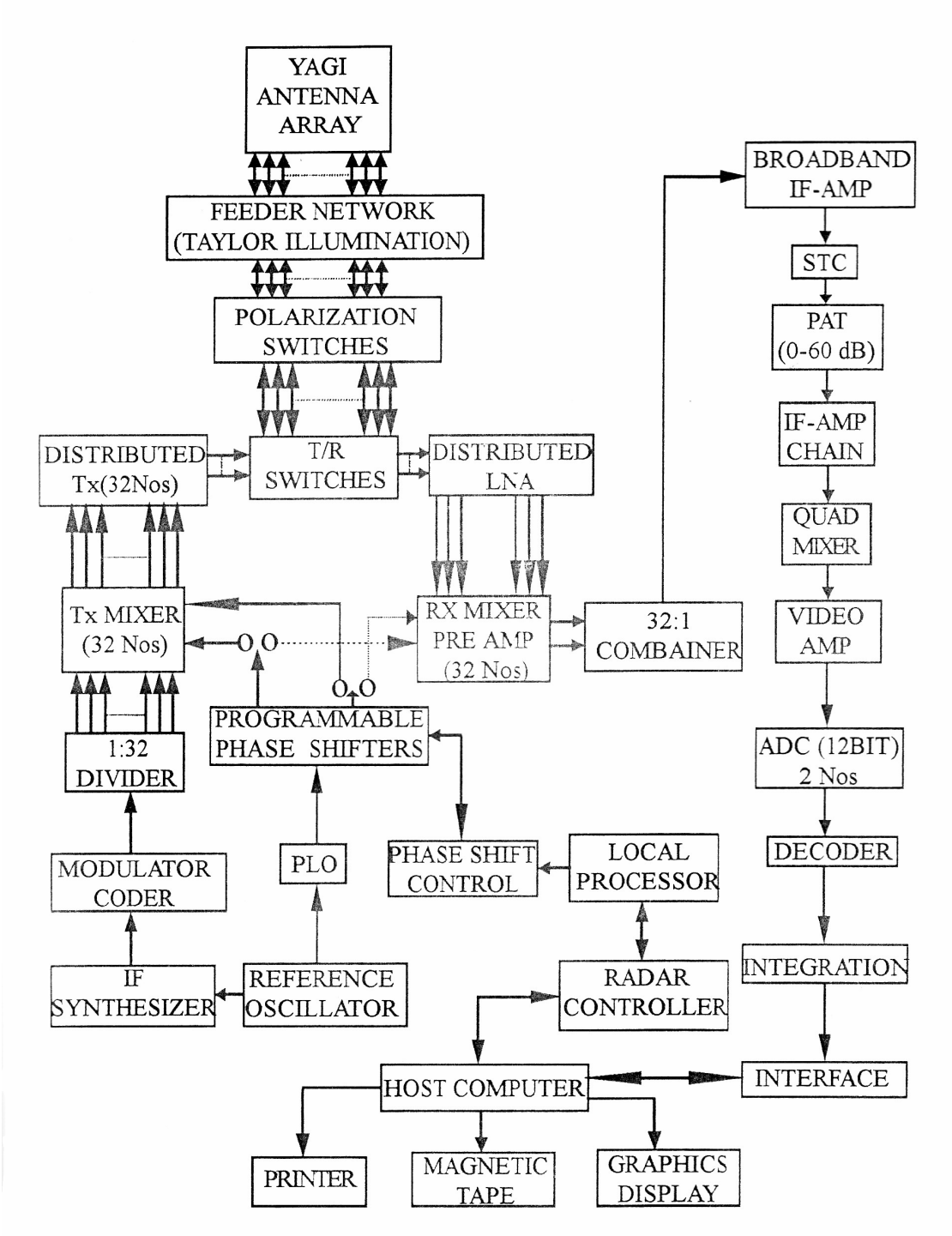

Figure -2.2 A block diagram of Indian MST Radar system (After Jain et al.,)

Indian MST radar a phased array radar consisting of planar array of 32 X 32 (=1024) dual Yagi antenna. There are 32 high power transmitters. One transmitter feeds a row of 32 Yagi antenna through a series feed of directional coupler. Transmitted powers and directional coupler outputs are tapered to achieve modified Taylor distribution with a design side lobe level of -20dB for the planar array. The beam is tilted by the low power phase shifters associated with exciters of the transmitters.

Each transmitter of MST radar consists of exciter (inclusive of a biphase complementary code), solid state amplifier, 2 stages of triode of triode drive amplifiers and finally high power amplifier.

The duplexer provides more than 60 dB isolation between the receiver and transmitter. The polarization switch allows selecting eight E-W or N-S polarization. The received signals are fed through blanking switches (necessary to provide extra isolation between receiver and transmitter) to individual front end amplifiers with a nominal noise figure of around 3dB. After suitable amplification the received signals are down converted to 5 MHz, combined and fed to a quadrate mixture. The I and Q outputs are then sent to the data acquisition system, which processed the raw data and display it in a suitable format. The final parameters read out are signal amplitude, Doppler and Doppler width for different heights. The whole operation is controlled by ‘radar controller’. It is a PC based subsystem using which the user controls the whole operation of the radar. All parameters necessary for radar operation namely bema selection, phase loading, pulse width and PRF selection and duration of operation are selected through radar controller.

2.6 Scattering Mechanisms of MST radar

The scattering and reflection mechanisms responsible for the MST radar signal return have been described in some detail by Balsley and Gage (1980) and Gage and Balsley (1980) among others. They are classified generally as: (i) Turbulent scatter, (ii) Fresnel(Partial) reflection/scatter and (iii) Thermal (incoherent or Thomson) scatter. The first two mechanisms provide coherent

scatter which result from macroscopic fluctuation in refractive index associated with clear air turbulence. The third arises from Thomson scatter by free electrons in the ionosphere and the signal return is characterized by the statistical fluctuations of electron density due to random thermal motions of electrons and ions (Evans, 1969). While the turbulent scatter and the Fresnel reflection are the dominant mechanisms for the MST signal return, it has been shown that it is possible to map the mesospheric wind fields using the Thomson backscatter as well (Harper,1978).

The radio refractive index, n, relevant to the MST radar return is expressed approximately as:

$$n-1 = (3.73 \times 10^{-1}\, e/T^2) + (77.6 \times 10^{-6}\, P/T) - (N_e / 2N_c) \qquad (2.8)$$

where, e (mbar) is the partial pressure of the water vapour, P(mbar) the total atmospheric pressure, T(K) the absolute temperature, N_e the number density of electron and N_c the critical electron density corresponding to the operating radar frequency. The first two terms, in the above expression, represent the contribution due to bound electrons of water vapor and dry air, while the third expresses the contribution due to the presence of free electrons. The refractive index fluctuations arising from the first two terms contribute to the radar returns from troposphere and stratosphere. The neutral turbulence induced electron density fluctuations represented by the third term become the major factor contributing to the radar return from the mesosphere.

2.6.1 Turbulent scatter

The basic theory of radiowave scattering by turbulent fluctuations of the atmosphere was developed originally by Booker and Gordon (1950) to explain 'over the horizon' tropospheric radio propagation. According to the theory of radio wave scattering from turbulent fluctuations of refractive index the radar backscattered signal arises from the spatial Fourier component whose wavelength is equal to one half of the radar wavelength λ_R as illustrated in figure 2.3 a. Hence, in order to have coherent backscatter, the

condition to be satisfied is $\lambda_{min} < \lambda_R/2 < \lambda_{max}$ where λ_{min} and λ_{max} are related to the inner (l_o) and outer (L_o) scale sizes of the turbulence. The height variation of minimum scale of turbulence λ_{min} , adapted from Balsley and Gage (1980), is shown in figure 2.3b.

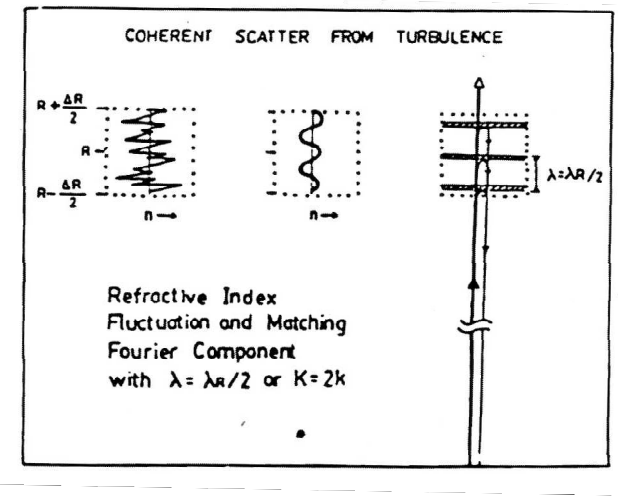

Figure 2.3 (a) Coherent backscatter from a spatial Fourier component whose Wavelength (λ) is one half of the radar wavelength(λ_R) (Rao,1990)

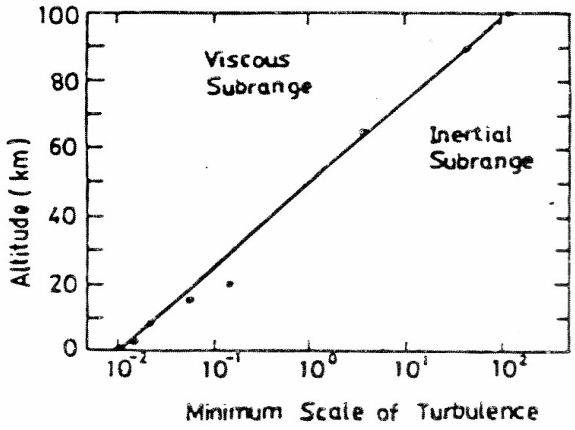

Figure 2.3 (b) Height Variation of minimum scale of turbulence (Balsley & Gage,1980)

The general expression for reflectivity for backscattering due to turbulence is given by

$$\eta = (\pi^2 / 2) K^4 \varphi_n (k) \qquad (2.9)$$

Where, k is the wave number of the Fourier spectral component to which the radar is sensitive and φ_n (2k) is the three dimensional wavenumber spectral

density for refractive index fluctuations. For locally homogenous and isotropic inertial range turbulence, the wave number spectrum is given by (Gage and Balsley,1980);

$$\varphi_n\ (2k) = 0.033\ C^2_n\ k^{-11/3} \qquad (2.10)$$

Where the refractivity structure constant is expressed as

$$C^2_n = 5.45\ (\overline{\Delta n})^2\ L_o^{-2/3} \qquad (2.11)$$

Substitution of eq. (2.10) and (2.11) in eq. (2.9) Leads to

$$\eta = 2.07(\overline{\Delta n})^2\ L_o^{-2/3}\ \lambda_R^{-1/3} \qquad (2.12)$$

For mesosphere, the mean square refractive index fluctuation may be expressed in terms of mean square electron density fluctuation $(\overline{\Delta N_e})^2$

$$(\overline{\Delta n})^2 = (f_p^2 / 2 f_r^2\ N_e)^2\ (\overline{\Delta N_e})^2 \qquad (2.13)$$

Where f_p is the plasma frequency and f_r is the radar frequency. Substituting Eq.(2.13) in Eq.(2.12) and replacing f_p by the corresponding electron density, we get

$$\eta = 3.25 \times 10^3 (\overline{\Delta N_e})^2\ c^{-4}\ L_o^{-2/3}\ \lambda_R^{11/3} \qquad (2.14)$$

from eqs. (2.12) and (2.14) it can be seen that the reflectivity of turbulent scatter varies with the radar frequency as $f_R^{1/3}$ for troposphere and stratosphere and so sensitivity as $f_R^{-11/3}$ for mesosphere.

Radar equation for Turbulent Scatter

The received backscattered power from a distributed target such as atmospheric turbulence may be expressed as (Sato.1989):

$$P_r = P_t\ A_e^2\ L\ \sigma / 4\ \pi^2\ \lambda_R\ R^4 \qquad (2.15)$$

Various symbols in the above equation carry the usual meaning. Defining the reflectivity as radar cross-section per unit volume, we have $\sigma = \eta dV$, where dV is the volume element illuminated by the radar pulse. For radar beam width θ and pulse length of ΔR, dV may be expressed as

$$dV = \pi^2 (R \lambda_R)^2 \Delta R / 16 A_e \quad (2.16)$$

Expressing σ in terms of reflectivity and using Eq.(2.16), Eq.(2.15) can be written as

$$P_r = \pi P_t A_e L \Delta R \eta / 64 R^2 \quad (2.17)$$

2.6.2 Fresnel Reflection and Scattering

Fresnel (Partial) reflection occurs from a sharp vertical gradient in refractive index that is horizontally coherent over a scale greater than a Fresnel zone. Radar observations at VHF have shown evidence for the importance of Fresnel reflections from horizontally layered structures in the neutral atmosphere of troposphere and stratosphere (Gage and Green 1978; Röttger and Liu, 1978) and electron density stratifications in the mesosphere (Fukao et al., 1978) Radar returns from the mesosphere, particularly at long wavelengths, are generally referred to as partial reflections. It should, however, be noted that there is observational evidence to suggest the radar returns are due to both Fresnel reflections from coherent density gradients and scattering from turbulent irregularities.

The general expression for power reflection coefficient $|\rho|^2$ for an electromagnetic wave reflected vertically from an infinite horizontal layer is given by Wait (1962) as:

$$|\rho|^2 = (1/4) \left| \int_{-t/2}^{t/2} (dn/dz) \exp(-i2kz) dz \right|^2 \quad (2.18)$$

$$= |\Delta n|^2 /4 \left| \int_{-t/2}^{t/2} (d(n/\Delta n)/dz] \exp(-2kz) dz \right|^2 \quad (2.19)$$

Where, z is the altitude, t the thickness of the layer and Δn the total change of n across the layer. For simple layer shapes, the integral can be expressed in closed form. For a step of magnitude Δn

$$|\rho|^2 = |\Delta n|^2 /4 \quad (2.20)$$

For a smoothly varying layer of the form

$$n = n_o + \Delta n [\exp (4z/t) / \{ 1+ \exp (4z/t)\}] \quad (2.21)$$

The reflection coefficient is give by Friend (1949) as

$$|\rho|^2 = (|\Delta n|^2 / 4)\,[(9t / \lambda)/ \sinh(9t / \lambda)] \qquad (2.22)$$

The general case of partial reflection in which there are many closely spaced layers randomly distributed in height is called Fresnel scatter. It is contrast to Fresnal reflection which arises from a single layer or a coherent distribution of layers.

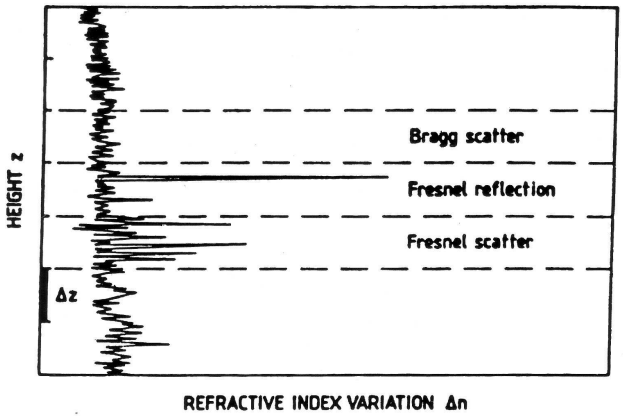

Figure 2.2 (c) A schematic depiction of the spatial variations ∆n of the ref Refractive index n in the vertical direction z leading toBragg scatter, Fresnel reflection and Fresnel scatter Rottger and Larsen,1990)

Figure 2.3c illustrates the processes of Bragg scatter, Fresnel reflection and Fresnel scatter in terms off the spatial variations of the refractive index n in the vertical direction z within the radar range gate ∆z (Röttger and Larsen,1990). In view of the random stratification of n, the problem of Fresnel scatter can be treated only through statistical approach. The power reflection coefficient, expressed as ensemble average, is given by Farly (1983) as:

$$<|\rho|^2> = (1/4) \int_{-\Delta R/2}^{\Delta R/2} dz_1 \int_{-\infty}^{\infty} dz_3 x < n'(z_1) n'(z_1 - z_3) > \exp(-i2kz_3) \qquad (2.23)$$

Where n'(z)= dn/dz is taken as a random variable. Eq.(2.23) is based on the assumption that the correlation length of n'(z) is much less than ∆R. The integration in z_3 is just the Fourier transform of the spatial ACF of n' and it is the

power spectrum S_n (2k) of the fluctuation of n'. Taking the spectrum to be independent of Z_1 over ΔR Equation (16) reduces to

$$< |\rho|^2 > = (1/4)\, \Delta R\, S_n(2k) \qquad (2.24)$$

Radar Equation for Fresnel Scatter

The radar equation for Fresnel reflection can be given on the basis of a source located at the mirror image distance of 2R and weighted by the factor of power reflection coefficient $|\rho|^2$. accordingly (Sato, 1989),

$$P_r = P_t\, G\, A_e\, L\, |\rho|^2\, 4\pi\, (2R)^2 \qquad (2.25)$$

Substituting $4\pi Ae/\lambda^2_R$ for G,

$$P_r = P_t\, A^2_e L\, |\rho|^2 / 4\, \lambda^2_R\, R^2 \qquad (2.26)$$

The signal power of Fresnel scatter has range dependence of R^{-2} as for the case of distributed targets and it is proportional to A_e^2 / λ^2_R like that of a hard target. Fresnal reflection is aspect sensitive and Eq.(2.26) assumes that the antenna beam is directed perpendicular to the layer for which he received signal power has its maximum value.

2.6.3 Thomson (Incoherent) Scatter

Thomson scatter, often referred to as incoherent scatter, is clearly the most potent of the ground based radar techniques to probe the earth's ionosphere (Evans 1969). Recent advances extending its application to mesospheric studies have been described in some detail by Mathews (1984).Thomson backscattered radar signal from the ionosphere is extremely weak, as it arises from small electron density fluctuations due to random thermal motions of the ions and electrons. When the radar wavelength is much larger than the Debye length, the scattering can no longer be regarded as from the individual electrons, but, instead, is best thought of as arising from density fluctuations associated with plasma waves.

The principal waves contributing to the radar-backscattered signal are the ion-acoustic and electron plasma waves. The two spectral components are ermed ionic and electronic. The scattering cross-section for unit volume per Hertz is expressed as (Mathews,1984):

$$\sigma(\omega_i + \omega) = N_e \sigma_e \sigma_n(\omega) \quad (2.27)$$

Where N_e is the steady state electron, σ_e the radar cross-section of an electron and $\sigma_n(\omega)$ the normalized scattering coefficient per electron per Hertz. Following Farley (1966), under the conditions of $1 \leq T_e / T_i \leq 3$ and no negative ions, the total normalized scattering coefficient per electron is given as

$$\sigma_n = \alpha^2_e / (1+ \alpha^2_e) + [1/(1+ \alpha^2_e) \{1+ (T_e / +T_i) + \alpha^2_e\}] \quad (2.28)$$

Where T_e and T_i are the electron in temperature and $\alpha_e = 4\pi \lambda_D / \lambda_R$, λ_D and λ_R being Debye length and radar wavelength respectively. In eq. (2.28) the first and second terms represent the electron and ion line contributions, respectively, to the total scattered power. When $\alpha^2_e >> 1$ (i.e., $\lambda_D >> \lambda_R$), $\sigma_n \approx 1$ and the contribution is essentially from the electron line. For $\alpha^2_e << 1$, the contribution is from the ion line which is expressed by

$$\sigma_n = 1/ [1+ (T_e + T_i) \quad (2.29)$$

In the mesosphere, where the collisions are important, both the electron and ion components the spectrum become significantly narrowed. The effect of the collisions on the spectrum is characterized by a parameter ψ given by the ratio of the radar wavelength to mean free path.

2.7 Method of Vector wind measurement

There are basically two methods which are applied by MST radar, in particular to measure velocities, as is sketched in Fig -2.3 (Röttger, 1981). One method uses a narrow radar beam pointed into various directions and measures the Doppler shift of echoes scattered from irregularities. This method is usually called the Doppler method" and for this reason these radars are also called the Doppler radars". The other method uses three or more spaces antennas and the received echoes are cross-correlated to determine the drift speed of irregularities

and are called “spaced antenna or SA method”. Since the irregularities are usually moving with the wind velocity, both methods are cable to measure the wind velocity. The SA method can also be applied in the spatial domain interferometer mode, which is advantageous for studying the structure of the scattering/ reflecting irregularities.

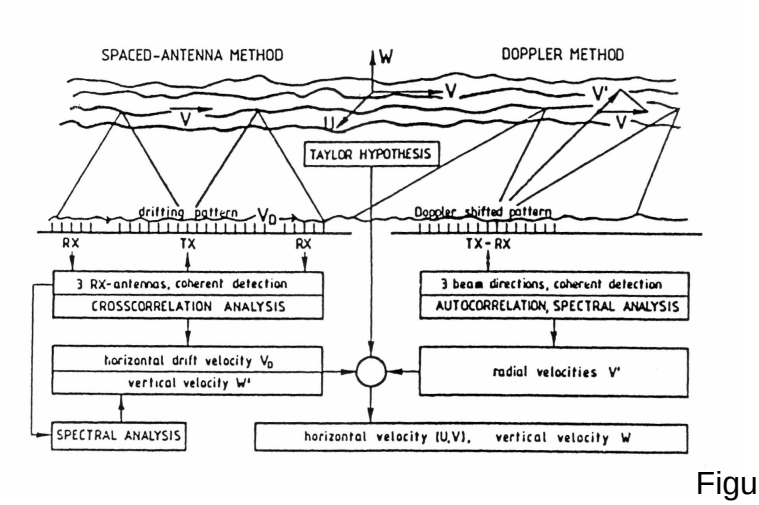

Figure 2.3 A Schematic representa
(DBS) and spaced antenna (SA) methods of drift velocity measurement (Röttger,1981)

2.7.1 Moments Estimation

The steps involved in the estimation of moments as given by Anandan (1997) are

(a) Re-order the spectrum to its correct index of frequency in the following manner 0,1,---- N/2------- N-1, Where 0 represent corresponds to ambiguous frequency, 1 corresponds to maximum negative frequency, N/2 corresponds to zero frequency and N-1 corresponds to maximum positive frequency.

(b) Subtract noise level from spectrum:

(c) Find the index of the peak value of the spectrum and the minimum index of positive point corresponding to the valley point of the detected Doppler spectrum.

(d) Computation of moments M0, M1, and M2 using the following expressions

(i)
$$M0 = \sum_{t=m}^{n} Pi \qquad (2.30)$$

represent the zeroth moment or total power in the Doppler spectrum.

(ii) $$M1 = (1/M_0)\sum_{i=m}^{n} Pfi \qquad (2.31)$$ (2.31)

represent the first moment or mean Doppler in Hz.

Where $f_i = (i - N/2) / IPP * NCI * N$

NCI = number of coherent integrations,

IPP= interpulse period and N is Number of FFT point.

$$M2 = (1/M_0)\sum_{i=m}^{n} P(fi - M1)^2 \qquad (2.32)$$ (

Represent the second moment of variance, a measure of dispersion from the central frequency.

(iii) Doppler spectral width = $2\sqrt{M2}$ Hz

(v) Signal to noise ratio (SNR)= 10log[M0/N*L)] dB (2.33)

Where L is the mean noise level.

2.7.2 uvw computation

Calculation of radial velocity and height:

For representing the observation results in physical parameters, the Doppler frequency and range bin have to be expressed in terms of corresponding radial velocity and vertical height.

Velocity $V = (c * f_D) / (2 * fc)$ or $(f_D * \lambda)/ 2$ ms^{-1}

Height $H = (c* t_R * \cos\theta)/2$

Where c= velocity of light in free space

f_D = Doppler frequency

f_c = carrier frequency

λ = carrier wavelength (5.86 m)

θ = Beam tilt angle

t_R = Range time delay

Computation of absolute wind vectors (UVW):

After computing the radial velocity in for different beam positions, the absolute velocity (UVW) can be calculated. To compute the UVW, at least three non-coplanar beam radial velocity data is required. If higher number of different beam data are available, then the computation will give an optimum result in the least square method.

Line of sight component of the wind vector $V(V_x V_y V_z)$ is

$$V_D = \mathbf{V.\ i} \mathrel{+}= v_x \cos\theta_x + v_y \cos\theta_y v_z \cos\theta_z \qquad (2.34)$$

where x, y and z directions, which are aligned to East-West, North-South, and Zenith respectively. Appling least squares method, residual

$$\varepsilon^2 = (v_x \cos\theta x + v_y \cos\theta_y + v_z \cos\theta_z - v_{Di})^2 \qquad (2.35)$$

where $v_{Di} = f_{Di} * \lambda / 2$ and i represents the beam number

To satisfy the minimum residual, $\partial \varepsilon^2 / \partial V_k = 0$ k corresponds to x, y and z thus,

$$\begin{bmatrix} V_x \\ V_y \\ V_z \end{bmatrix} = \begin{bmatrix} \sum_i \cos^2\theta_{xi} & \sum_i \cos\theta_{xi}\cos\theta_{yi} & \sum_i \cos\theta_{xi}\cos\theta_{zi} \\ \sum_i \cos\theta_{xi}\cos\theta_{yi} & \sum_i \cos^2\theta_{yi} & \sum_i \cos\theta_{yi}\cos\theta_{zi} \\ \sum_i \cos\theta_{xi}\cos\theta_{zi} & \sum_i \cos\theta_{yi}\cos\theta_{zi} & \sum_i \cos^2\theta_{zi} \end{bmatrix} * \begin{bmatrix} V_{Di}\cos\theta_{xi} \\ V_{Di}\cos\theta_{yi} \\ V_{Di}\cos\theta_{zi} \end{bmatrix} \qquad (2.36)$$

on solving this equation we can derive the V_x, V_y, V_z which are corresponding to U (zonal), V(meridional), W (vertical) components of velocity.

2.8 Sample Observations from MST Radar

Figure 2.4 shows a display of Doppler Power spectra from a typical 6 beam (East, West, Zenith X- Zenith y , North , South) scam using 16 μs coded pulses, 512 fft points, 64 coherent integrations, 1 incoherent integration, 1000 μs Interpulse period, providing a height resolution 150 m. The signal can be upto 20 km. The vertical component of the wind velocity is very small compared to the horizontal and merdional component.

Figure -2.5 presents a set of height profile of the three wind components , zonal (U), meridional (V), Vertical (W) . The zonal wind is found to vary with height from easterly with peak value of about 40 ms^{-1} The meridional component is found to be very smaller and more variable compared to the zonal component. It is northerly below 7 km and the value about 3 ms^{-1} above this height it is becomes southerly reaching a maximum of about 12 ms^{-1} at height of about 13 km again it goes to northerly reaching a maximum value about 5 ms^{-1} above the 14 km it has gone to southerly and reaching and maximum value about 12 m/s at the 18 km. vertical component is small peak value ~ 1 ms^{-1} at 17 km.

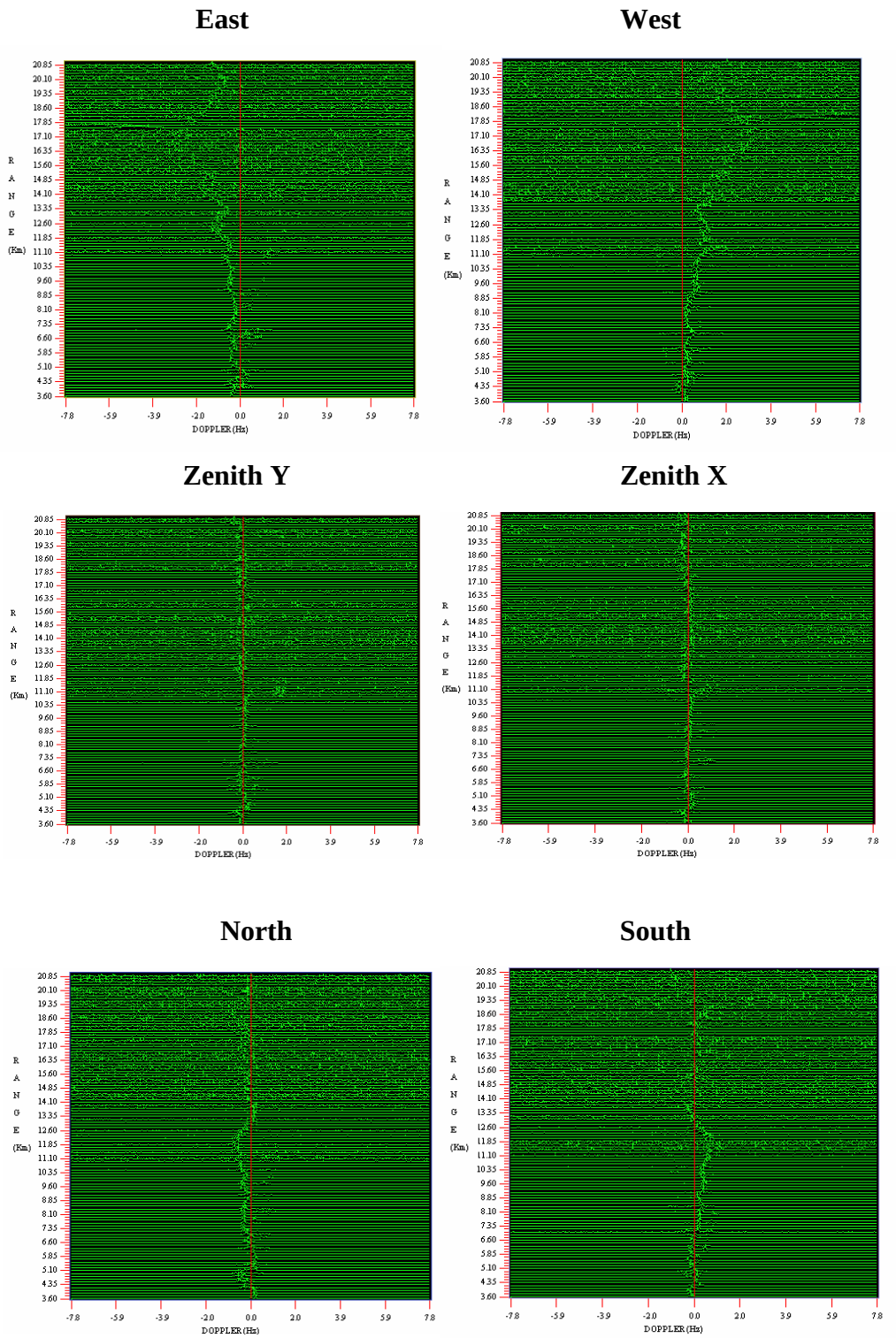

Figure 2.4 Doppler spectra of typical six beam scan taken on 12 August 2003

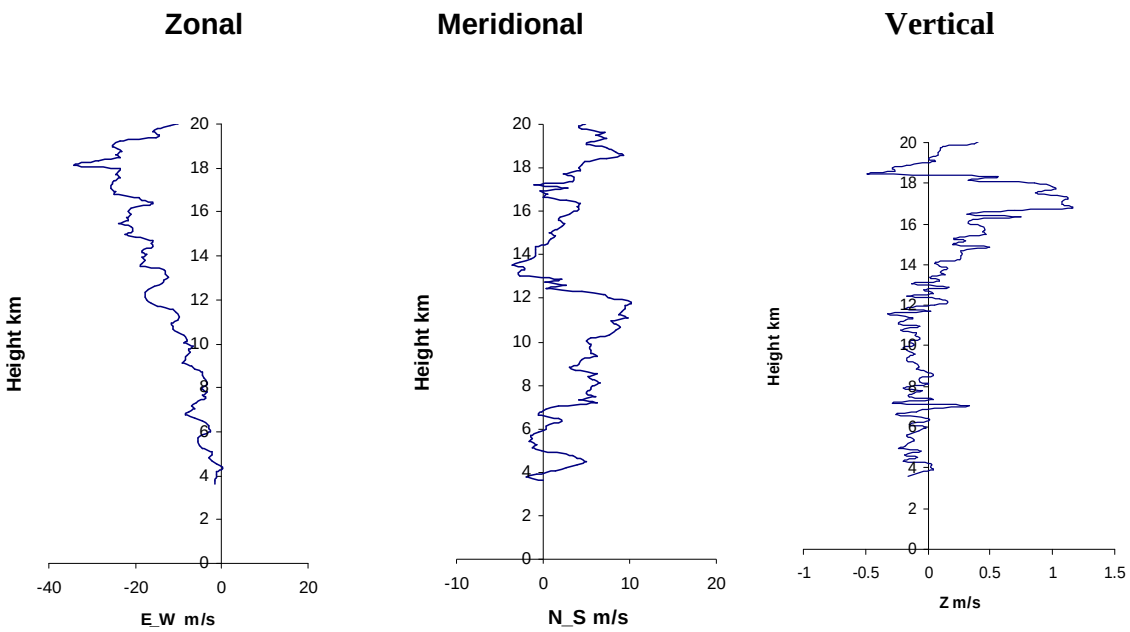

Figure 2.5 Typical height profile of zonal, meridional and vertical wind Component of the wind Vector derived from the Doppler Spectra observed by the MST Radar on 12 August 2003

3.1 Introduction:

The term wind is generally used to describe air in motion. Wind systems generally arise from gradient in atmospheric pressure. The most important cause of pressure gradient is differential heating of the atmosphere; due to change is zenith angle with latitude, or due to changes in surface characteristics affecting the terrestrial long wave radiation or due to change in atmospheric concentration of the gases that absorb the radiation such as O_3 , O_2, H_2O.

In upper troposphere, near 200 mb (hPa) level, there are two well-marked westerly wind maxima, one in each hemisphere. In the winter hemisphere, the maxima is close to latitude 30^o ; in the summer hemisphere, it is close to latitude 45 ^{o}. During the winter season, the maximum is stronger and more equatorward than during the summer season, in any hemisphere. Over the equatorial region, winds are general easterly, these are Trade winds. Equatorial tropospheric easterlies are strongest during the northern summer (June- August). This is due to the existence of the easterly jet stream over the south Asia during this season. The tropics have relatively stronger easterlies in the lower stratosphere compared to the troposphere. (Asnani, 1993).

When the force of earth's gravity and the magnitude of the stabilizing restoring force introduced by the density gradient become comparable with compressibility forces, the resulting waves are called acoustic gravity waves or simply gravity waves. Atmospheric gravity waves can exist only when the atmosphere is stably stratified. It is generally believed that gravity waves are the main cause of wind and temperature fluctuations with periods of a few hours and less, down to a few minutes. The waves have the curious property that the phase velocity and group velocity are almost proportional to each other and when group velocity is upward, the phase velocity is downward. Gravity wave appears to be the most important means of dynamical coupling between the middle atmosphere and the thermosphere. Their sources are in troposphere. They grow in amplitude as they propagate upwards into higher regions of the atmosphere (Figure -3.1). In the absence of any dissipation, the wave amplitude grows with altitudes as the wave propagates into the higher regions of the atmosphere. However, as the

wave approaches the critical level (where its phase velocity is equal to the background wind velocity) or when the wave amplitude grows sufficiently to cause turbulence the wave looses its energy. As the amplitude grows, the waves become unstable and saturation and wave breaking occur (Fritts, 1984). There exist basically three theoretical treatments of the wave saturation, which can be categorized as linear and non –linear. The simplest theory, developed conceptually, of gravity wave saturation and breaking is the linear saturation theory developed by Lindzen (1981). The basic premise of the linear theory is that convectively unstable regions appearing within the wave field result in generation of turbulence and just that level of eddy diffusion necessary to restrain wave amplitudes to values near natural stability. The other two involves non-linear interaction among the components of the gravity wave spectrum. One of these theories invokes wave-wave interactions at the small scale end of the gravity wave spectrum to produce non-linear diffusion of the energy from the longer scale waves (Weinstock, 1990). The other theory by Hines (1991) employs non-linear Doppler spreading of medium scale waves into the small scale end of the spectrum by the winds of the longer scale waves coupled with dissipation at the smallest scale of the spectrum. Van Zandt (1982) proposed that the spectral distribution of gravity wave energies is not a strong function of latitude, longitude or time of the year but, in fact is almost invariant. Figure 3.2a shows typical experimental gravity wave spectra. The long wave number part of the spectra is the saturated spectrum whereas the short wave number region is the unsaturated one. However, the transition from unsaturated to saturated part changes with increasing altitude with this transition shifting to shorter wave numbers with increasing altitude. Recent studies (Wilson et al, 1991; Rajeev et al,2002) have shown departures of the observed saturated gravity wave spectra from the m^{-3} dependence which is attributed to processes other than convective instabilities (e.g, non-linear interactions) being active in the saturation process.

A major consequence of gravity wave saturation in the mesosphere, which has implications to the thermosphere, is the generation of turbulence. It was mentioned above that gravity wave saturation occurs as they propagate through

the middle atmosphere resulting in turbulence. The generated turbulence is expected to be intermittent both in time and space depending on the characteristics of the causative gravity waves. The eddy diffusion coefficient depends upon the strength of the turbulence generated. From the linear theory Lindzen (1981) showed that the eddy diffusion coefficient in the upper mesosphere and lower thermosphere could be drastically different in summer and winter.

3.2 Generation of gravity waves

The proposed mechanisms of gravity wave generation generally fall into two categories namely, mountain waves and waves due to unstable wind shears. Mountain waves are forced by flow over mountains and are associated with phase speeds close to zero. However, the phase speed need not be zero when the flows are unsteady.

Windshear, tropospheric convection and frontal systems are considered to be major sources of gravity waves (e.g., Nastrom and Fritts, 1992). Unstable vertical shears of horizontal winds can excite gravity waves. The excitation mechanism appears to be inherently non-linear (Fritts, 1982., 1984). The gravity wave due to shear excitation is constrained to have phase speeds comparable to the mean flow velocities. The tropical troposphere in the south and southeast Asian region exhibits a strong easterly jet just below the tropopause at ~10^{o} N latitude in the south west monsoon season. The altitude region of the jet could be unstable due to wind shears and can act as a source of gravity waves. The MST radar data at Gadanki (13.5^{o} N ,79.2^{o} E) indeed shows strong vertical shears of ~0.03m/s in general in the jet region and large day to day variability (Krishna Murthy,1998). This potential source of gravity waves has a strong longitudinal and seasonal variability. It is extremely important to investigate this source both in its ability to generate gravity waves and in the effects of the gravity waves generated on thermospheric phenomena such a equatorial spread F and equatorial ionization anomaly. Yamanaka et al (1989) from the MU radar observation in Japan reported upward wave emission from the troposphere jet

stream. Sasi et al (2000) from MST radar observation at Gadanki reported Inertia Gravity wave generation associated with the easterly jet.

Another important source of gravity wave generation is convection in the troposphere (Fritts and Nastrom 1992). Two mechanisms have been considered for gravity wave excitation by convection. In the first mechanism (thermal forcing) oscillating updrafts and downdrafts impinging on the interface between the unstable and stable regions cause oscillatory displacements of the isentropes at the base of the stable layer leading to excitation of vertically propagating gravity waves. The second mechanism envisages gravity wave generation by a rising convective element acting as an obstruction to the ambient horizontal flow. Similar effect can also occur in the case of convective downdraft. Convectively generated gravity waves are expected to scales representative of the underlying convection, to respond episodically to strong local forcing and to have a broad range of phase speeds. Thus the convective source could be an important source for gravity wave generation. This source is also highly longitude dependent. Tropical convection is quite frequent especially in the monsoon and pre-monsoon seasons in the south and Southeast Asian regions. In this chapter we study the salient features of gravity wave activity in the troposphere and lower stratosphere of a low latitude station using wind data obtained by MST Radar at Gadanki.

3.3 Theoretical Treatment of Atmospheric Gravity waves.

Considering a plane wave in a vertical plane oriented in the azimuthal direction x in the horizontal plane.

The equations of motion of the wave perturbation are

$$\rho_0 \frac{\partial u_x}{\partial t} = -\frac{\partial p_1}{\partial x} \tag{3.1}$$

$$\rho_0 \frac{\partial u_z}{\partial t} = -\frac{\partial p_1}{\partial z} - \rho_1 g \tag{3.2}$$

The thermodynamic energy equation can written as

$$\frac{\partial p_1}{\partial t} = c^2 \left[\frac{\partial p_1}{\partial t} + u_2 \frac{\partial \rho_0}{\partial z} \right] - u_z \frac{\partial p_0}{\partial z} \tag{3.3}$$

The continuity equation is

$$\frac{\partial \rho_1}{\partial t} + u_z \frac{\partial \rho_0}{\partial z} + \rho_0 \left[\frac{\partial u_x}{\partial x} + \frac{\partial u_z}{\partial z} \right] = 0 \tag{3.4}$$

The above equations are used together with the auxiliary equations of hydrostatic balance;

$$-\frac{\partial p_0}{\rho z} = \rho_0 g \text{ ; so that } \quad p_0, \rho_0 \alpha \exp(-Z/H)$$

$$\frac{\partial p_1}{\partial t} = c^2 \gamma \frac{p_0}{\rho_0}; \quad c^2 = \frac{\gamma_0}{H}; \quad H = \frac{KT}{mg} = \frac{c^2}{\gamma g}$$

It is assumed that wave perturbations are small and sinusoidal so that they can be treated as liner additions to background values neglecting non-linear terms. They can be represented by

$$\frac{\frac{p_1}{p_0}}{P} = \frac{\frac{\rho_1}{\rho_0}}{R} = \frac{u_x}{X} = \frac{u_z}{Z} = A \exp i\{\omega t - K_x X - K_z Z\} = \Phi$$

K_x K_z are complex horizontal and vertical wave numbers respectively. ω is real angular frequency of the wave and A is arbitrary constant of wave amplitude. P, R, X and Z are parameters which involve parameters of the wave and the medium of propagation.

Further,

$$\frac{\partial}{\partial t} = i\omega; \quad \frac{\partial}{\partial x} = -iK_x \qquad \frac{\partial}{\partial z} = -iK_z$$

Substituting these in equation (3.1) to (3.4)

$$\rho_0 X i\omega\phi = p_0 P i K_x \phi$$

$$\rho_0 Z i\omega\phi = \left\{ -g_0\rho_0 R + p_0 P i K_z - P\frac{d\rho_0}{dz} \right\}\phi$$

$$p_0 P i\omega\phi + Z\phi\left\{ \frac{dp_0}{dz} - c^2\frac{d\rho_0}{dz} \right\} = c^2\rho_0 R i\omega\phi$$

$$\rho_0 R i\omega\phi + Z\phi\frac{d\rho_0}{dz} - \rho_0\phi i K_x X - \rho_0\phi K_z Z = 0$$

Canceling φ and dividing by ρo these can be written in terms of the unknowns P,R ,X and Z. if we consider horizon

$$\frac{pc^2}{r}K_x + o\cdot R - \omega\cdot X + o\cdot Z = 0$$

$$P\left[\frac{c^2}{\gamma} iK_z + g\right] - gR + o\cdot X + \frac{\gamma-1}{H}\cdot Z = 0$$

$$pi\omega - ri\omega R + o\cdot X + \frac{\gamma-1}{H}\cdot Z = 0$$

$$o.p - i\omega R + iK_x X + (iK_z + \frac{1}{H}) = 0$$

For the above equations to have a non-zero solution for P,R,X and Z the determinant of coefficients must be 0 , i.e

$$\begin{vmatrix} c^2K_x & 0 & -i\omega & 0 \\ (\frac{c^2 iK_z}{\gamma} + g) & -g & 0 & -i\omega \\ i\omega & -ri\omega & 0 & \frac{\gamma-1}{H} \\ 0 & i\omega & iK_x & (\frac{1}{H} + iK_Z \end{vmatrix} = 0$$

Expanding the determinant leads to the wave **dispersion equation**

$$\omega^4 - \omega^2 c^2 (K_x^{\ 2} + K_z^{\ 2})(\gamma - 1) g^2 K_x^{\ 2} + ig\omega^2 K_Z = 0 \qquad (3.5)$$

and the **polarization relations**

$$P = \gamma\omega^2 K_z - \frac{i\omega^2}{H} \qquad (3.6)$$

$$R = \omega^2 K_z + i(\gamma - 1) g K_x^{\ 2} - \frac{i\omega^2}{H} \qquad (3.7)$$

$$X = c^2 \omega K_x K_z - i\omega g K_x \qquad (3.8)$$

$$Z = \omega^3 - \omega c^2 K_x^{\ 2} = \omega(\omega^2 - c^2 K_x^{\ 2}) \qquad (3.9)$$

Equations (3.6)-(3.9) show that the relative magnitudes and phases of perturbations in density, pressure and wind velocities are related to each other in a specified way. The temperature perturbations are related to p_1 *and* $E\rho_1$ by the perfect gas law

$$\frac{p_1}{p_0} = \frac{\rho_1}{\rho_0} + \frac{T_1}{T_0}$$

The dispersion equation (3.5) does not have solutions with both K_x and K_z real and finite. If we consider horizontal propagation without dissipation then K_x and K_z real and finite.

If we consider horizontal propagation without dissipation then K_x is real. Equation (3.5) has two solutions

(i) K_z is purely imaginary

(ii) K_z is real

$$K_z = K_z + \frac{ir\gamma g}{2c^2} = K_z + \frac{i}{2H} \qquad (3.10)$$

When K_z *is* purely imaginary, no vertical propagation can take place from the source. Therefore, only a surface (evanescent) wave can propagate horizontally (external). Internal waves are waves propagating in vertical direction corresponding to condition (ii).

When (3.10) is substituted in (3.6), it is seen that the wave perturbation has a growth factor $e^{\frac{z}{2H}}$ with altitude arising from the imaginary part of K_z .This is due to decrease in ρ with z; as $\rho = \rho_0 e^{-\frac{z}{H}}$

In the absence of dissipation, the K E density associated with wave perturbation is preserved as the wave propagates upwards, $\frac{1}{2}\rho U^2 = const.$,

Hence

$$U\alpha \frac{1}{\sqrt{\rho}} \alpha e^{\frac{z}{2H}}$$

This is a characteristic of all internal waves like tides, planetary waves, etc. it is convenient to separate out the imaginary part $\frac{i}{2H}$ from the real part K_z in equations (3.5) to (3.9) by representing

$$\frac{\frac{p_1}{p}}{p} = \frac{\frac{\rho_1}{p}}{p} = \frac{u_x}{x} = \frac{u_z}{z} = Ae^{\frac{z}{2H}} \exp i\{\omega t - K_z x - K_z z\} \qquad (3.11)$$

$$\omega^4 - \omega^2 c^2 (K_x^{\ 2} + K_z^{\ 2}) + (\gamma - 1) g^2 K_x^{\ 2} - \frac{\gamma^2 g^2 \omega^2}{4c^2} = 0$$

and

$$P = r\omega^2 \left[K_x - i(1 - \frac{\gamma}{2}) \frac{g}{c^2} \right]$$

$$R = \omega^2 K_z + i(\gamma - 1) g K_x^{\ 2} - i\gamma g \omega^2 / 2c^2$$

$$X = \omega K_x c^2 \left[JK_z - i(1 - \frac{\gamma}{2}) \frac{g}{c^2} \right]$$

$$Z = \omega \left[\omega^2 - K_z^{\ 2} c^2 \right]$$

Equation(3.11) reveals that any pair of real wave numbers(K_x, K_z) can be associated with either of two distinct values of ω^2 and so with either of two values of ω if attention is confined to values (positive roots . One of these ω is greater than $\omega_\alpha = \frac{\gamma g}{2c}$ and the other is less than $\omega_g = (\gamma-1)^{1/2} g/c$. Also $\omega_a > \omega_g$ (γ less than 2). Therefore, two distinct sequences of internal waves can occur, the one at high frequency ($\omega > \omega_a$) and the other at low frequencies ($\omega < \omega_g$) and that a gap in the frequency spectrum exists $\omega_g \leq \omega \leq \omega_a$ in which no internal waves can propagate. It indicates in figure 3.2b **The two sequences will be termed as acoustic waves and internal gravity waves respectively**. The energy of the acoustic waves propagates in much the same direction as does the phase pattern. **The energy of the internal gravity waves may propagate in directions radically different from the corresponding phase normal, by as much as 90^0 and for longer periods the flow tends to be horizontal. For IGWs , the vertical component of the energy flow is opposite to that of the phase propagation.**

Equation (3.11) can be written as

$$\frac{\omega^2 - \omega_\alpha^{\,2}}{c^2} - \omega^2(K_x^{\,2} + K_z^{\,2}) + \omega_g^{\,2} K_z^{\,2} = 0$$

$$\omega^2 = \frac{c^2}{(K_x^{\,2} + K_z^{\,2})}$$

The corresponding waves are not free from gravity ; the exponential amplitude factor applies. Under asymptotic conditions; simplified relations for IGWs can be obtained when $K_z^{\,2} >> \frac{\omega_\alpha^{\,2}}{c^2}$

At low frequencies

$$\omega^2 K_z^{\,2} \approx \omega_g^{\,2} K_x^{\,2}$$

$$\frac{Z}{X} \approx \frac{-K_z}{K_x}$$

$$\frac{R}{X} = \frac{i(\gamma-1)^{1/2}}{c}$$

3.4 Experimental set-up, Observations & Method of Data Analysis

The Indian MST Radar offers an excellent opportunity for the study of the dynamics of the tropical middle atmosphere, by virtue of its unique location. It is highly sensitive phased array Doppler VHF radar operating at 53 MHz with an average power aperture product of 7 X 10 ^{8} Wm^2. The peak transmitted power is 2.5 MW.It is fed to the 32 × 32 Yagi antenna array, generating a radiation pattern with a one way beam width of 3^o with a gain of 36 db and a side lobe level of -20 dB. Details of Indian MST radar system can be found in **Rao et al. (1995).** The radar antenna beam was pointed toward six present directions viz. east, west north, south inclined at an angle of 10^o from the zenith and along two vertical beams, one is the east-west polarization and the other in the north-south polarization.

MST radar observations have been taken for a number of days during the during the monsoon (August 2001, 2002 and 2003) , autumn equinox (October - November 2004), winter (December 2004; January–February 2005) Vernal equinox (April 2005) seasons. The schedule and details of the experiments conducted in all the campaigns are given in **Table 3.1**

Table 3.1

Date of Experiment	Time & Height Resolution	Duration of Experiment
16, 17 ,20, 21, 23 August 2001	4 min 150 m	21:30 to 01:30 hrs
5 - 9 August 2002	4 min 150 m	2130 to 01:30 hrs
12–14 and 18 – 19 August 2003	4 min 150 m	10:00 to16: 00 hrs
18 - 21 October 2004	4 min 150 m	19:00 to 01:00 hrs
11 ,13,15 November 2004	4 min 150 m	19:00 to 01:00 hrs
20 – 24 December 2004	4 min 150 m	19:00 to 01:00hrs
21, 22, 23 January 2005	4 min 150 m	19:00 to 01:00hrs
16 - 20 February2005	4 min 150 m	21:30 to 01:30 hrs
21- 23 April 2005	4 min 150 m	21:30 to 01:30 hrs

For these observations the following radar configuration was used: Pulse Repetition Frequency = 1000 Hz. Pulse Width = 16 μs, No. of coherent integrations = 64, No. of FFT points = 512, No. of beams =6 (oblique beams 10^0).

The Doppler spectra obtained as output were subjected to moments analysis. The first moments give the Doppler shift (v_d) and it represents a line-of-sight velocity which is the projection of the velocity vector in the radial direction. The 'Doppler Beam Swing (DBS), method is used here to determine the three component v_x, v_y, v_z of the wind vector from the v_d profiles.

The line-of-sight component of the wind velocity vector V= (v_x , v_y, v_z) at a given height is expressed as

$$v_d = V.i = (v_x\cos\theta_x, + v_y\cos\theta_y + v_z\cos\theta_z) \quad (3.12)$$

where, i is a unit vector along the antenna beam direction and θ_x , θ_y , θ_y are the angles between i and the x, y, and z axes, respectively.

$$V = \begin{bmatrix} \cos\theta_{x1} & \cos\theta_{y1} & \cos\theta_{z1} \\ \cos\theta_{x2} & \cos\theta_{y2} & \cos\theta_{z2} \\ \cos\theta_{x3} & \cos\theta_{y3} & \cos\theta_{z3} \end{bmatrix}^{-1} \begin{bmatrix} v_{d1} \\ v_{d2} \\ v_{d3} \end{bmatrix} \quad (3.13)$$

If we observe more than three directions, as is the present case, then the estimate of V can be made in a least squares, manner in which the residual given by the following can be minimized.

$$E_v^{\,2} = \sum_{i=1}^{m} (v_x \cos\theta_{xi} + v_y \cos\theta_{yi} + v_z \cos\theta_{zi} - v_{di})^2 \quad (3.14)$$

where m is the number of beam direction used

$$V = \begin{bmatrix} v_x \\ v_y \\ v_z \end{bmatrix} = \begin{bmatrix} \sum\cos^2\theta_{xi} & \sum\cos\theta_{xi}\cos\theta_{yi} & \sum\cos\theta_{xi}\cos\theta_{zi} \\ \sum\cos\theta_{yi}\cos\theta_{xi} & \sum\cos^2\theta_{yi} & \sum\cos\theta_{yi}\cos\theta_{zi} \\ \sum\cos\theta_{zi}\cos\theta_{xi} & \sum\cos\theta_{zi}\cos\theta_{yi} & \sum\cos^2\theta_{zi} \end{bmatrix}^{-1} x \begin{bmatrix} \sum v_{di}\cos\theta_{xi} \\ \sum v_{di}\cos\theta_{yi} \\ \sum v_{di}\cos\theta_{zi} \end{bmatrix} \quad (3.15)$$

where, the summations are taken for i=1 to 6. (Iyer et .al. 1994)

Time series of V_x, V_y and V_z thus obtained at height intervals of 150 m for duration of 4-6 hrs are subjected to a ten point moving average.

3.5 Results and Discussion:

(a) Back ground winds

For the period of the months (June- August), the presence of easterly jet is common over the Indian sub-continent (Asnani, 1993). The maximum wind in such jet stream normally occurs between 13 and 17 km that maximizes near tropopause. The magnitude of the wind speed associated with the jet stream is usually found to be of the order of about 40 m/s. To study the prevailing wind structure at different height regions during the period of observation, we plotted the altitude variation of mean wind in figure 3(a, b, c, d, e, f).

During the month of August (2001,2002,2003) the altitude variation of vertical wind field on sampled days viz. 16-17,20-21, 23 August 2001,6-9 August 2002 and 12-14 and 18-19 August 2003 has been plotted, respectively (Figure 3.3 a,b,c,d,e,f) . The mean zonal wind is mostly easterly all the days above the 10 km while it westerly below 10km.it lies between +20 m/s and -40 m/s. There is a tendency for reversal of wind direction in many of the profiles at about 8 km in both components. Below 10km the magnitude of the wind speed ~ 15 m/s and reverse above this altitude reaching a maximum value of ~40 m/s at a height of about 18 km .The meridional component is found more variable compared to the zonal component. It lies between mostly + 10 m/s and -10 m/s while the vertical component of the wind as a function of height lies between +0.5 m/s and -0.5 m/s.

The mean variation of zonal, meridional and vertical wind velocity with height for the different days during the months of October 2004 has been given in Figure 3.3(g,h). The mean zonal wind on all the four days of observation remains easterly. The meridional wind remains northerly up to around 10km altitude and above it is southerly. The mean vertical wind values vary between +0.5 to -0.5 all the days. Here we see the zonal wind velocity value is less compared to the August month. The magnitude of the zonal wind velocity is about 20 m/s and for the meridional wind it varies from -20 m/s to +20 m/s.

During the three days of observation for the month of the November 2004 low values of the mean zonal wind velocity are observed. It can be see in figure

3.3(i) that mostly the wind is easterly except on 11 November 2004 and the maximum value observed of the zonal wind velocity is -10 m/s. while in the case of meridional component it is mostly southerly. The magnitude of the meridional wind speed is about 12 m/s. The vertical wind velocity a between +0.5 to -0.5 all the days. Heare +ve sign indicates the upward direction and – ve sign indicates the down ward direction of vertical wind velocity.

For the period of the winter seasons (December, January and February) , the altitude variation of mean zonal, meridional, and vertical velocity on a number of days viz. 21-22, 24 December 2004 , 22-24 January 2005 and 17-20 February 2005 has been plotted, respectively (Figure 3.3 j,k,l) . The mean zonal wind is mostly westerly all the days. The magnitude of the wind velocity is about 20 m/s in January month and it has seen about 40 m/s in February month. The meridional component is found more variable compared to the zonal component. It's magnitude observed about 20 m/s and while the vertical component of the wind as a function of height very between +0.5 m/s and -0.5 m/s.

During the number of the days of observations for the month of the April 2005 the value of mean zonal wind velocity is about 30 m/s observed. It can be see in Figure 3.3 (m). Mostly it is seen westerly while in the case of meridional component it's fluctuates between northward and southward. The magnitude of the meridional wind speed is about +10 m/s and -10 m/s. The mean vertical wind pattern very between +0.3 to -0.3 all the days. On 21st April 2005 good wave like structure is observed in meridional component.

. During monsoon the zonal wind is significantly high, while meridional wind is low in comparison with any other seasons. It may be noted here that August is the month of south-west monsoon when the wind will be southwesterly and westerly with significant zonal wind and low meridional wind. It is suggested that the Inter-Tropical Convergence Zone (ITCZ) signature of easterly wind is suppressed by the strong eastward monsoonal winds giving rise to no clear reversal of zonal wind at lower levels due to passage ITCZ (Krishna Murthy et al. (2000)).

(b) Wind fluctuations: Gravity wave signatures

The wind field in the middle atmosphere can be decomposed into a continuum of spatial and temporal scales. Van Zandt (1985) stressed that a complete description of atmospheric fluctuations requires an analysis of the horizontal and vertical velocity verses frequency and horizontal and vertical wavenumber spectra and that both velocity should be measured simultaneously.

Time series of u, v and w are obtained at height intervals of 150 m from these wind profiles. The length of the time series in the present study is 4-6 hrs. A ten point moving height average is subtracted from the observed values of u, v and w to obtain the fluctuations u', v', w'.

Figure 3.4(a) shows Vertical profile of u',v',w' at different time on 17 August 2001. Good wave like structure is observed in zonal, meridional and vertical component. The range of the fluctuation is observed for zonal and meridional component +4 to -4 m/s respectively while for vertical component the range is observed between +0.5 to -0.5 m/s.

Good wave like structures have been observed in zonal component, meridional and vertical component on 8 August 2002 (Figure 3.4 b). The zonal component vary from mean position is +6 m/s to -6 m/s, meridional component vary form +4 to -4 m/s and vertical component +0.2 to -.2 m/s.

Figure 3.4(c) shows Vertical profile of u',v',w' at different time on 15 November 2004. Good wave like structure is observed in zonal, meridional and vertical component. The range of the fluctuation observed for zonal component is from +2 to -2 m/s for meridional component +6 to -6 m/s while for vertical component the range is observed between +0.2 to -0.2.

On 22 January 2005 good wave like structures have been observed in zonal component, meridional and vertical component. Figure 3.4(d) shows vertical profile of u', v', w' at different times. The range of the fluctuation is observed zonal component to be from +10 to -10 m/s, in meridional component +4 to -4 m/s and in vertical component the range is observed between +0.6 to -0.6 m/s.

Figure 3.4(e) shows Vertical profile of u', v', w' at different times on 17 February 2005. Good wave like structure is observed in zonal, meridional and vertical component. The range of the fluctuation is observed for zonal and meridional component +10 to -10 m/s respectively while in vertical component the range is observed between +0.4 to -0.4.

On 22 January 2005 good wave like structured has been observed in zonal component, meridional and vertical component. Figure 3.4(f) shows vertical profile of u', v', w' at different time. The range of the fluctuation is observed in zonal +6 to -6 m/s, in meridional component +4 to -4 m/s and in vertical component the range is observed between +1 to -1

some details of the wave like structure observed in the vertical profile in u',v', w' like range of periods, vertical wavelength height range over which they exist etc has to be give here and concluded that they represent gravity wave signature.

3.4 Conclusion:

Wind observation from MST Radar situated at Gadanki(13 ^{o} N) were used to study the behavior of mean winds .

Westerlies are found to prevail between December to April and easterlies between August to November. The trend is opposite in the lower troposphere. A strong easterly jet (~ 40 m/s^{-1}) is observed during monsoon (August) between 14 to 18 km. Meridional wind velocity ranges between +10 to -10 and is found to be predominantly northerly. Wave like structures have been observed on many occasions. These are attributed to Gravity wave signatures.

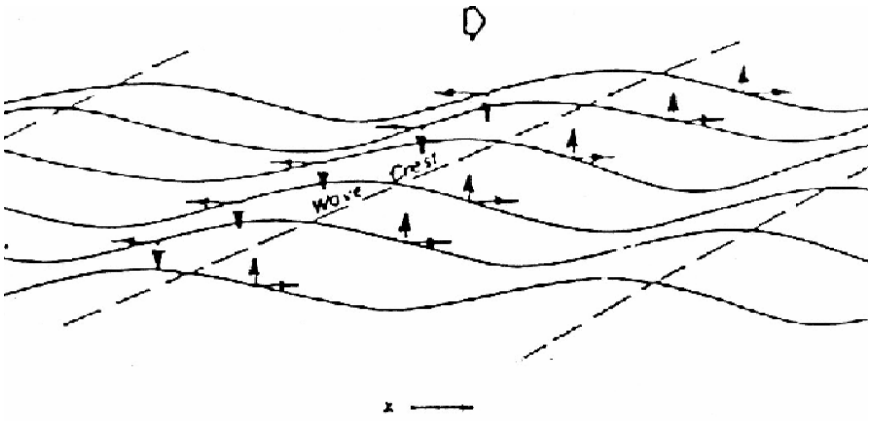

(Dunkerton, JAS,38 ,281-297,1981)

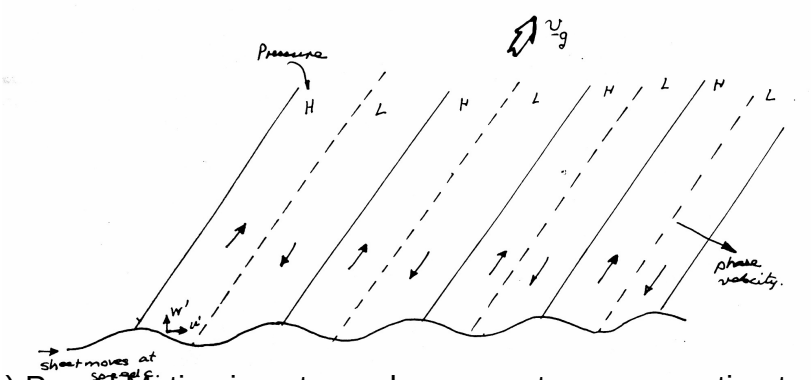

Figure 3.1(a) Parcel Motion in untapped wave system propagation to the right

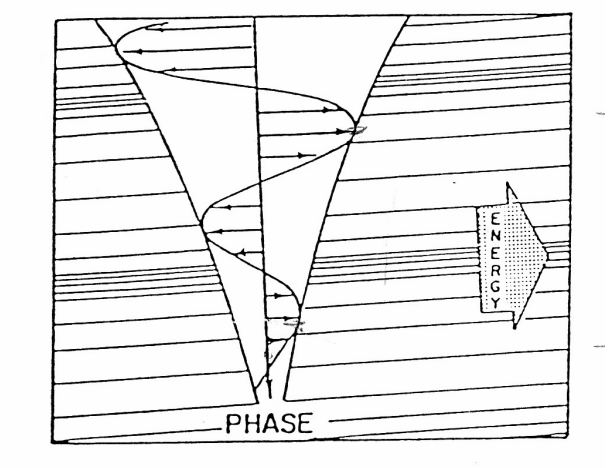

Figure 3.1(b) The wave grows exponentially with height

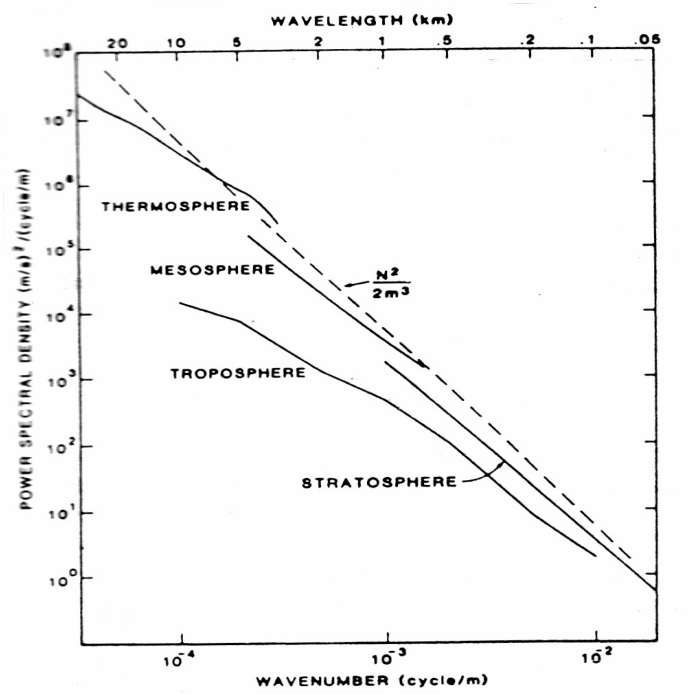

Figure 3.2a Typical experimental horizontal gravity wave spectra as a function of vertical wave number for four different altitude regimes. (Smith et al. 1987)

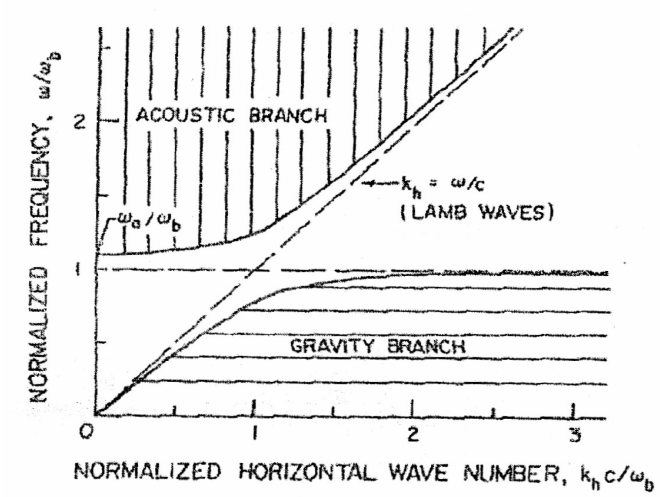

Figure 3.2 b Regions of propagation of the gravity branch and the acoustic branch in an isothermal atmosphere. The bounding curves are given by k_z=0.The regions corresponds to finite real k_z values are shown hatched.

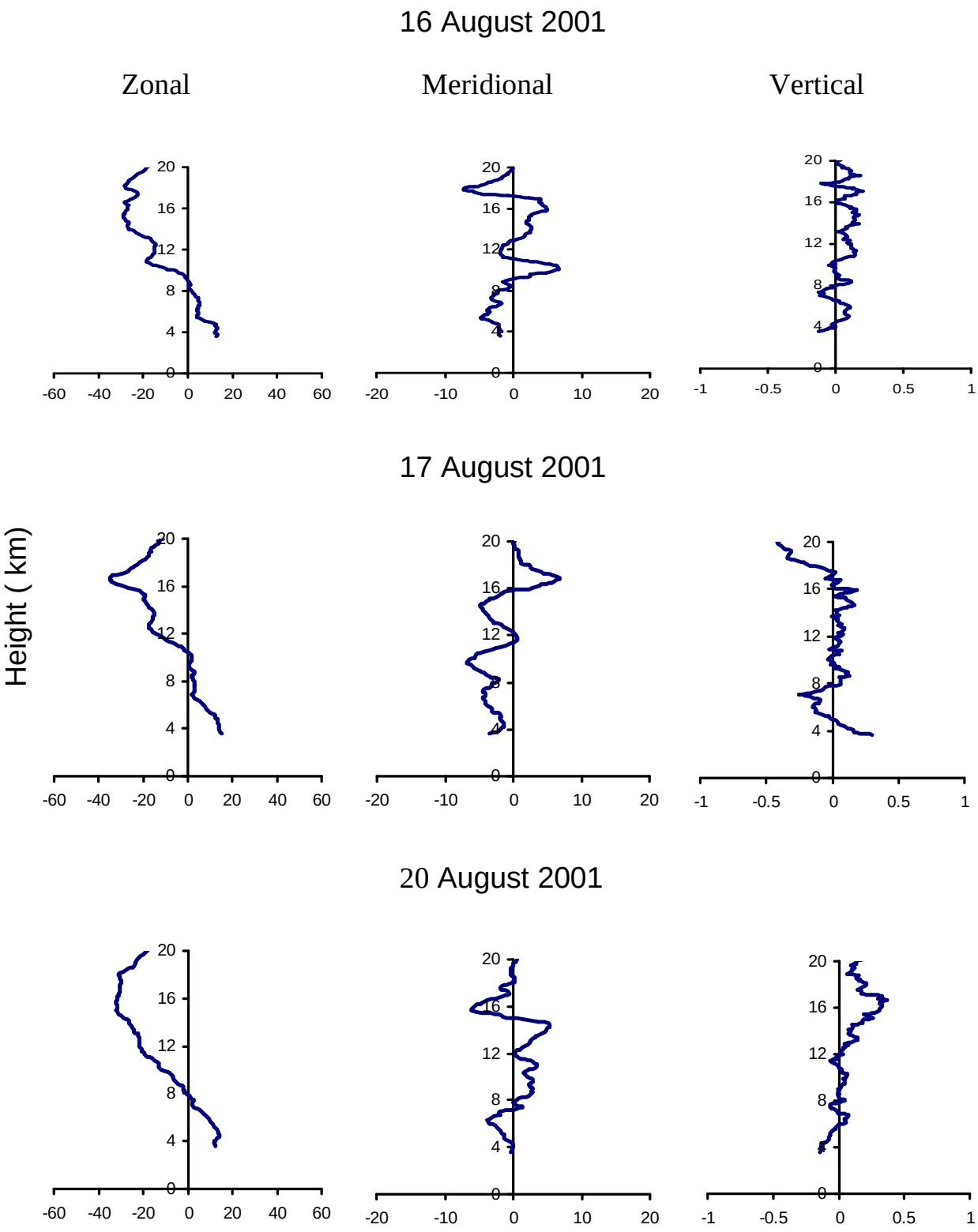

Figure -3.3 (a) Mean Vertical Profiles of U, V,W with height resolution of 150m after10 Points moving average in time of the time series with observation every 4 min spanning

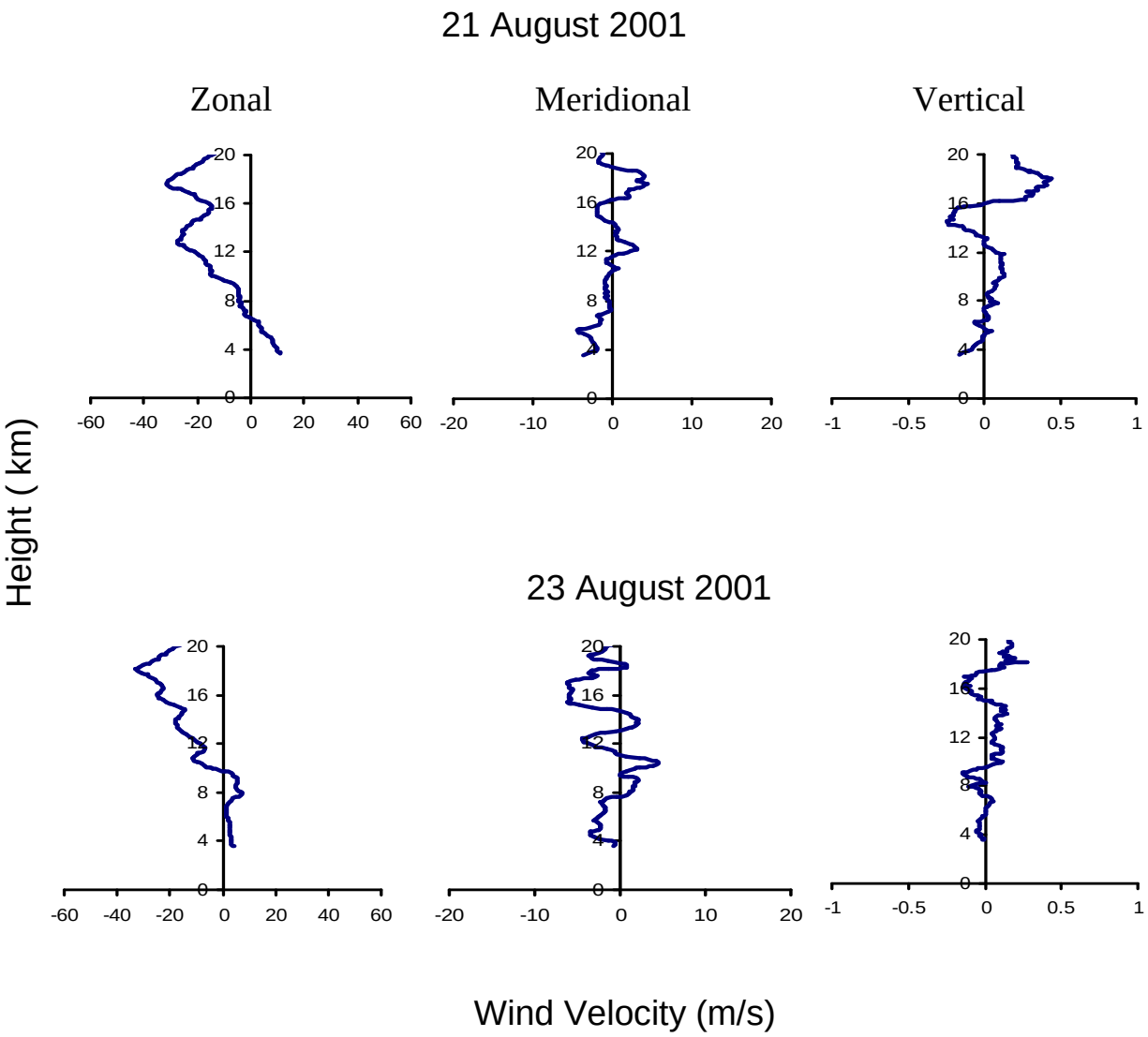

Figure -3.3 b same as Figure 3.3 (a) but for different days

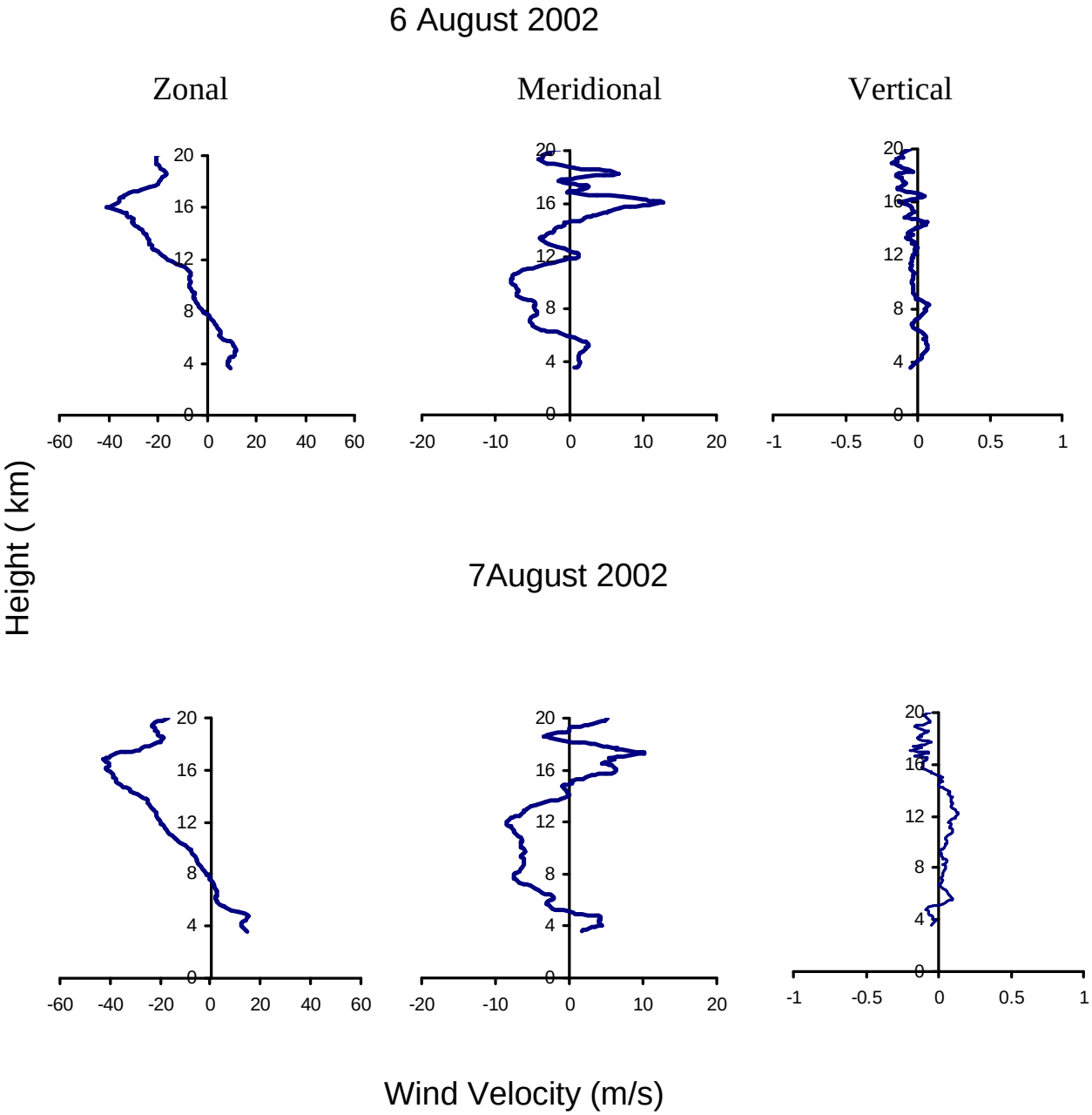

Figure -3.3 (c) same as Figure 3.3 (a) but for different days

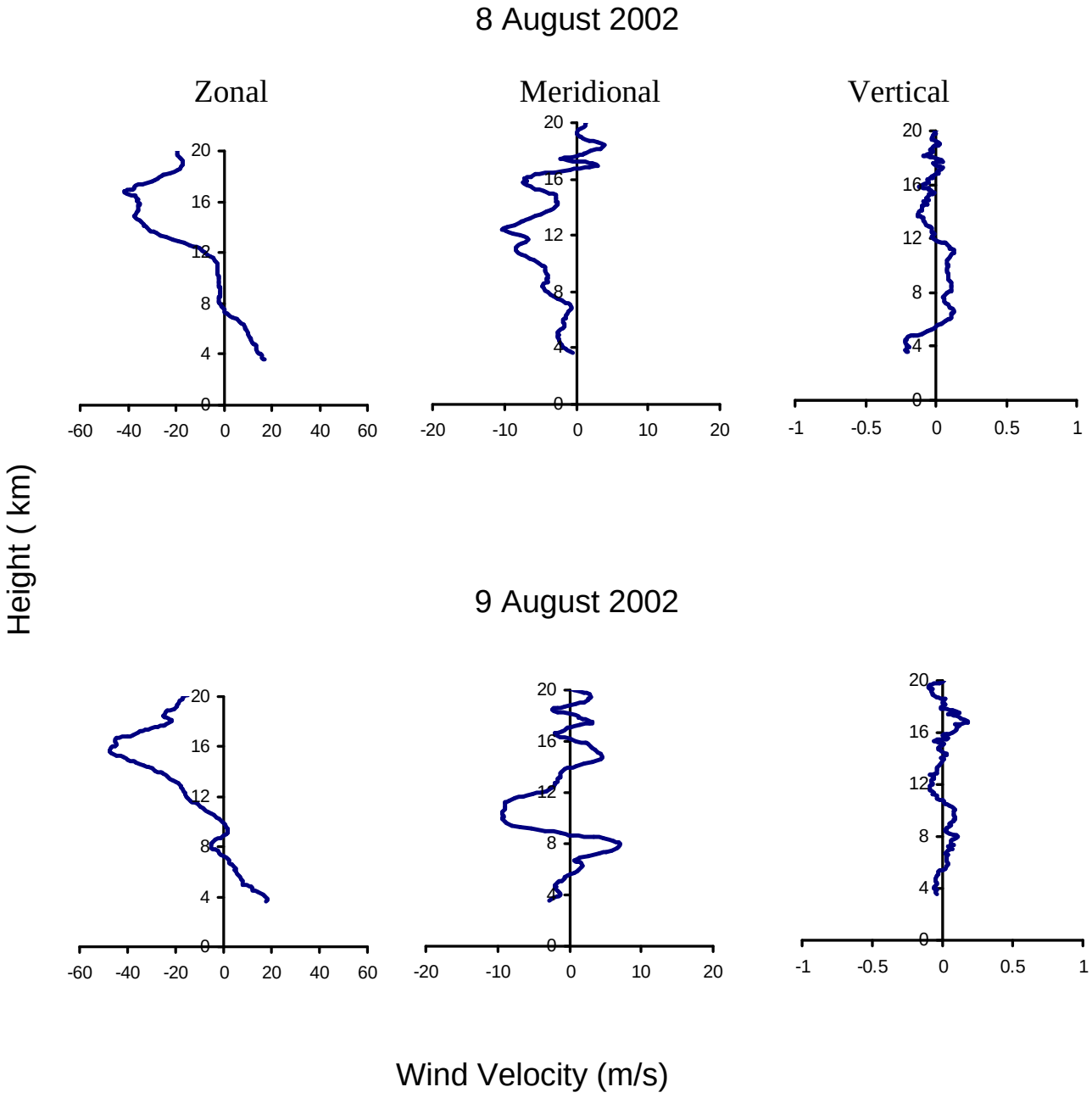

Figure -3.3 (d) same as Figure 3.3 (a) but for different days

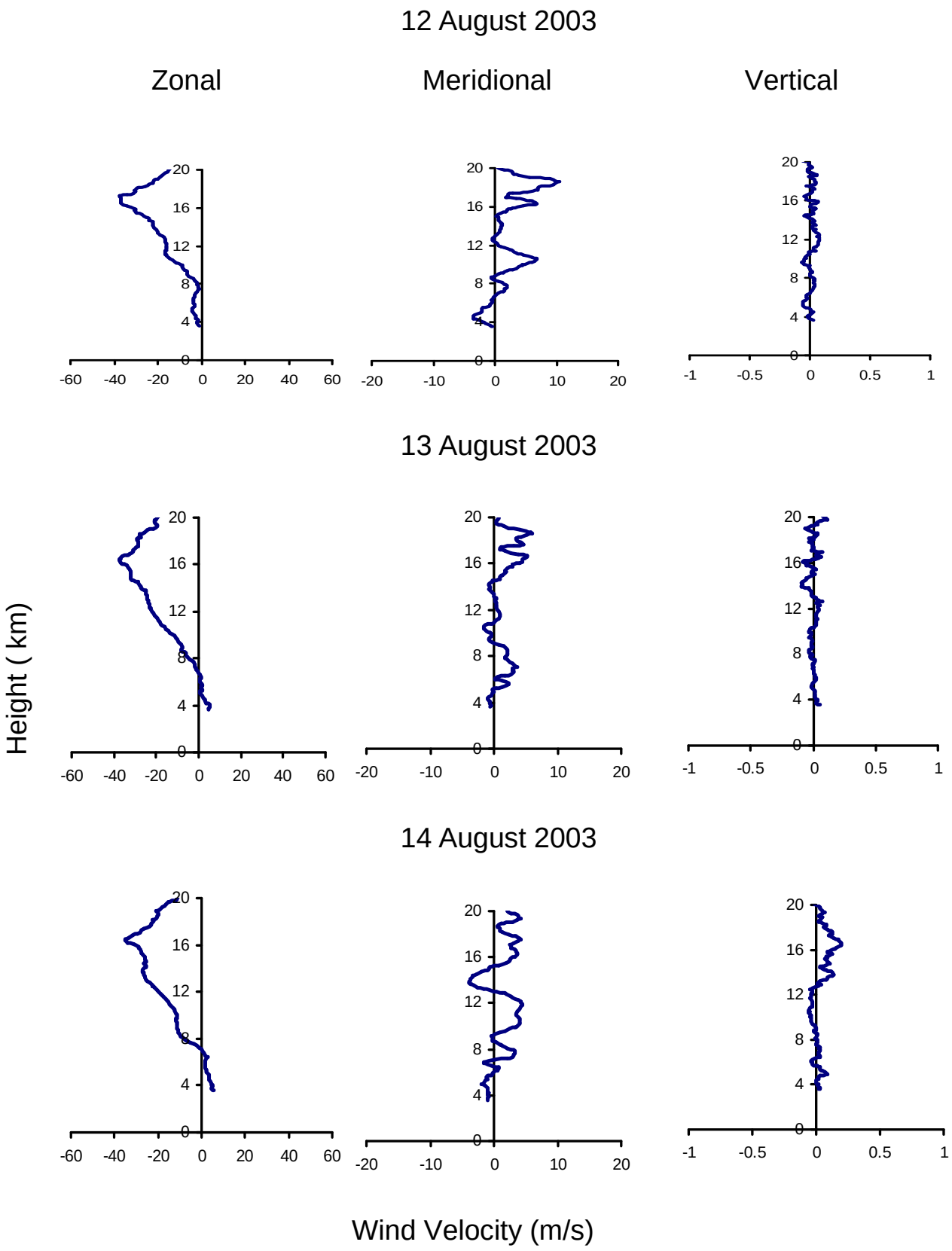

Figure -3.3 (e) same as Figure 3.3 (a) but for different days

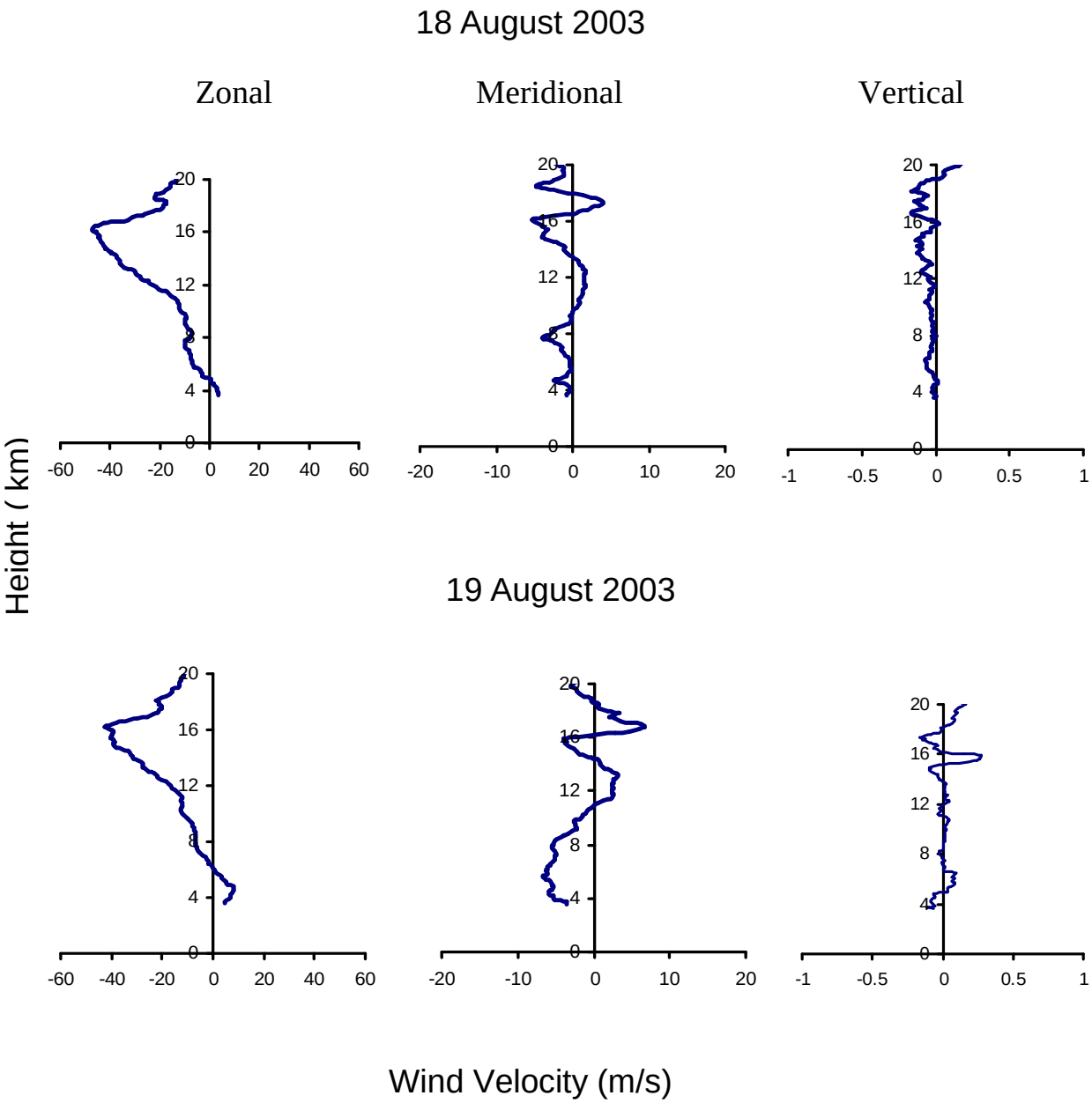

Figure -3.3 (f) same as Figure 3.3 (a) but for different days

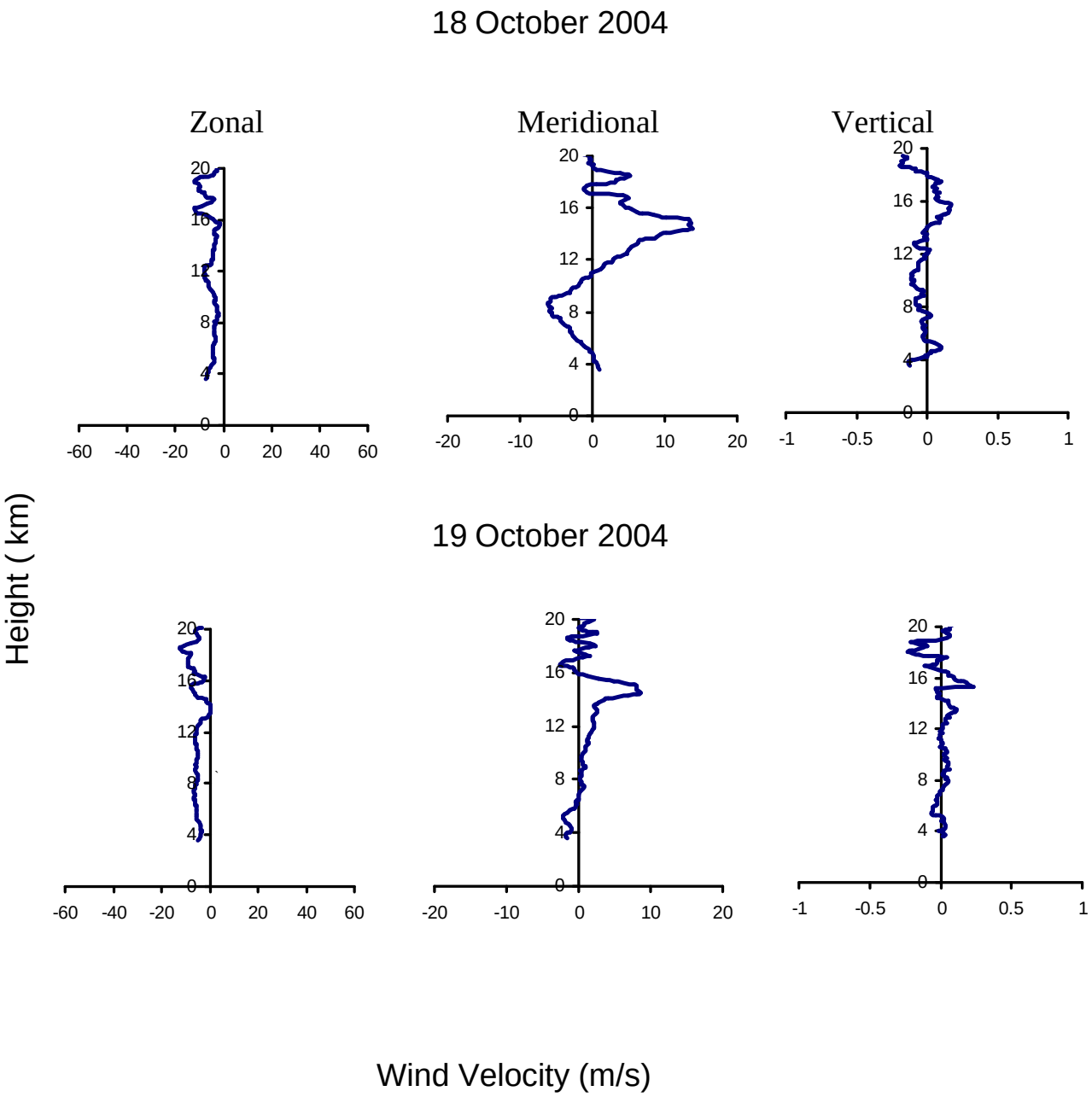

Figure -3.3 (g) same as Figure 3.3 (a) but for October month

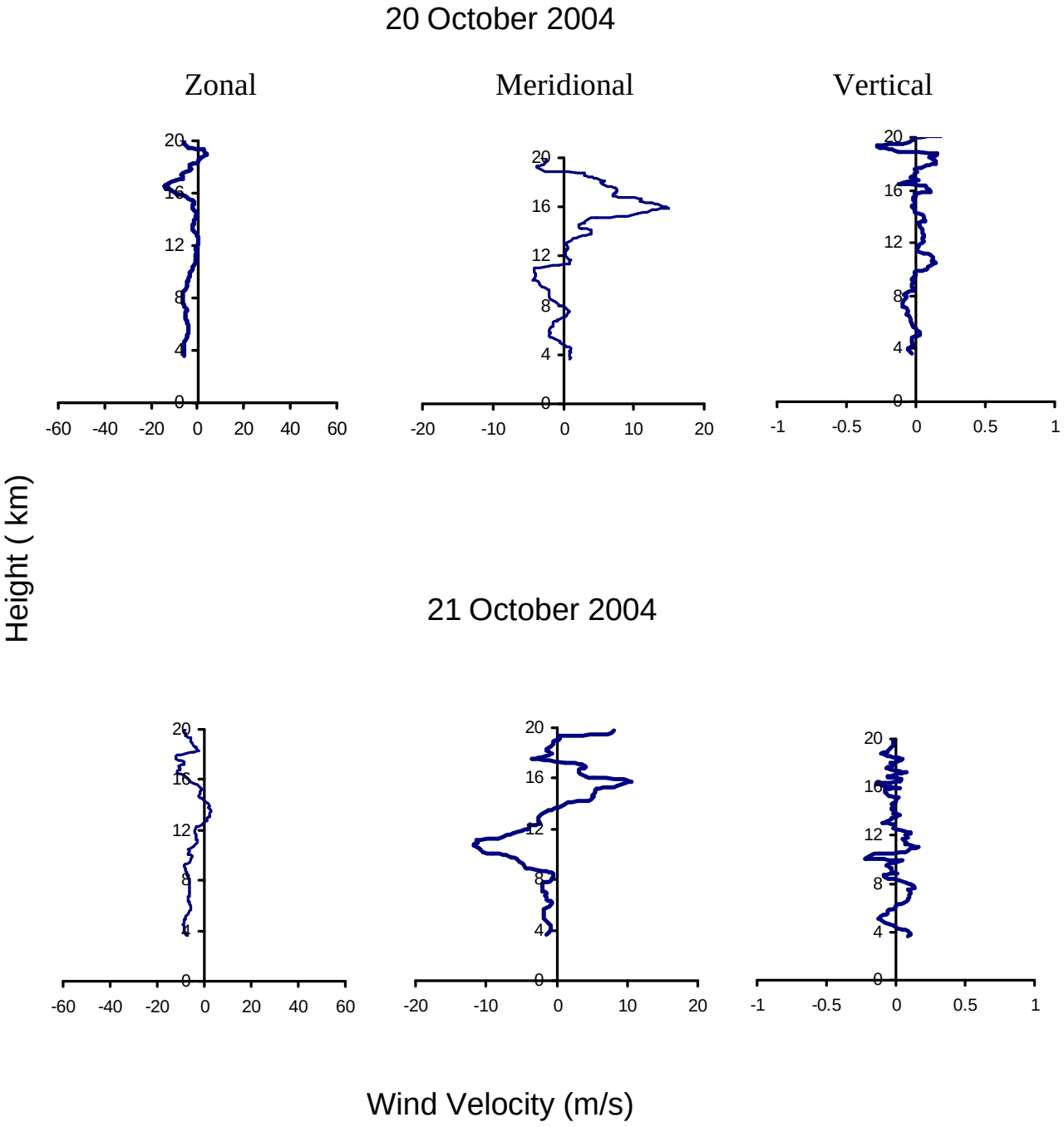

Figure -3.3 (h) same as Figure 3.3 (a) but for October month

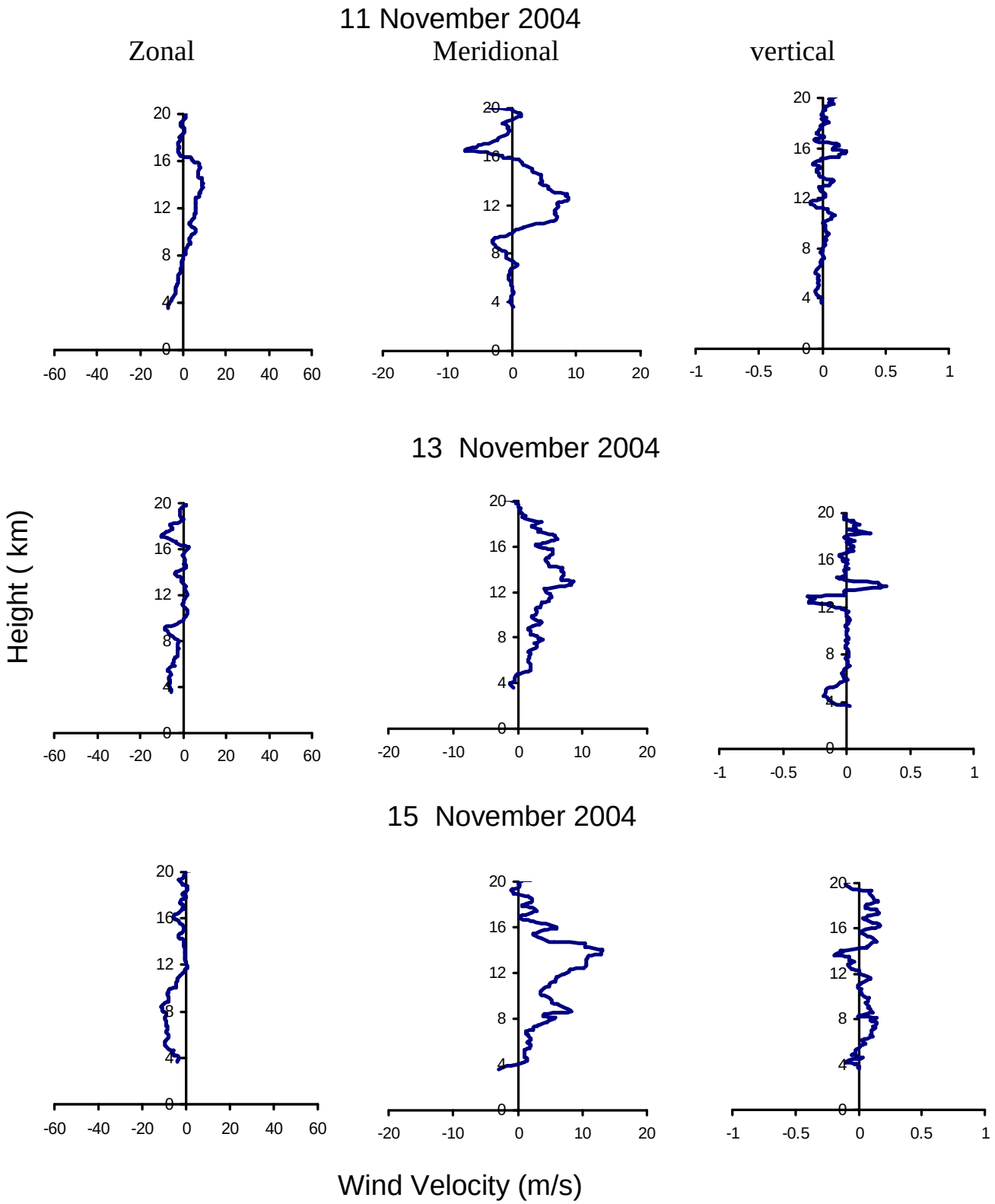

Figure -3.3 i same as Figure 3.3 (a) but for November month

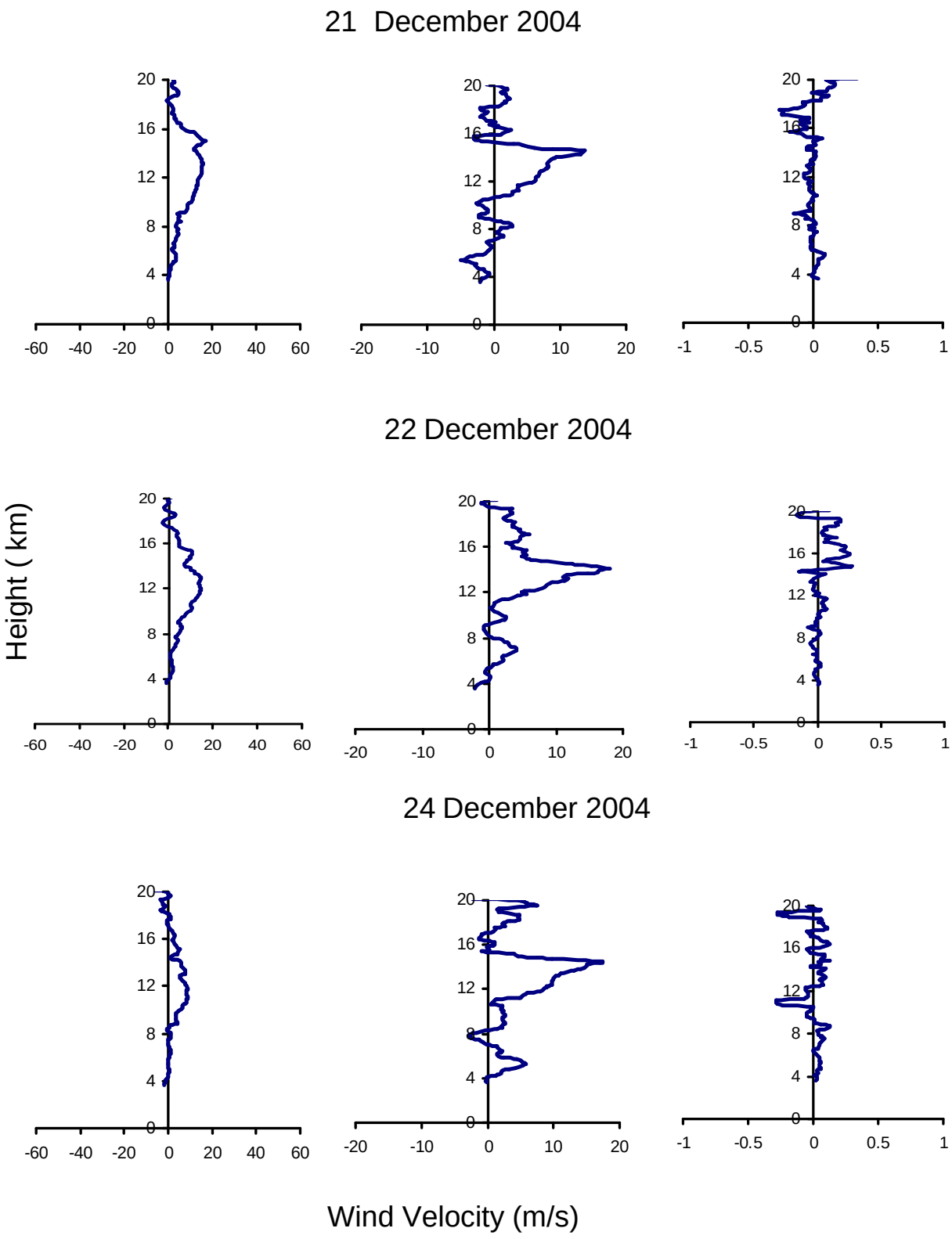

Figure -3.3 (j) same as Figure 3.3 (a) but for December month

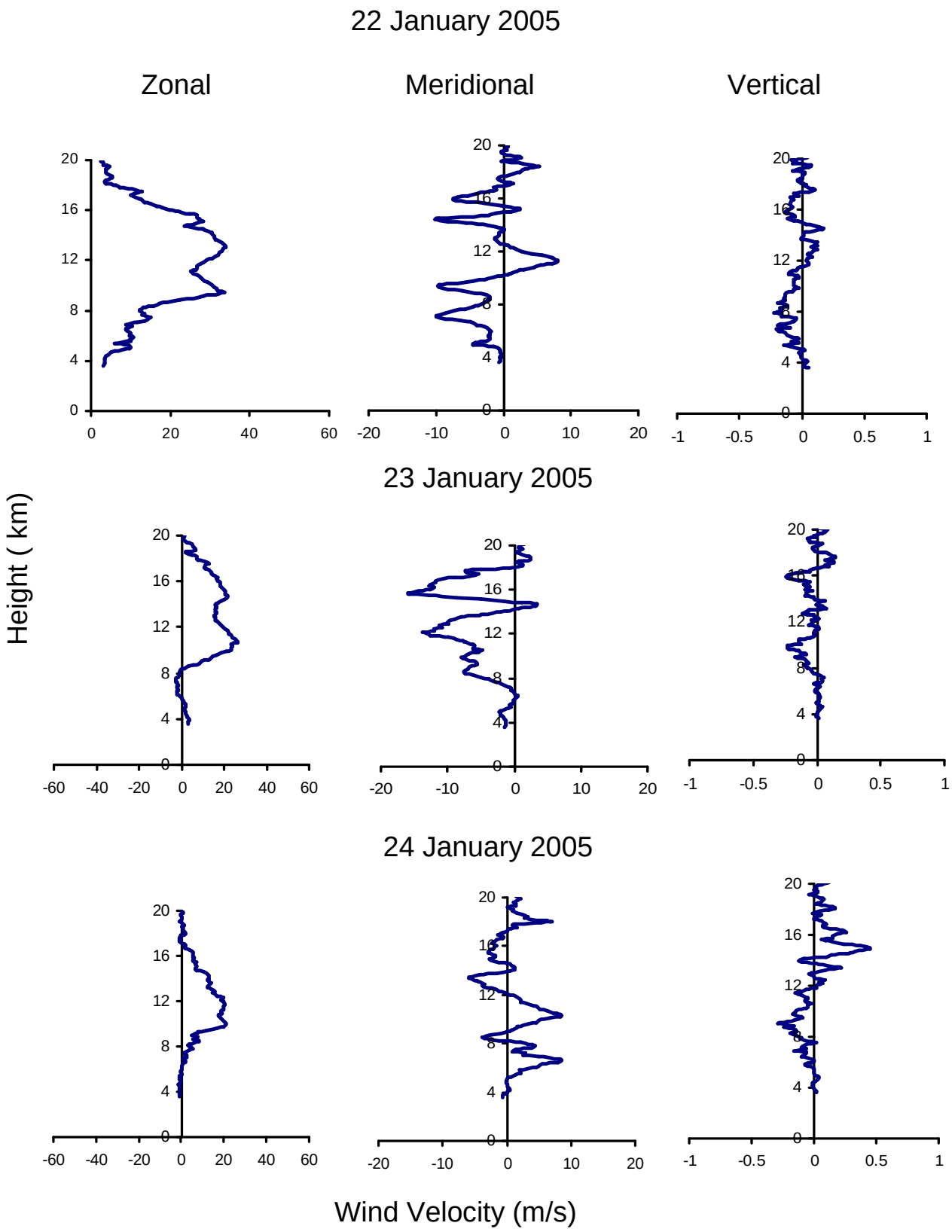

Figure -3.3 (k) same as Figure 3.3 (a) but for January month

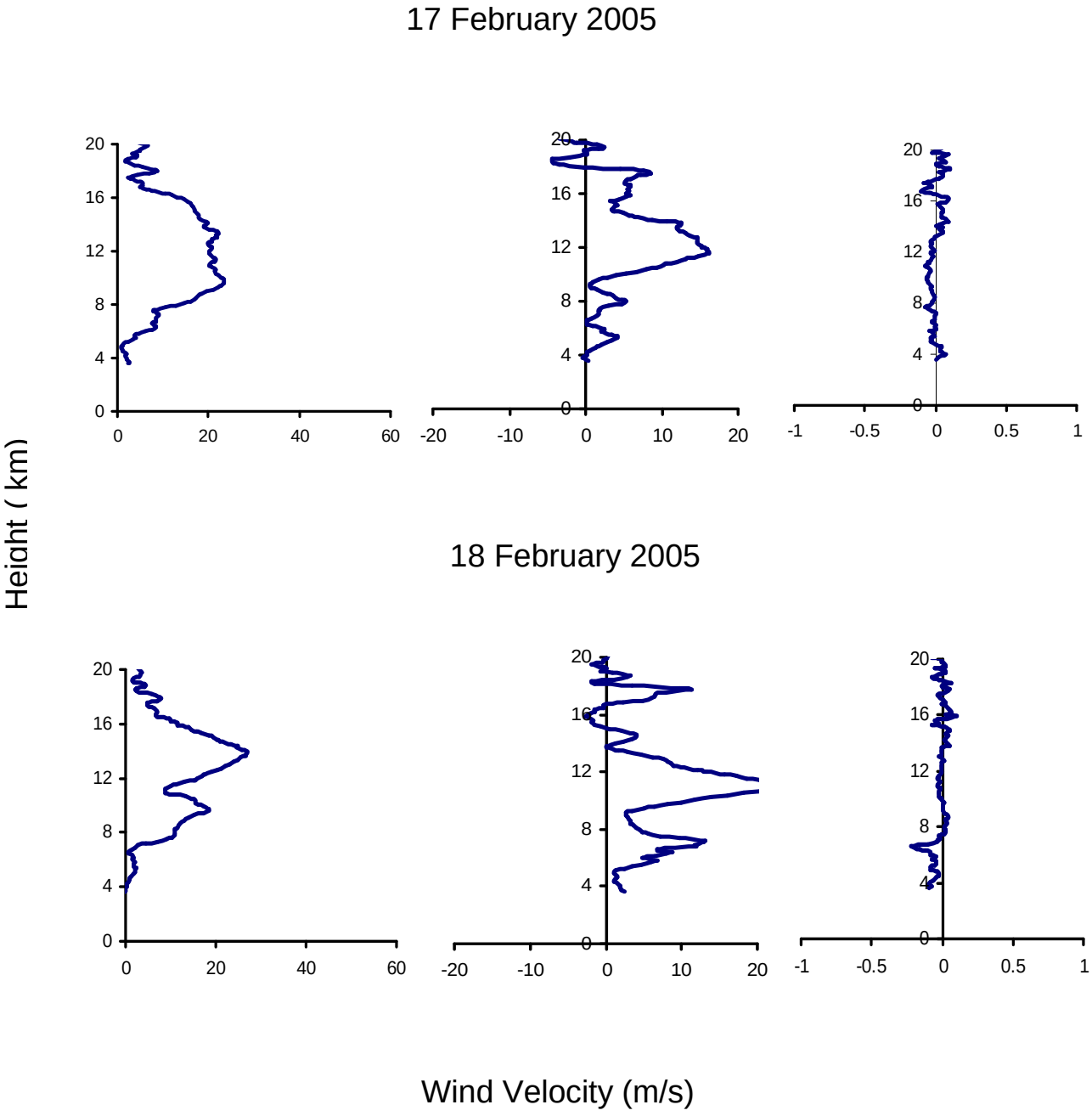

Figure -3.3(l) same as Figure 3.3 (a) but for February month

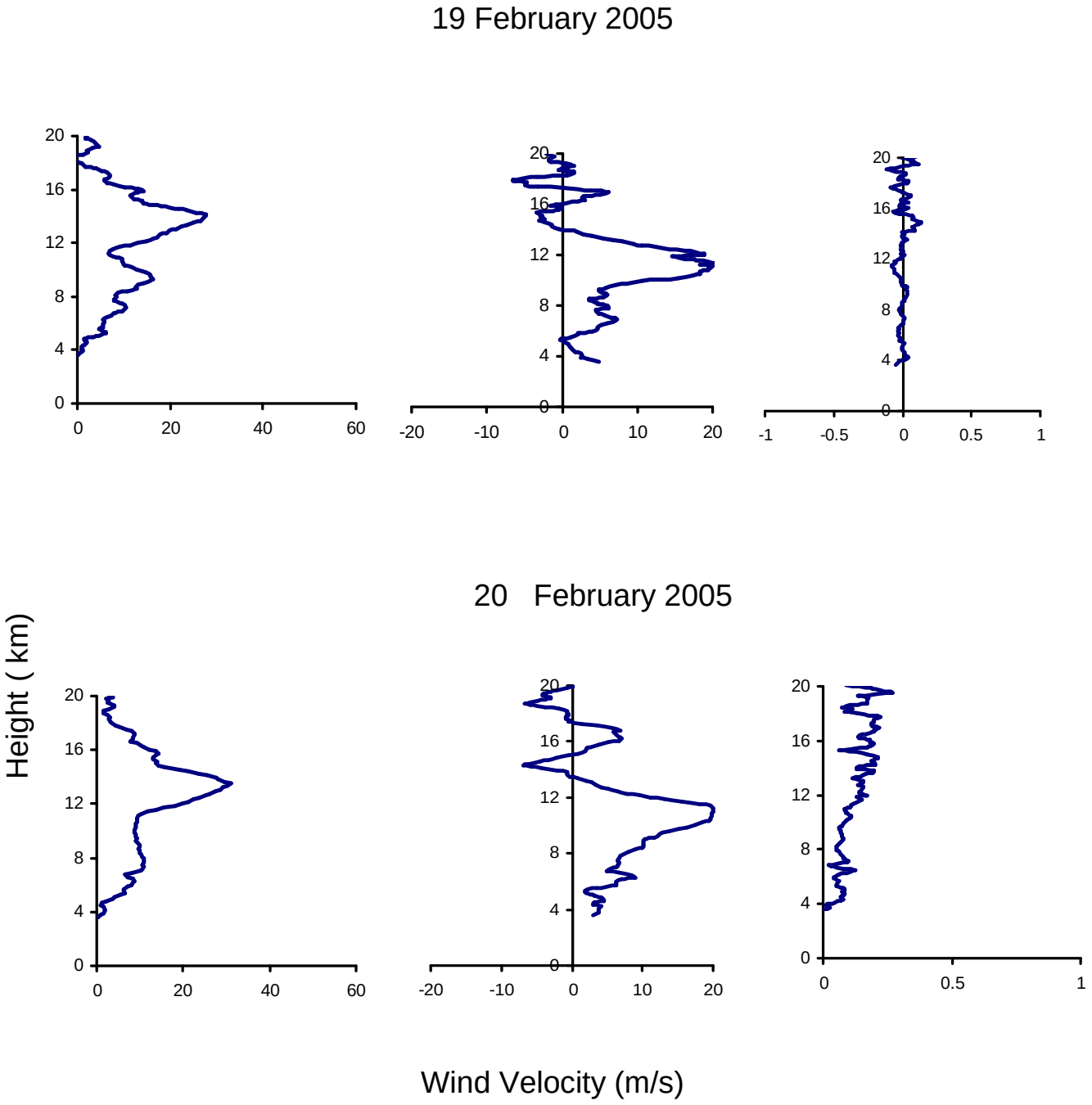

Figure -3.3 (m) same as Figure 3.3 (a) but for February month

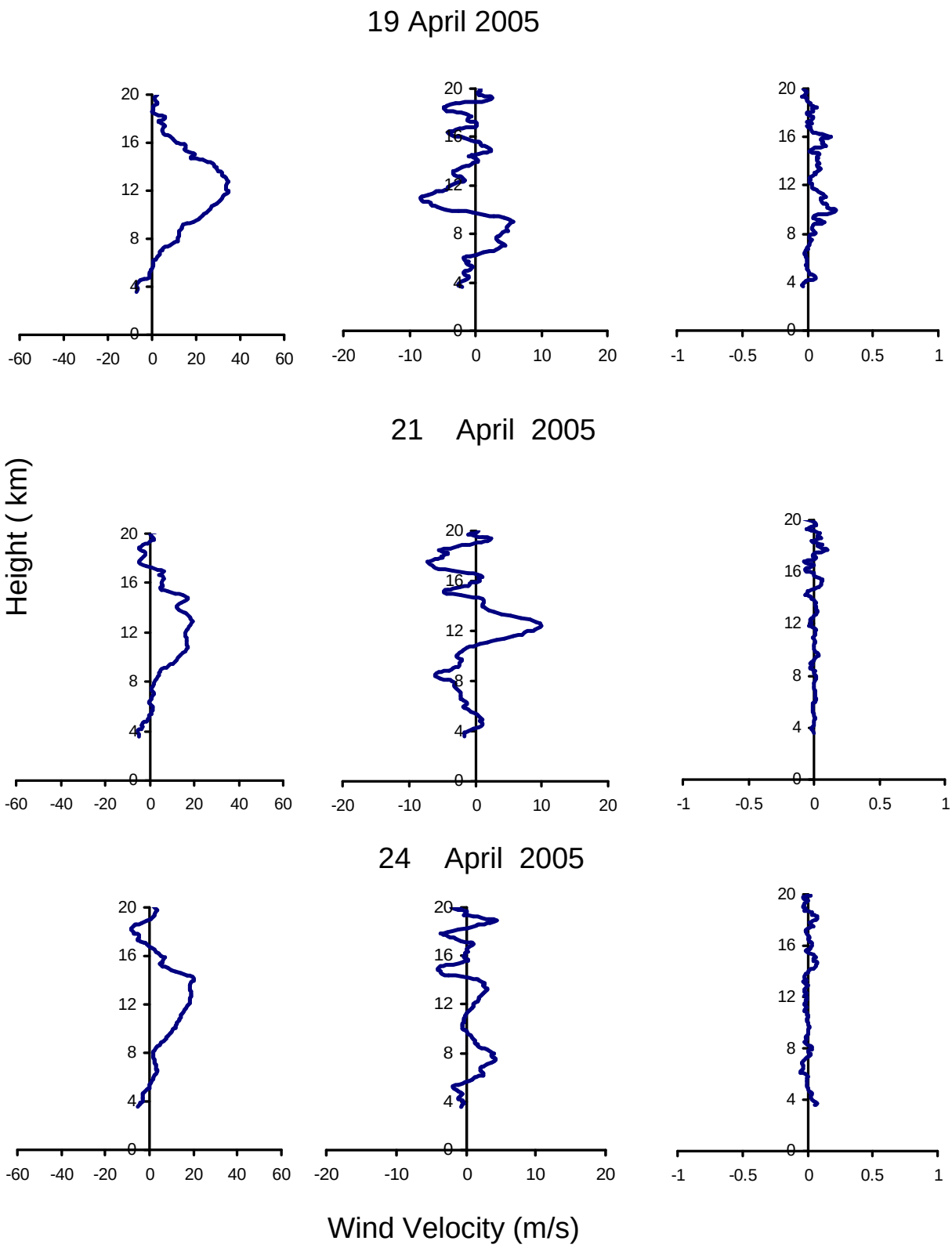

Figure -3.3 (n) same as Figure 3.1 (a) but for April month.

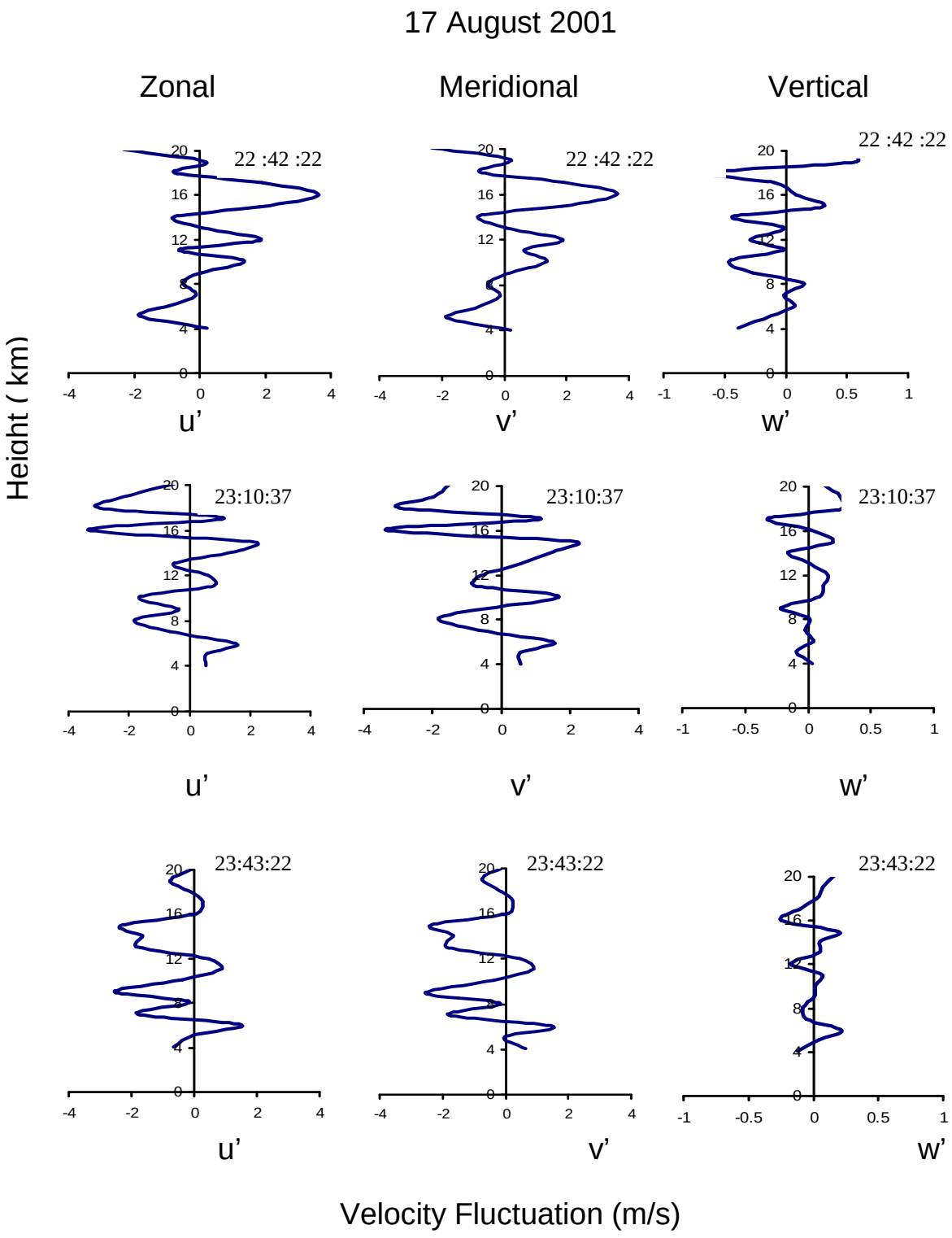

Figure 4.1(a) Vertical profile of u',v',w' showing wave like structure

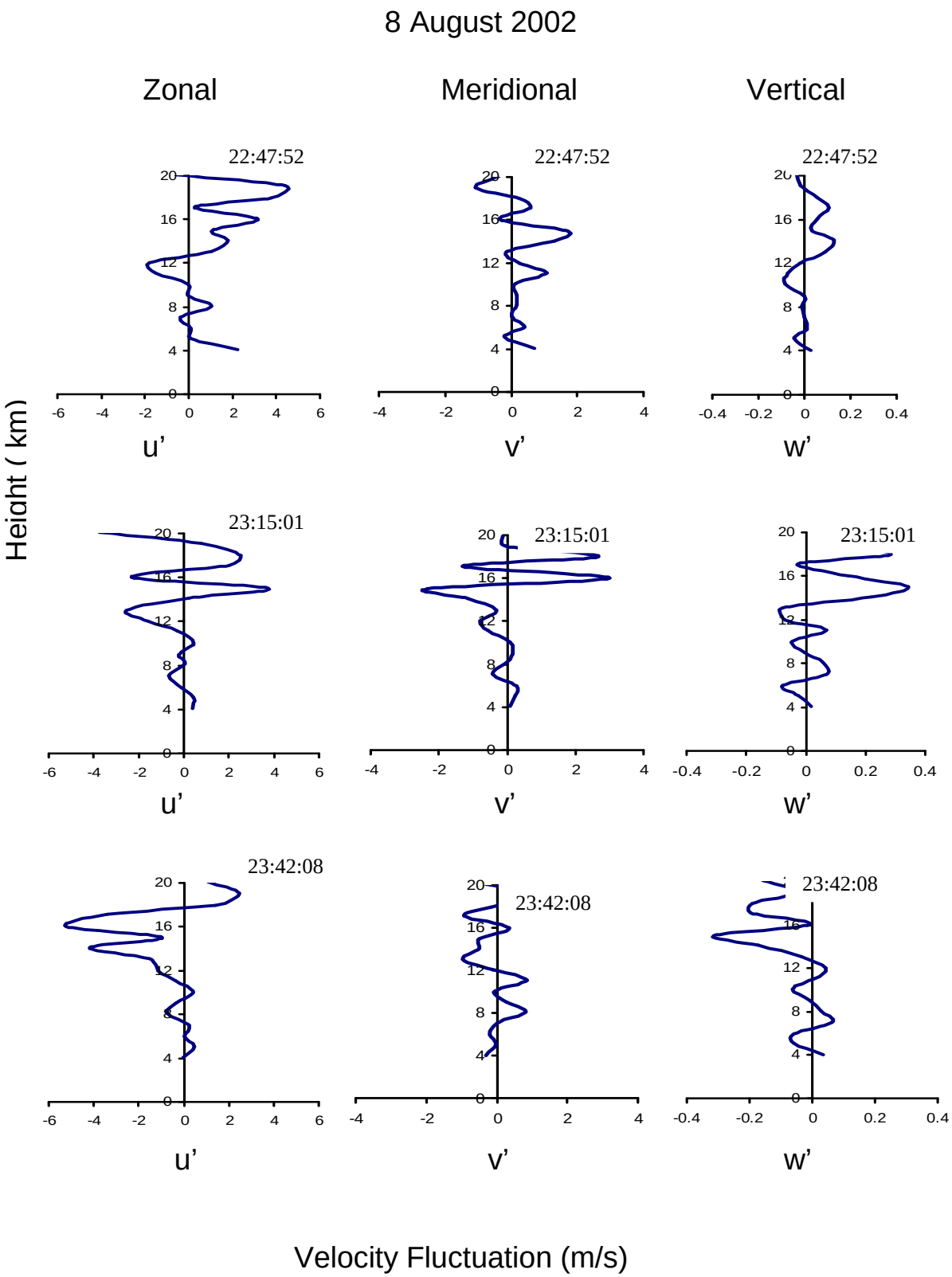

Figure 4.1 (b)Vertical profile of u',v',w' showing wave like structure

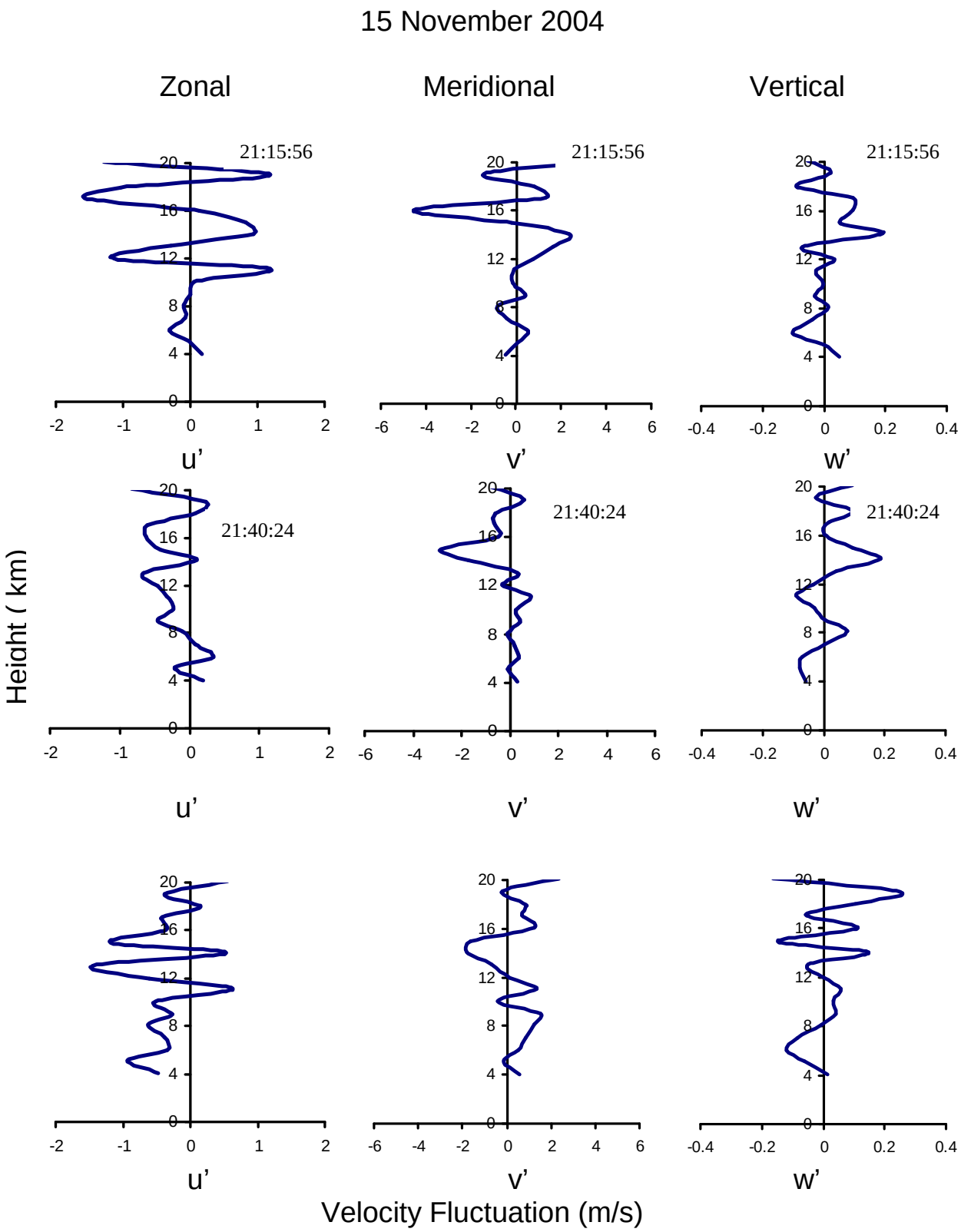

Figure 4.1(c) Vertical profile of u',v',w' showing wave like Structure

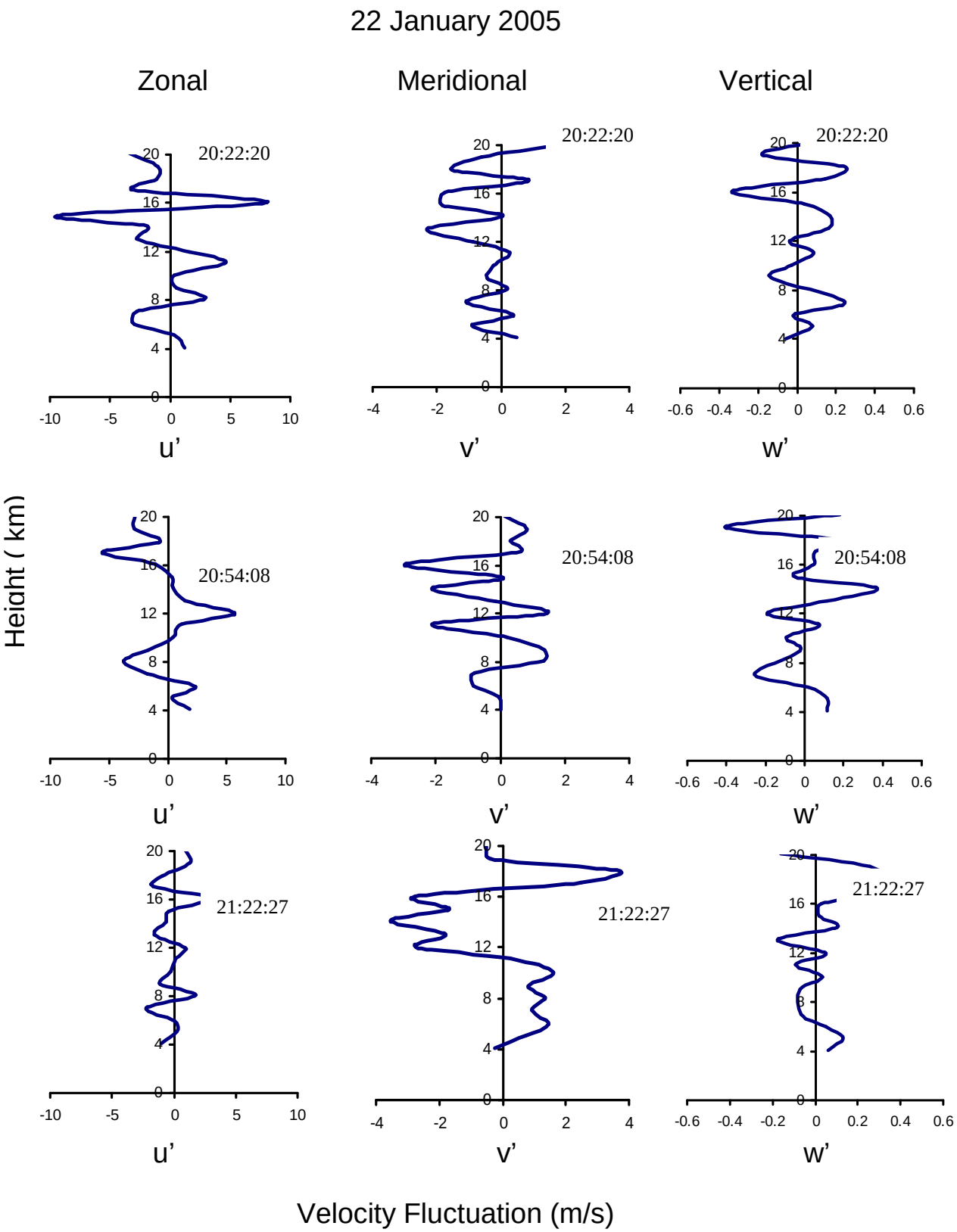

Figure 4.1 (d) Vertical profile of u',v',w' showing wave like structure

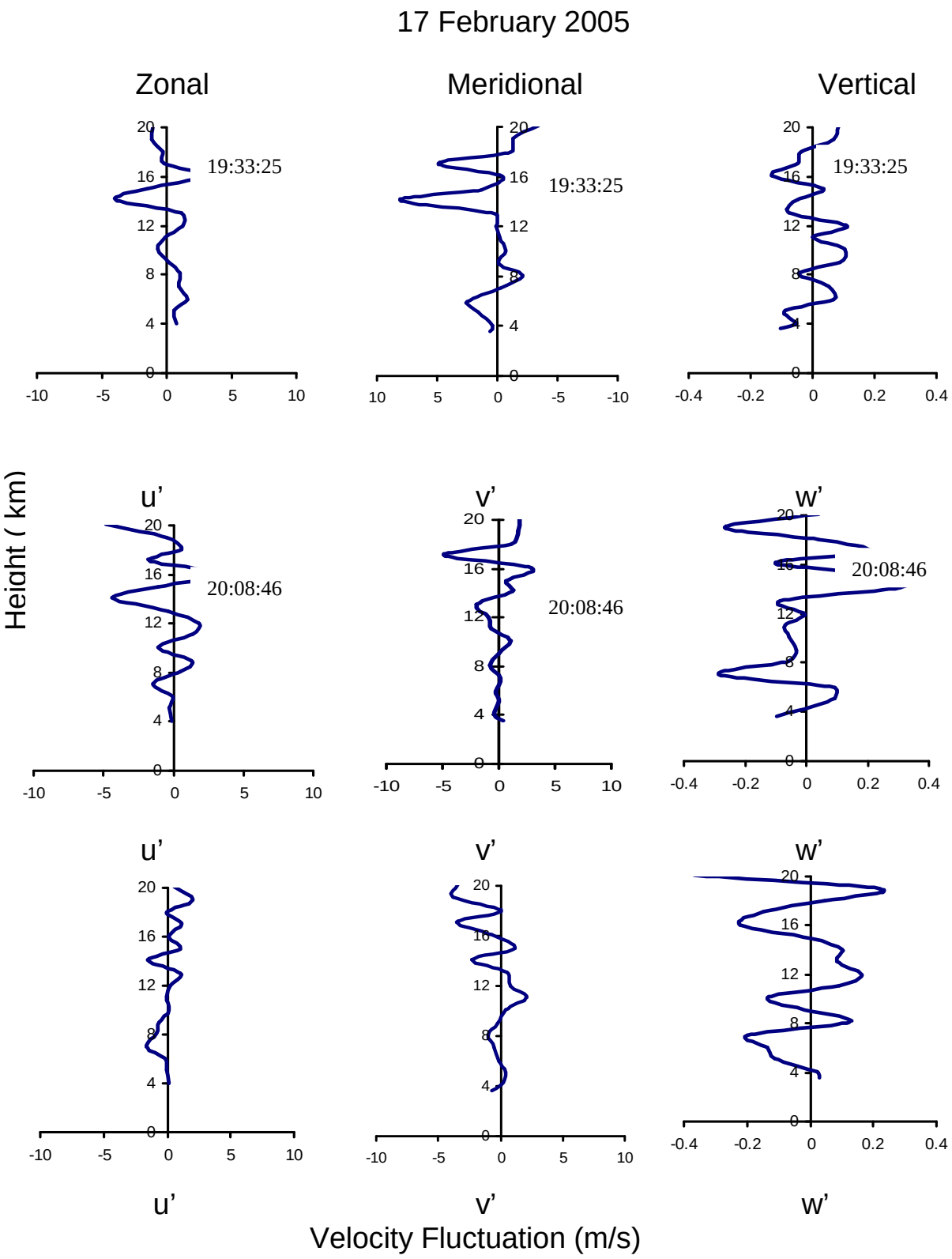

Figure 4.1 (e) Vertical profile of u',v',w' showing wave like structure

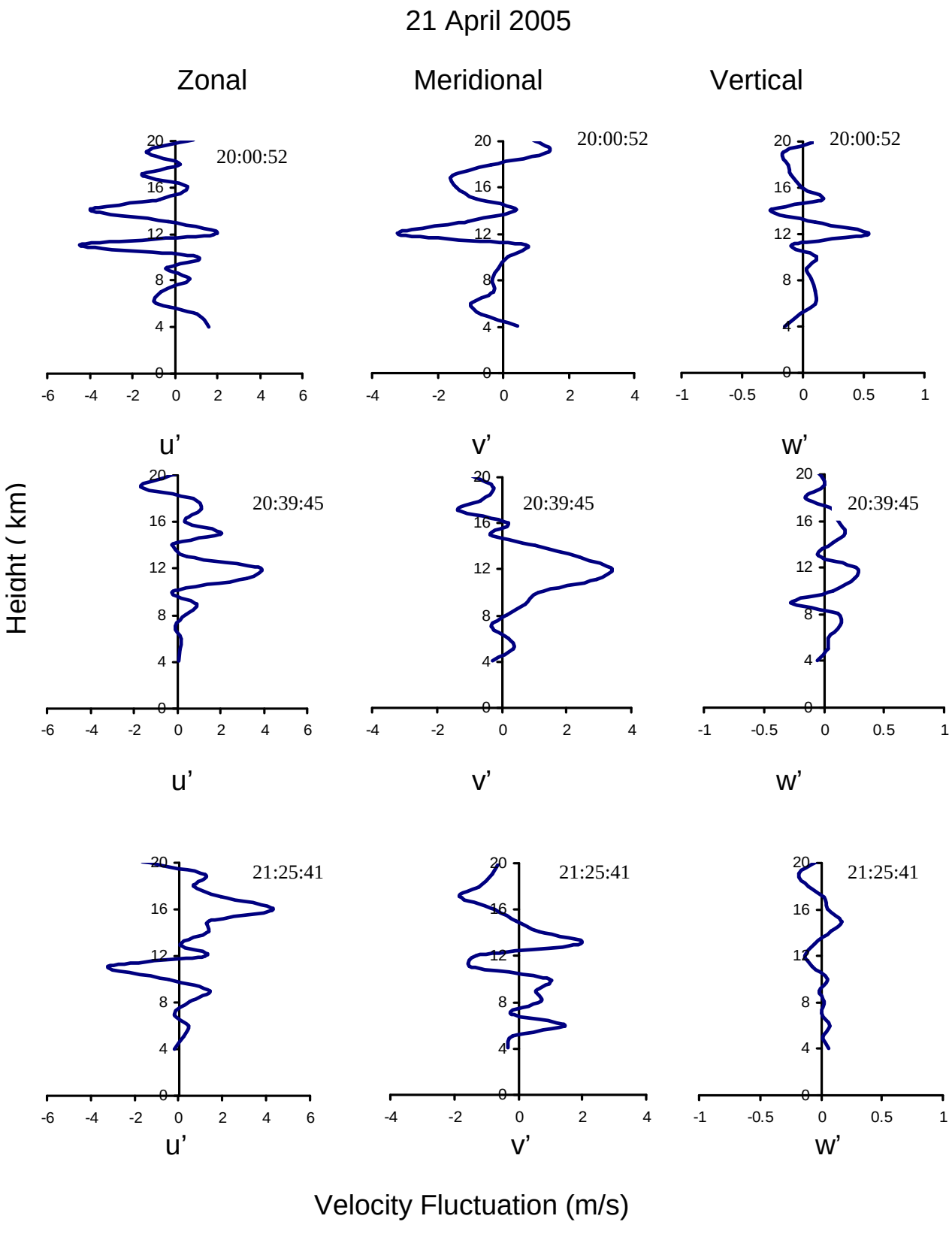

Figure 4.1 (f) Vertical profile of u',v',w' showing wave like structure

4. 1 Introduction

Atmospheric Gravity waves have been a subject of intense research activity in recent years because of their myriad effects and their major contributions to atmospheric circulation, structure and variability. Gravity waves also play very important role in carrying energy & momentum from lower to middle atmosphere and hence in coupling between troposphere and stratosphere. Their sources are in troposphere. They grow in amplitude as they propagate upwards into higher regions of the atmosphere .In the absence of any dissipation, the wave amplitude grows exponentially with altitudes as the wave propagates into the higher regions of the atmosphere.

Topographically generated internal gravity waves can transport significant momentum vertically in the atmosphere. The dissipative nature of internal gravity waves (Elisassen and Palm 1960) may allow the wave stress at the ground surface to be transferred far into the upper atmosphere where the density is small. Wave stress divergence associated with wave breaking acts as a drag on the mean flow at the wave braking level. The impact of gravity wave drag is known to be especially important for large-scale motions on time scales longer than one weak over continental areas during winter time. Spectral analysis show that the mesoscale variances are clim atologically much larger over mountainous area than over flat land surfaces or the ocean, and the observed differences are mostly due to gravity wave activity in the atmosphere.

Momentum transfer by gravity waves can be locally important on smaller time scale above significant topography. In the upper troposphere and lower stratospheric region, the vertical flux of horizontal momentum is generated primarily by the longer-period fluctuations. In this height range, the long –period momentum flux is due primarily to intense vertical air motion. For the lower stratosphere and troposphere there have been many studies conducted which correlate with high convection, fronts and orographic forcing. The frequency range of the gravity waves that can propagate upward should be fairly wide, because wave trapping is not significant owing the low inertial frequency near the equator. Since gravity waves with small vertical scales can easily be saturated,

they can effectively produce turbulence in the stratosphere and further act to enhance the eddy diffusion, which seems to have an important effect on the transportation of minor constituents in the equatorial middle atmosphere.

Early estimates of the energy and momentum fluxes associated with gravity waves suggested that their effect at upper heights could be important (e.g. Gosard,1962 ; Hines 1972). However, the role of such waves in balancing the momentum and energy budgets of the mesosphere awaited studies such as those of Houghton (1978) and Lindzen (1981). Interest in the momentum budget at lower height was inspired by the observation of substantial fluxes associated with mountain waves (e.g Lilly and Kennedy, 1973) and the realization that the flux divergence could affect the large scale circulation at the lower heights (Lilly,1972).

Observational techniques to measure the vertical transport of horizontal momentum have included the use of aircraft-mounted systems (e.g Lilly and Kennedy,1973; Bougeault et al., 1993; Alexander and Pfister,1995), radiosonde flights (e.g., Mobbs and Rees, 1989; Sutts et al., 1994) and mesosphere-stratosphere-troposphere (MST) radar (e.g. Fukao et al., 1988; Fritts et al., 1990). The symmetric-beam radar method of Vincent and Reid (1983) has been applied to measure momentum flux in both the lower atmosphere (e.g., Fukao et al., 1988; McAfee et al., 1989; Sato, 1990, 1993; Fritts et al 1990; Thomas et al ., 1992 ; Prichard and Thomas, 1993) and the mesosphere (e.g. Tsuda et al ., 1990; Reid and Vincent,1987). In this method, the momentum flux in a vertical plane is obtained using two radial radar beams in that plane, pointing at symmetric zenith angles +θ and – θ

$$uw = \frac{r^2_{+\theta} - r^2_{-\theta}}{2\sin 2\theta} \tag{4.1}$$

where u, w represent the horizontal and vertical perturbation velocities and $r_{+\theta}$, $r_{-\theta}$ represent the radial perturbation velocities in the two beams. For instantaneous measurements, this would require the horizontal scale of the gravity waves to be far greater than the spatial separation of the beams at the height of interest. However, for an averaging time much longer than the observed

wave periods, the velocities recorded by each beam are assumed to be statically similar; the momentum flux is given by the difference of the mean variance in the two beams and the beam separation is no longer important, what ever the horizontal wavelengths of the gravity waves.

Another approach (e.g Fukao et al. 1988) uses the product of the perturbation vertical wind component measured directly with the vertical radar beam, and the horizontal velocity derived from the vertical and a radial beam, to give the momentum flux in the vertical plane defined by the two beams.

$$uw = \frac{W(r^2_{+\theta} - W\cos\theta)}{\sin\theta} \tag{4.2}$$

where W represent the vertical beam measurement.

A third possible method, a “hybrid” of (4.1) and (4.2) measures the perturbation of vertical wind directly and those of the horizontal wind using a pair of radial beam.

$$uw = \frac{W(r_{+\theta} - r_{-\theta})}{2\sin\theta} \tag{4.3}$$

Generation mechanisms of gravity waves were also studied by means of observation made with aircrafts, radio sounds, rocket-sounds, MST Radar, and Rayleigh lidars. The MST radar at Jicamarca (12^o S), Peru, was used for observations of gravity waves in the middle atmosphere, detecting profile of wave induced momentum fluxes (Hitchman et al., 1992; Fritts et al., 1992).

4.2 Data and Method of Analysis

The Indian MST radar at Gadanki (13.2^o N, 79.2^o E) provide excellent opportunity to study momentum flux with high time and height resolution particularly in the Troposphere and Lower stratosphere. The Indian MST Radar is a high power density VHF Radar operating Frequency at 53 MHz with an average power-aperture product 7×10^8 Wm^2. The total transmission power

is 2.5 MW. The radar beam can be scanned in the North-South and East-West planes.

The present observation is made from the fixed ground station. The vertical flux of zonal and meridional momentum is calculated form the winds measured by the MST radar. For the momentum flux (u'w' and v'w') computation, a direct approach where time series of the perturbation component of u,v and w are obtained. Then products of u'w' and v'w' are formed and averaged over a suitable length of time. Vincent and Reid (1983) developed a method for radar measured winds. In this method two oppositely directed off-vertical symmetrical beam in the East-West or North-South plane are used to obtain line of sight (LOS) winds. Since the introduction of this dual beam method by Vincent and Reid(1983) numerous studies of gravity wave momentum fluxes in the troposphere, stratosphere and mesosphere have been carried out using radar data. However, when the vertical wind velocity can be obtained directly from the radar vertical beam data together with horizontal wind components (from oblique beam data) it is preferable to use direct method (Sasi et al. 1999). It is also noted here that the direct method make use of u, v and w obtained from the six LOS wind values, where as the Vincent and Reid (1983) method makes use of only two symmetrical oblique beams.

In the present study the VHF Radar at Gadanki (13.48º N, 79.18º E) a tropical station is used to study the gravity wave momentum fluxes in different months like August, October to February and April. Data is collected continuously for five hours for three to five days in a typical month during 9:30 to 1:30 LT on each day. The months of observations represent different seasons.

For this observation the following radar configuration was used :

Experiment Specification File

Pulse Repetition Frequency = 1000 Hz

Pulse Width = 16 µs

No. of coherent integrations = 64

No. of FFT points = 512

No. of beams =6 (oblique beams 10^0)

The Doppler spectra corresponding to the six beams, with a vertical resolution 150 m , where first converted to line-of-sight (LOS) wind profiles. From these vertical profiles of LOS corresponding to the six beams, the zonal (u) , meridional (v) and vertical components of the winds were derived using a least squares technique assuming a vertical wind contribution to the LOS winds obtained for the oblique beam (Sato,1989). Time series of u, v and w are obtained at height intervals of 150 m from these wind profiles. The length of the time series in the present study is 4-6 hrs. A ten point moving height average is subtracted from the observed values of u, v and w to obtain the fluctuations u', v', w' due to gravity waves. Products of u',w' and v',w' are taken and averaged over a suitable length of time represent zonal and meridional momentum flux and $\overline{u'^2+v'^2}$ the averaging being carried out during the length of observation, represents the gravity wave variance.

4.3 Result and Discussion

(a) **Gravity wave Variance**:

Variance represents the strength of the Gravity wave's activity. For the present study zonal and meridional wind data have been used to calculate fluctuating velocities u' and v', It is shown in Figure 4.1. Clear wave like fluctuations are seen on both days. Gravity wave variance has been computed for each height using the formula $\overline{u'^2+v'^2}$.

The mean variance plotted as function of height for the month of August (2001 -2003), is shown in Figures 4.2 (a, b, c). The prominent peaks of the variance are observed for all the days between ~ 14 km to ~ 17km. Gravity wave activity appear to increase exponentially with height. The values of variance observed on 16, 21 and 23 August 2001 (Figure 4.2 a) range between ~0.2 to 60 ~ m^2/ s^2 and on 17 August 2001 it observed ~0.2 to ~40 m^2/ s^2 while on 20 August 2001 the maximum value of variance is observed ~15 m^2/ s^2 . For the month of August 2002 mean variance plotted as function of height, (Figure 4.2 b) the prominent peaks of variance are observed for all the days between ~ 14 km to ~ 17 km. The value of variance observed range between 0.2 to 20 m^2/s^2 while

on August 2003 (Figure 4.2 c) the value of variance observed range between 0.1 to 40 m^2/ s^2.

In Figure 4.2 (d, e) is shown the variance of wind fluctuations around the mean values during the post monsoon season (18-21 October 2004 and 11-13-15 November 2004) using MST Radar. Very less value (< 10 m^2/s^2) of variance observed during October. The magnitude of the variance is observed around 5-8 m^2/ s^2 . No significant peak is seen during the observed days of this month. While on 11, 13 November 2004 the value of the variance is observed ~ 0.2 to 20 m^2/ s^2 and the prominent peak observed between 13 to 16 km, on 15 November 2004 less value of the variance observed compare to other two days.

The mean variance is plotted as function of height for winter seasons, (December 2004 – January 2005 and February 2005 in figures 4.2 (f,g,h). During the month of the December the prominent peaks of the variance is observed at ~ 16 km on 21 December 2004 and on 22 December peak observed ~ 14 km. The activity appears to increase exponentially with height and value observed in the present study range between 0.2 to 20 $m^2/s^{2.}$ There is no prominent peak observed on 24 December 2004.

Large variability can be observed in variance values observed in January 2005. The activity appears to increase exponentially with height and the values observed in the present study range between 0.2 and 60 m^2/s^2. The prominent peak has been obsvered all the days between ~ 14 km to 17 km while during the month of February 2005 the value of the variance observed ~0.2 to 40 m^2/s^2 and the peak observed between ~14 km to 17 km.

The mean variance plotted as function of height which for the number of the days of April 2005 is shown in Figure 4.2. The value observed in the present study range between ~0.2 to 20 ~ m^2/ s^2 . Two prominent peaks observed on 19th April 2005, at ~8 to 12 km and ~14 km to ~17 km and on 21 April 2005 and 22 April 2005 the value of variance increase with height. The activity appears to increase exponentially with height.

It is expected that as the density of neutral atmosphere falls exponentially upwards, the gravity wave amplitudes will grow accordingly. This clearly shows

that major sources of gravity waves are located in the troposphere. Using radio sonde measurements, Tsuda et al. (1994 a) showed that gravity waves were mostly generated in the middle troposphere and propagating upwards. Most of the work done on gravity waves in the mesosphere suggests that their sources are in the troposphere.

The maximum variance as observed in the present study ranges between ~0.2 and 60 m^2/ s^2 during the monsoon seasons (16, 21, 23 August 2001) and during winter (22, 23 January 2005) while during the October the variance observed (< 10 m^2 / s^2) . Tsuda et al. (1994a) estimated a wind velocity variance between 1 and 20 m^2/ s^2 over East Java, Indonesia. The average estimate of variance given by Chang et al. (1997) for Christmas Island ranges between 1 and 5 m^2/ s^2.

(b) Gravity wave power spectra and significant period.

The height-time structure of the periodicities of the gravity waves is obtained from the FFT analysis. Fourier transformation of the time-domain data converts the time-amplitude representation to a frequency amplitude representation and thus, can be utilized to analyze the frequency components which exist in the signal.

Time series of u, v and w are obtained at height intervals of 150 m from these wind profiles. The length of the time series in the present study is 4-6 hrs. A ten point moving height average is subtracted from the observed values of u, v and w to obtain the fluctuations u', v', w'.

For the power spectral analysis take the Time series of u' v',w' (Figure 4.3), are used. The meridional wind fluctuations (v') are taken for power spectral analysis to bring out the gravity wave periodicity because good wave like structure is observed in meridional component compared to the zonal and vertical.

Figure 4.4a shows the power spectrum on 16 August 2001. The observations were taken during 2230 LT on 16 August 2001 up to 0130 LT on next day morning. Below about 8 km very less power density is observed, and then it gradually increased with increasing height. Maximum power density

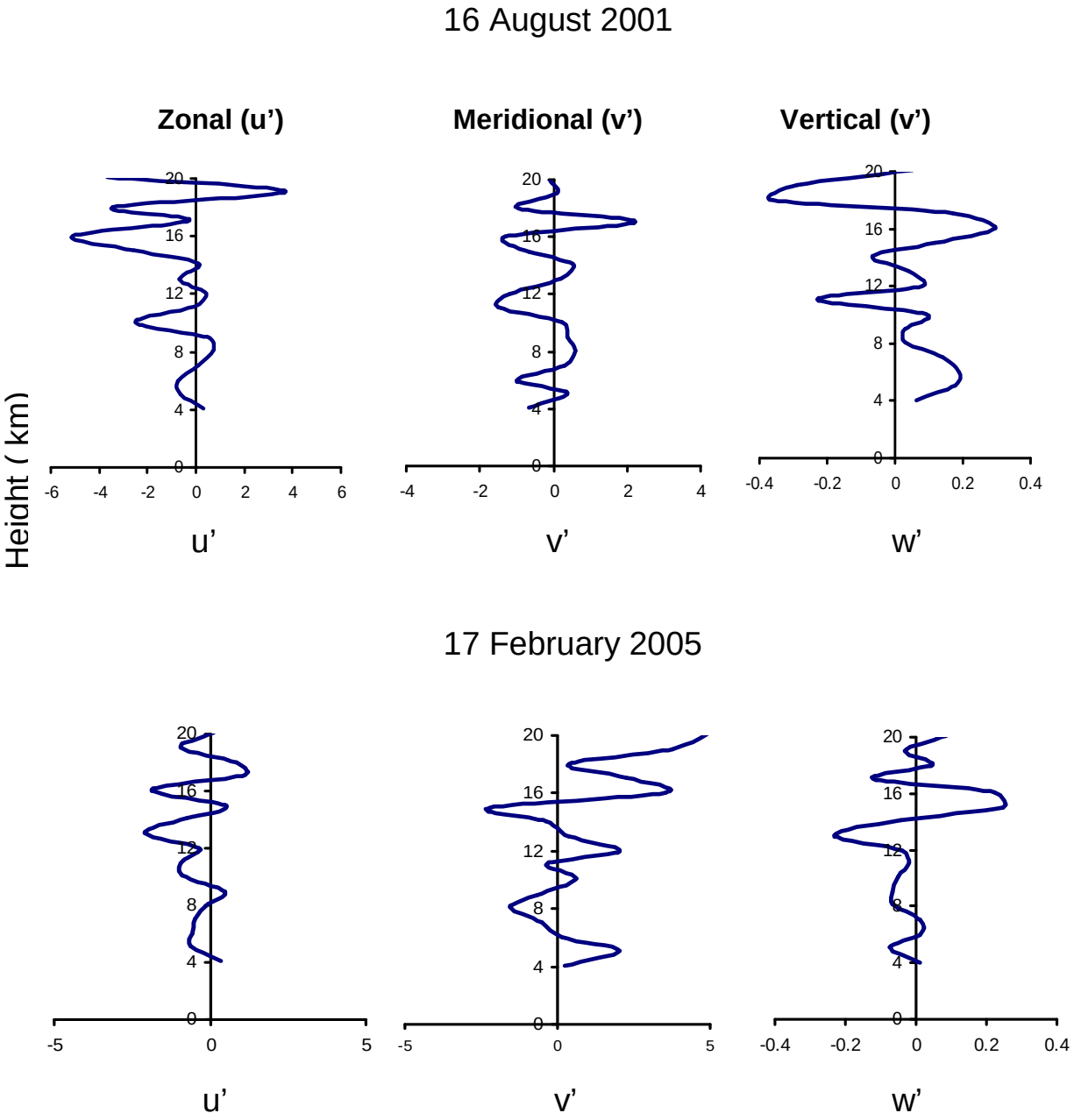

Figure 4.1 Vertical profile of u', v', w' showing wave like structure

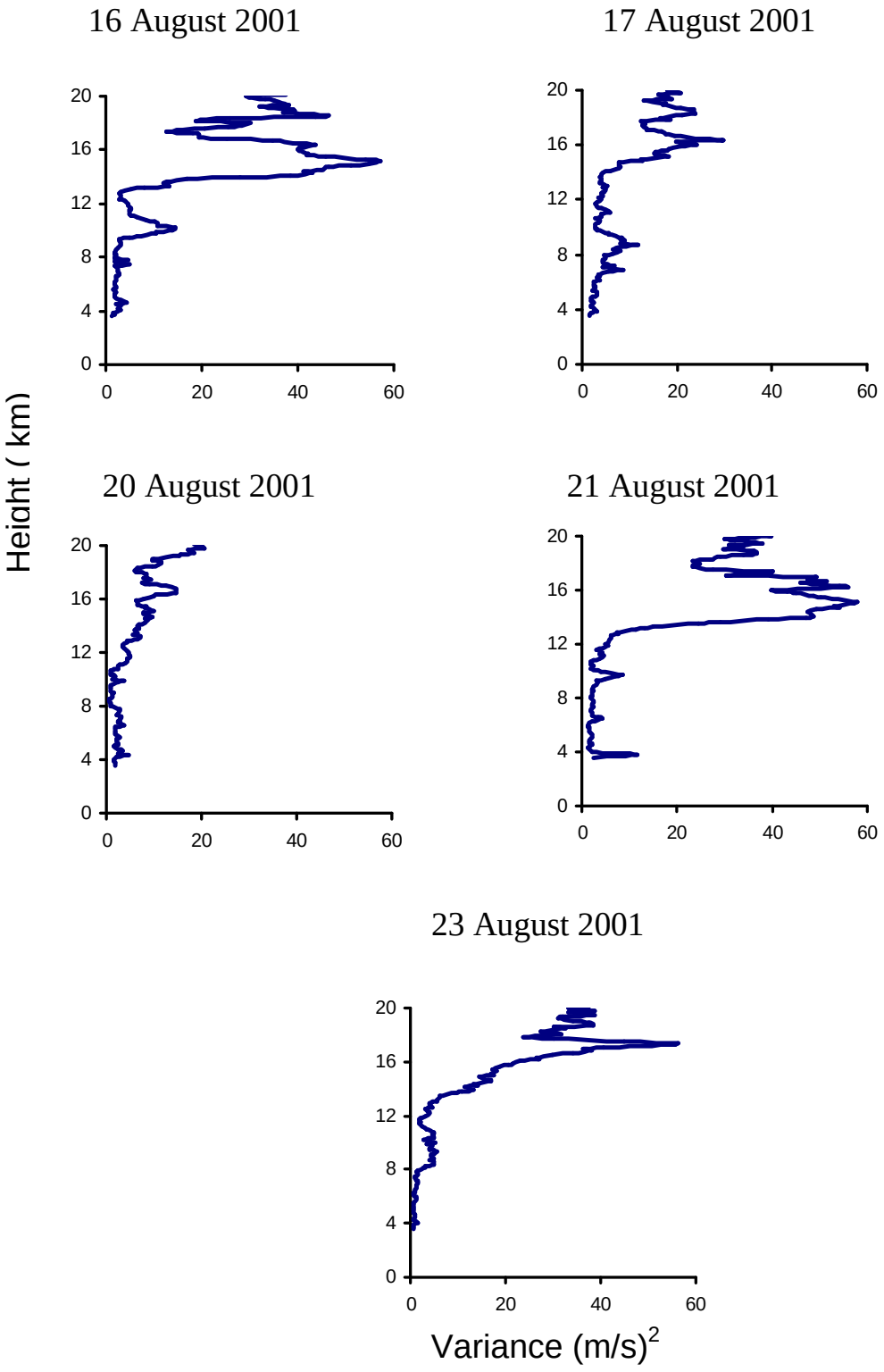

Figure 4.2 a: Mean profile of zonal and meridional Variance $(u'^2+v'^2)$

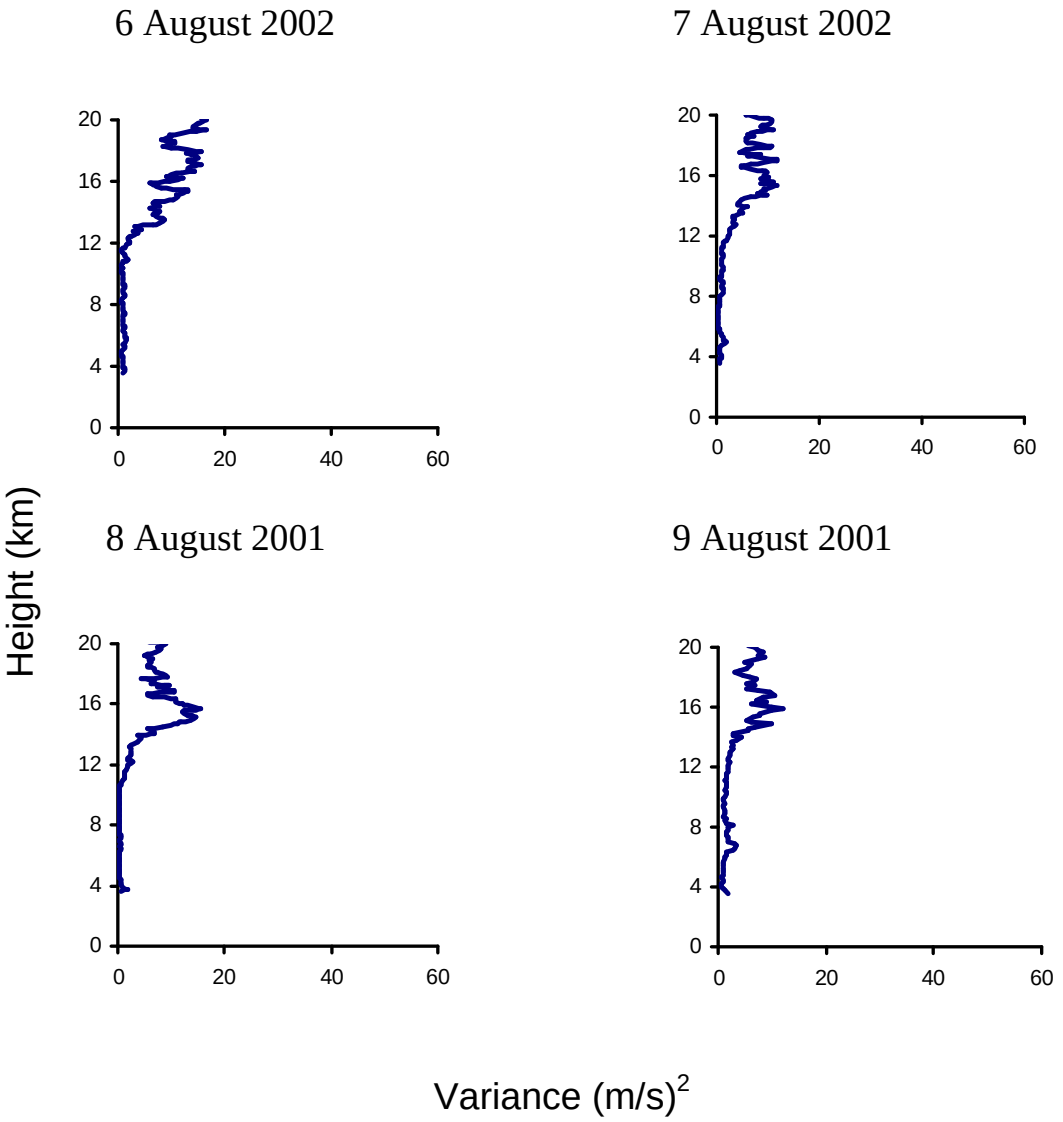

Figure 4.2 b: Mean profile of zonal and meridional Variance $(u'^2+v'^2)$

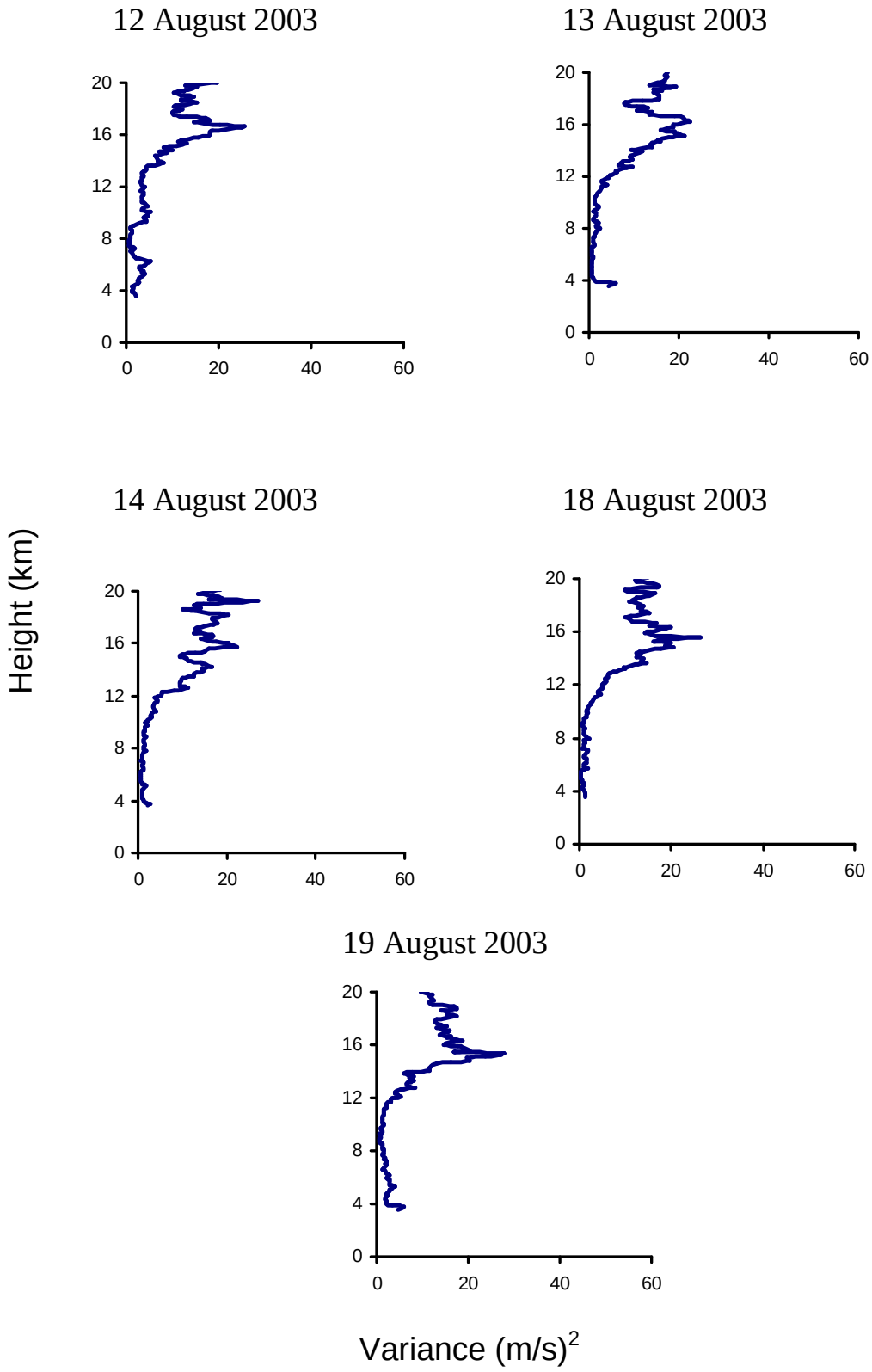

Figure 4.2 c : Mean profile of zonal and meridional Variance ($u'^2+v'^2$)

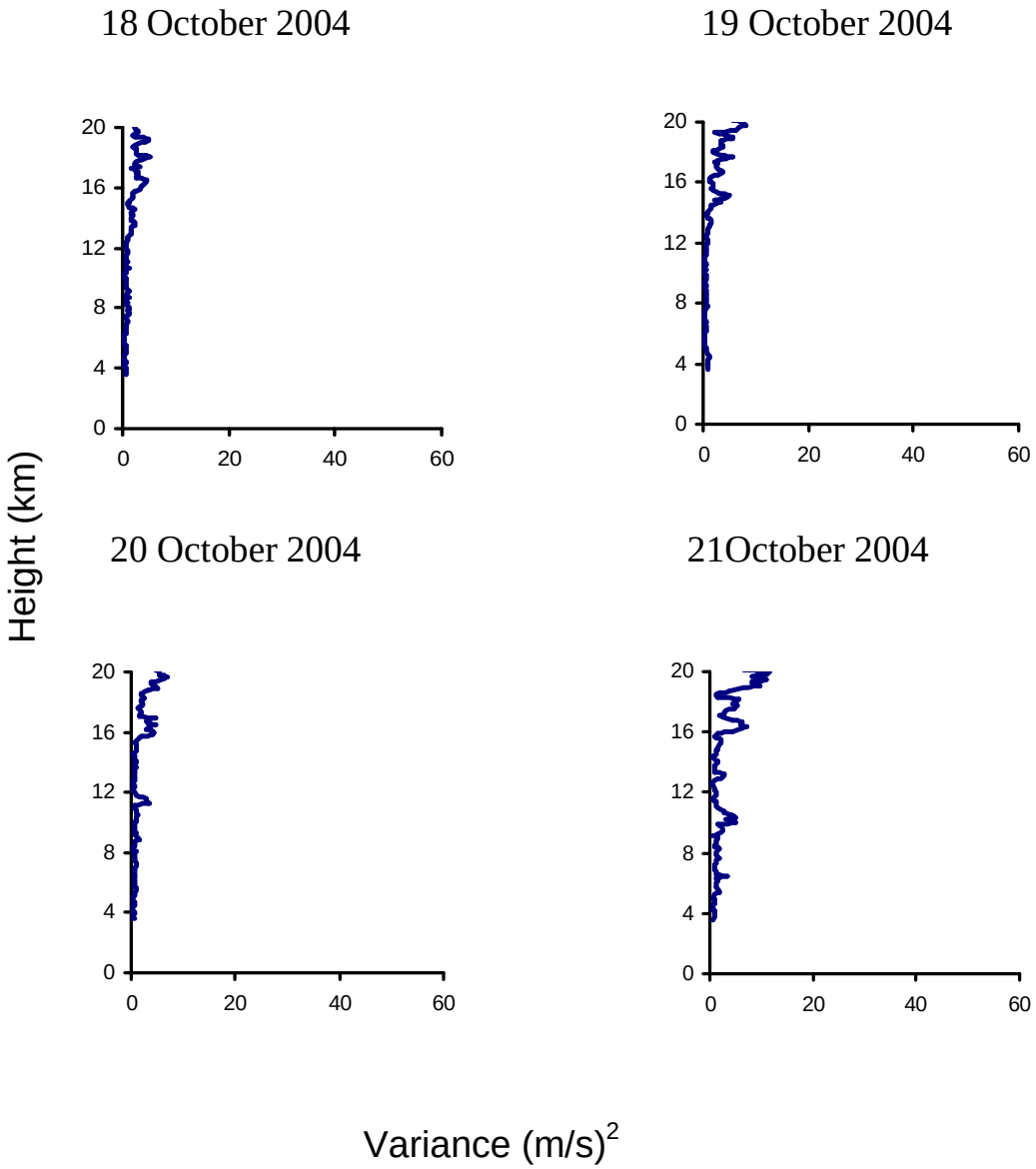

Figure 4.2(d Mean profile of zonal and meridional Variance $(u'^2+v'^2)$

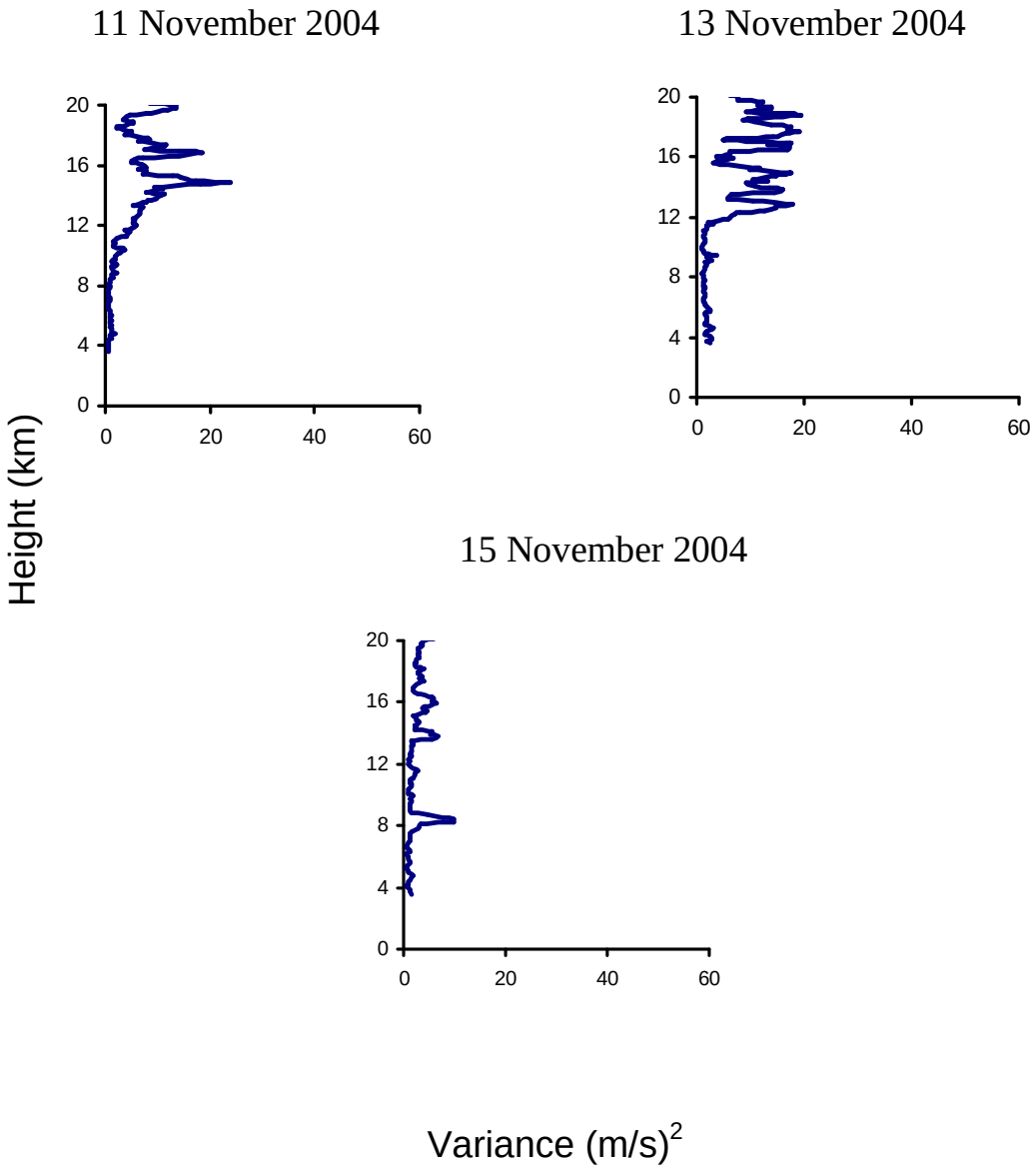

Figure 4.2 (e) Mean profile of zonal and meridional Variance $(u'^2+v'^2)$

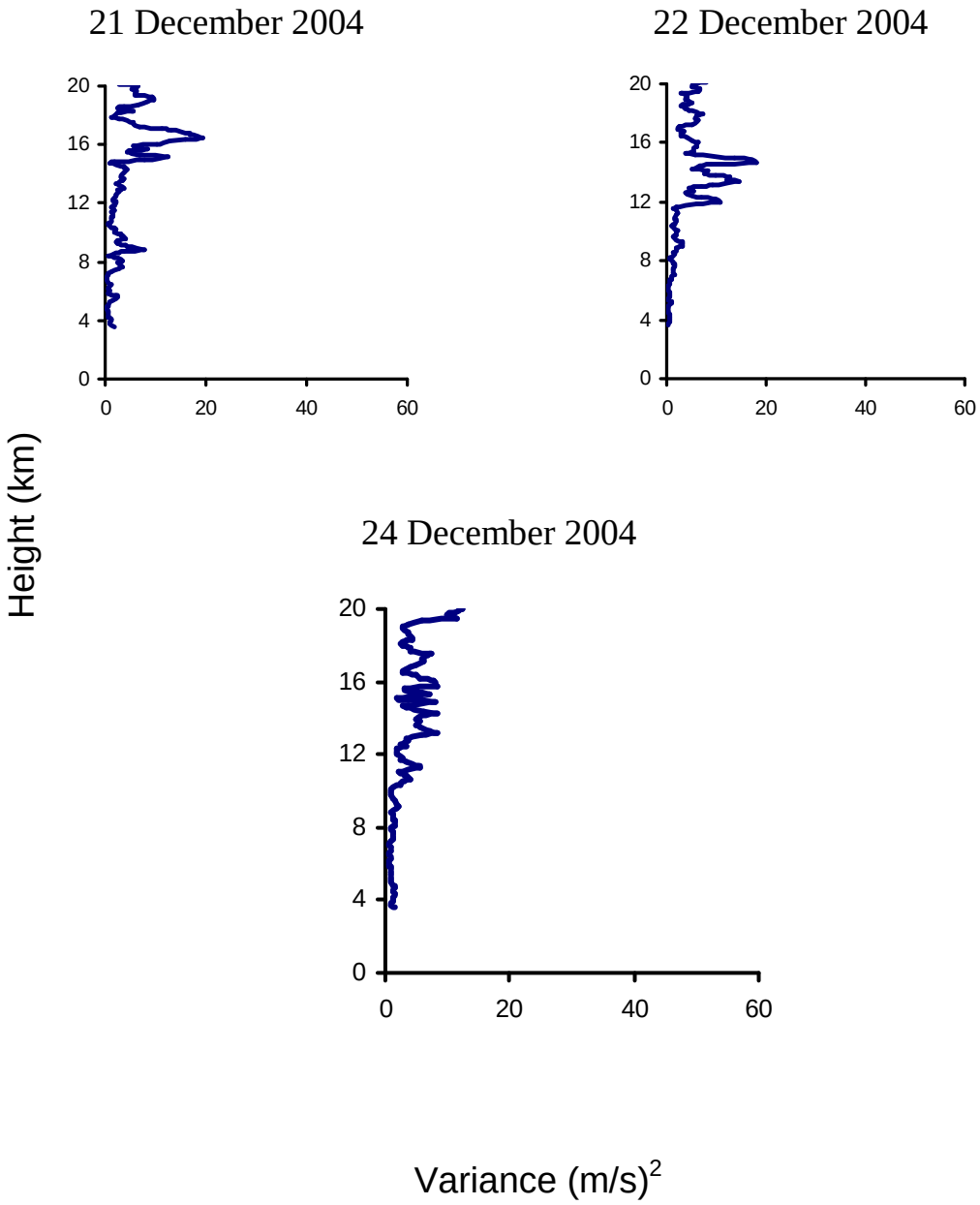

Figure 4.2 (f) Mean profile of zonal and meridional Variance $(u'^2+v'^2)$

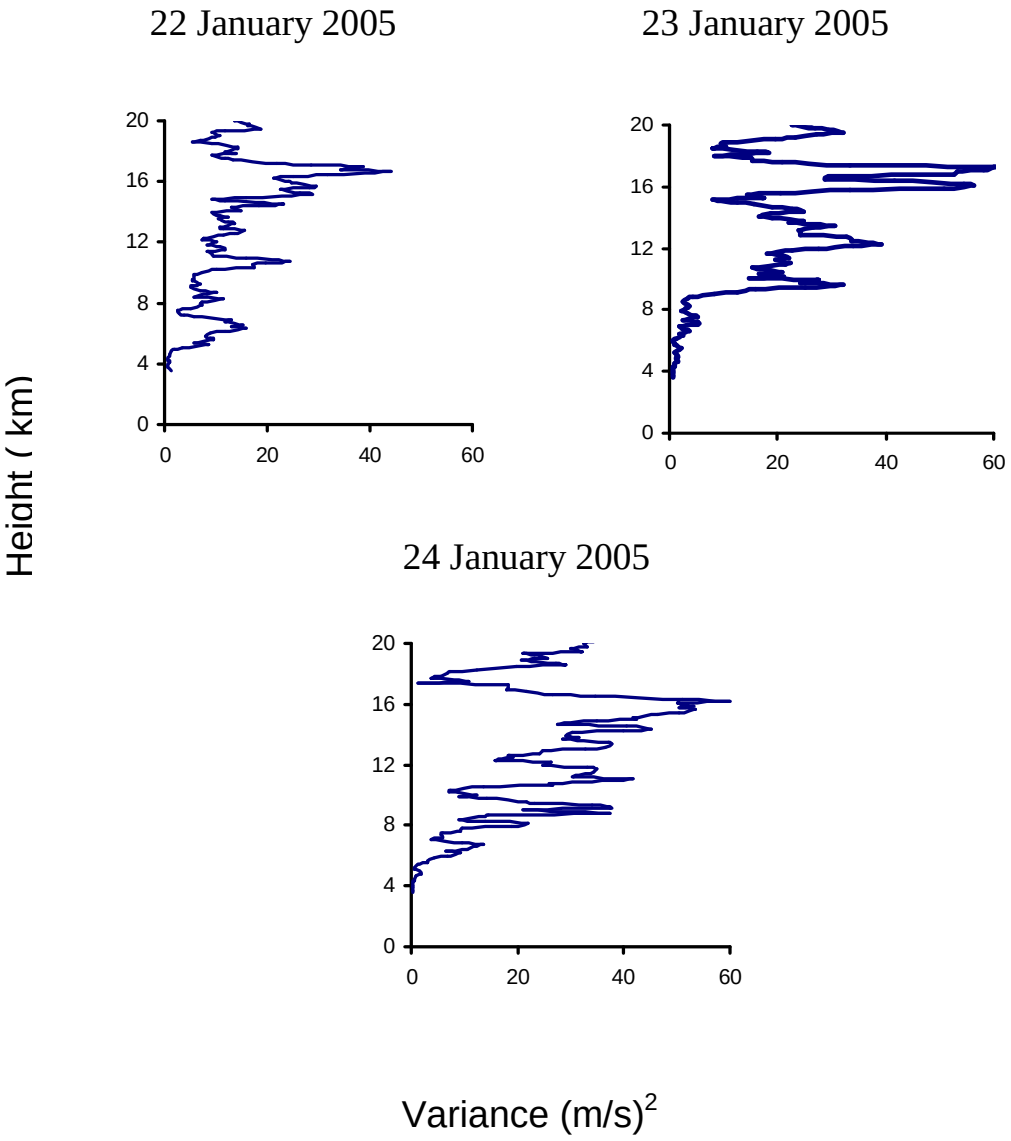

Figure 4.2 (g) Mean profile of zonal and meridional Variance ($u'^2+v'^2$)

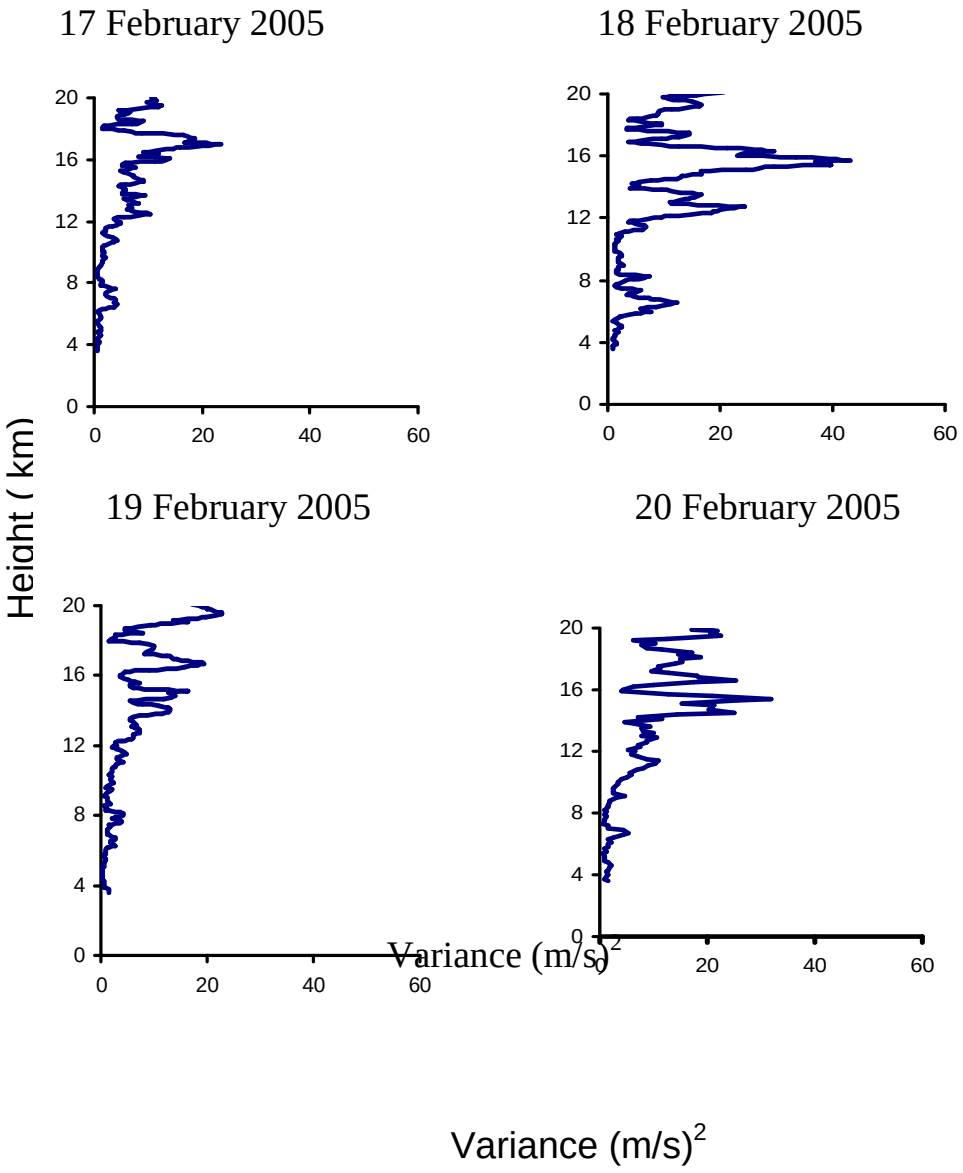

Figure 4.2 (h) Mean profile of zonal and meridional Variation ($u'^2+v'^2$)

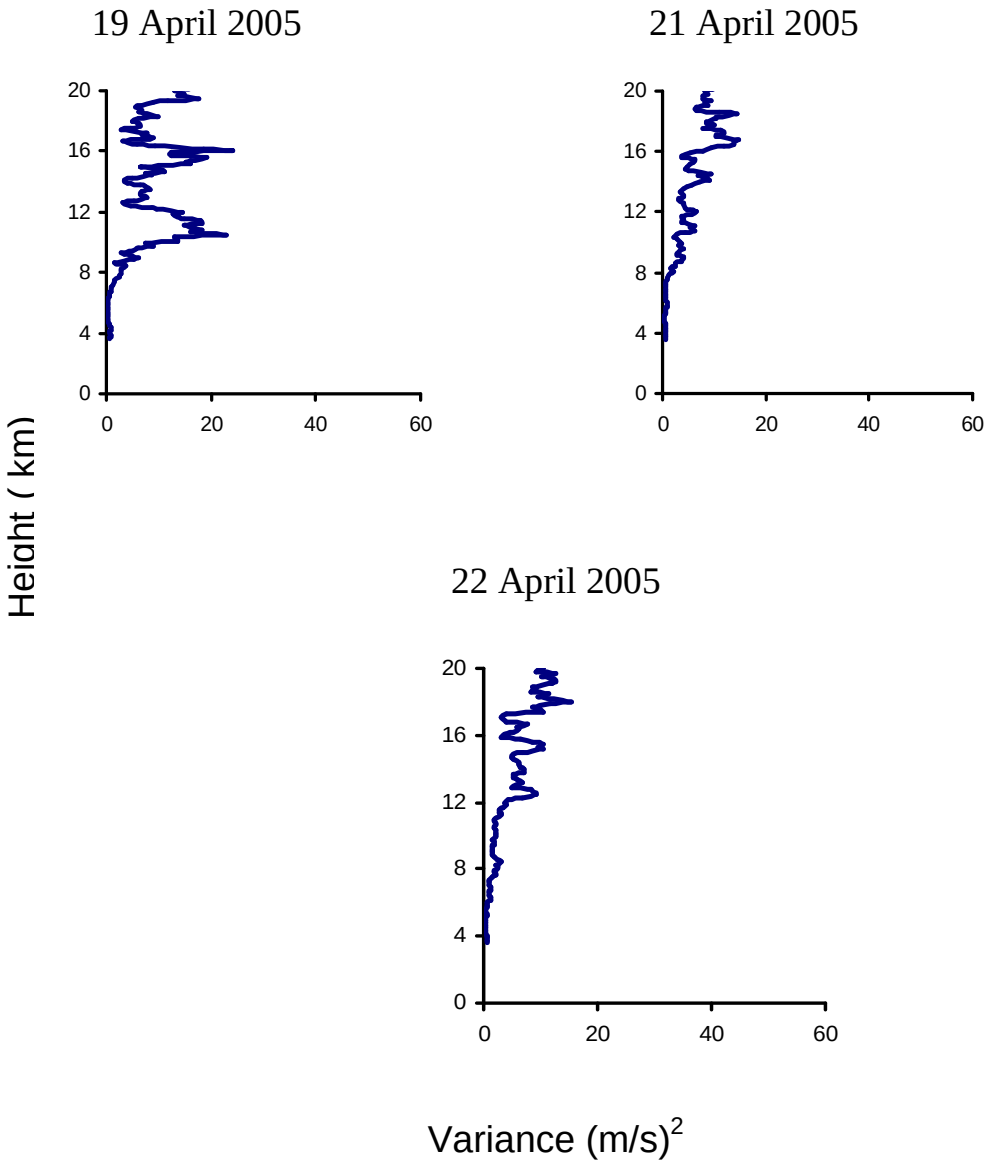

Figure 4.2 (i) Mean profile of zonal and meridional Variance ($u'^2+v'^2$)

is observed at 17.1 Km where the value of the power density is around 50 $(m/s)^2$. After this it slowly decreases with height around 20.1 km where least power density is observed. Governing period of the gravity waves is observed to be about 20 to 27 min.

The observations on 21 August 2001 were taken during 2230 LT up to 0130 LT on next day morning (Figure 4.4b). On this day, a very less power density has been observed up to 10.05 km, then it increases and reaches a maximum power density of 25 $(m/s)^2$ around the altitude at 16.5 km. And above this altitude, it slowly decreases. The prominent period of the gravity wave has been observed between 20 to 40 minutes, for this day.

As observed on 23 August 2001, less power density is found below 8 km and then it increases with height (Figure 4.4c). Maximum power density has been observed at 18.75 km, and then it decreases with height around 20.1 km where a very less power density has been observed. The dominating period of the gravity waves is observed about 20 to 27 min.

The observations on 12 August 2003 were taken for six hours from 1100 to 0400 LT (Figure 4.4 d). On this day, a very small power density has been observed up to 6.45 km, then it increases and reaches a maximum power density of 25 $(m/s)^2$ around the altitude of 16.5 km. And above this altitude, it slowly decreases. The same day, the dominant period of the gravity wave has been observed between 20 to 40 minutes.

On 18 October 2004, a very small power density (<0.3 $(m/s)^2$) has been observed The variance also showed very less values in this month. It can be concluded that gravity wave activity is practically absorb on this day.

Figure 4.4 (f) shows the power spectrum on 22 December 2004; the observations were taken for four hours from 2030 to 0030 IST up to the next morning. Below 12 km very small power density (< 5 m^2/s^2) is observed, then it increases and reaches a maximum power density of 40 $(m/s)^2$ at around 14.1 km and then it decreases with height .

The observations on 23 January 2005 were taken for four hours from 1930 to 1230 LT (Figure 4.4 g). On this day, a very less power density (<10 m^2 / s^2) been observed up to 7.95 km, but then it increases and reaches a maximum power density of 100 $(m/s)^2$ around the altitude of 17.1 km. And above this altitude, it slowly decreases. The same day, the prevailing period of the gravity wave has been observed between 20 to 40 minutes.

As observed on 17 February 2005, less power density is found below around 9.6 km and then it increases with height (Figure.4.4 h). Maximum power density has been observed around 17.55 km, and then it decreases with height. The governing period of the gravity waves are observed about 20 to 27 min. During the winter seasons the maximum variance observed in 23 January 2005 .it's value observed 60 m^2 / s^2 at height ~ 17 km and here the maximum power density (100 m^2/s^2) has been observed at ~17.4 km.

In Figure 4.4 (i) shows the power spectrum of 21 April 2005 .They are placed in columns in order of increasing heights. The observations on 21 April 2005 were taken for four hours from 1930 to 1230 LT .On this day, a very less power density (<10 m^2/s^2) has been observed up to 6.9 km, but then it increases and reaches a maximum power density of 20 $(m/s)^2$ around the altitude of 14 km. And above this altitude, it slowly decreases. The same day, the dominating period of the gravity wave has been observed between 20 to 30 minutes.

The mean variance is plotted as a function of height and power spectra for all three seasons are shown in figure 4.3 and figure 4.4. A peak in variance is seen between ~ 14 to ~18 km for mostly in all seasons and maximum value observed during monsoon season and winter seasons particularly on 16 ,21 and 23 August 2001 and 23 , 24 January 2005 it reaches maximum value of 60 $(m/s)^2$ at around 16 to17 km (Figure 4.2 a and Figure 4.2 g) . Similarly from the power spectra the maximum power (~50 m^2/ s^2) observed during monsoon on 16 ,21 and 23 August 2001 (figure 4.4 a-c)and (~100 m^2 /s^2) is observed during winter on 23 January 2005. The range of the period is same ~20-40 minutes in all seasons. The above results show that convective activity in monsoon season is

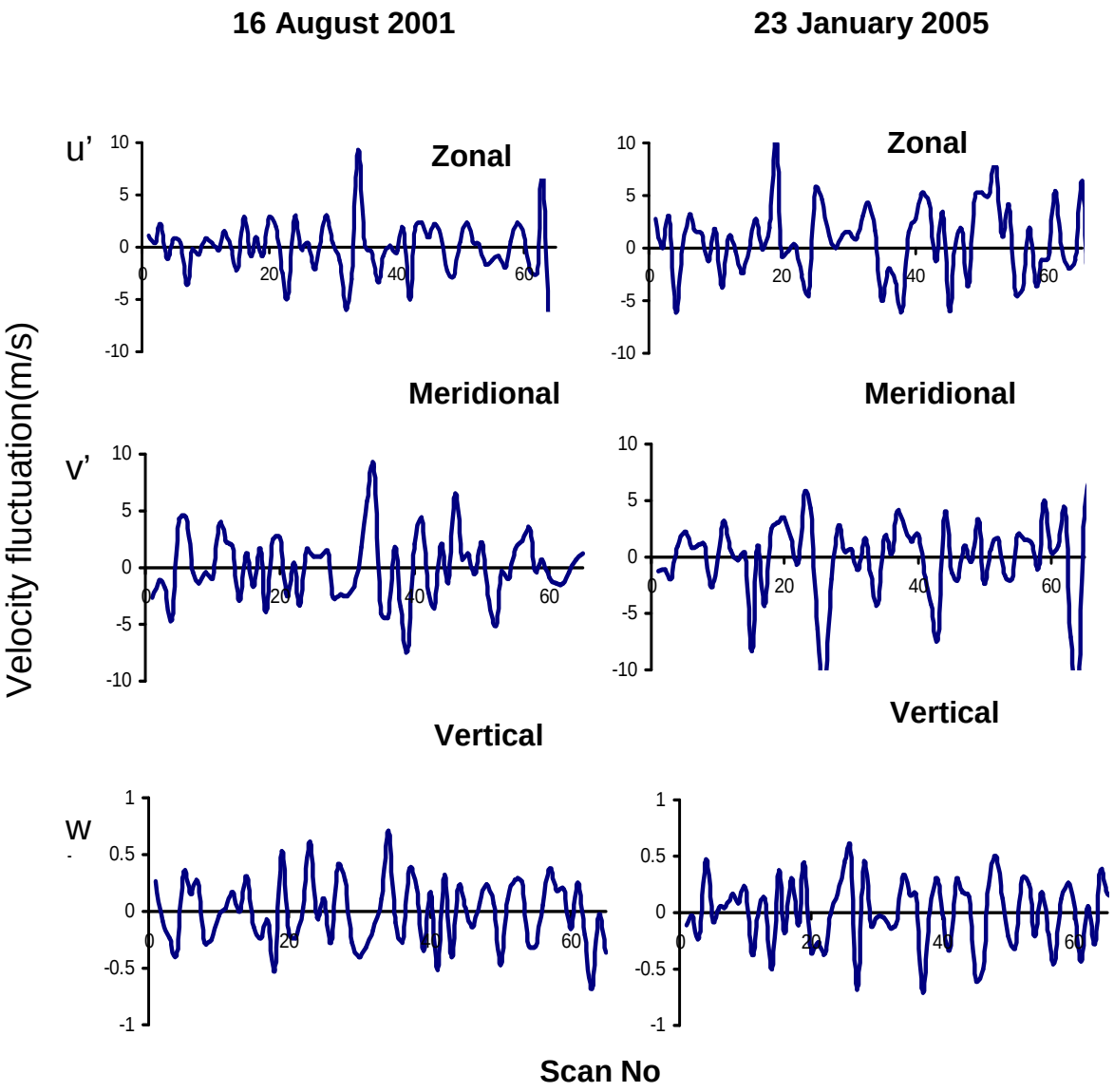

Figure 4.3 Typical Time series of u' v' w', Time interval between Successive scans is 4 mins (at 17.1 km for 16 august 2001 and at 17.4 km for 23 January 2005)

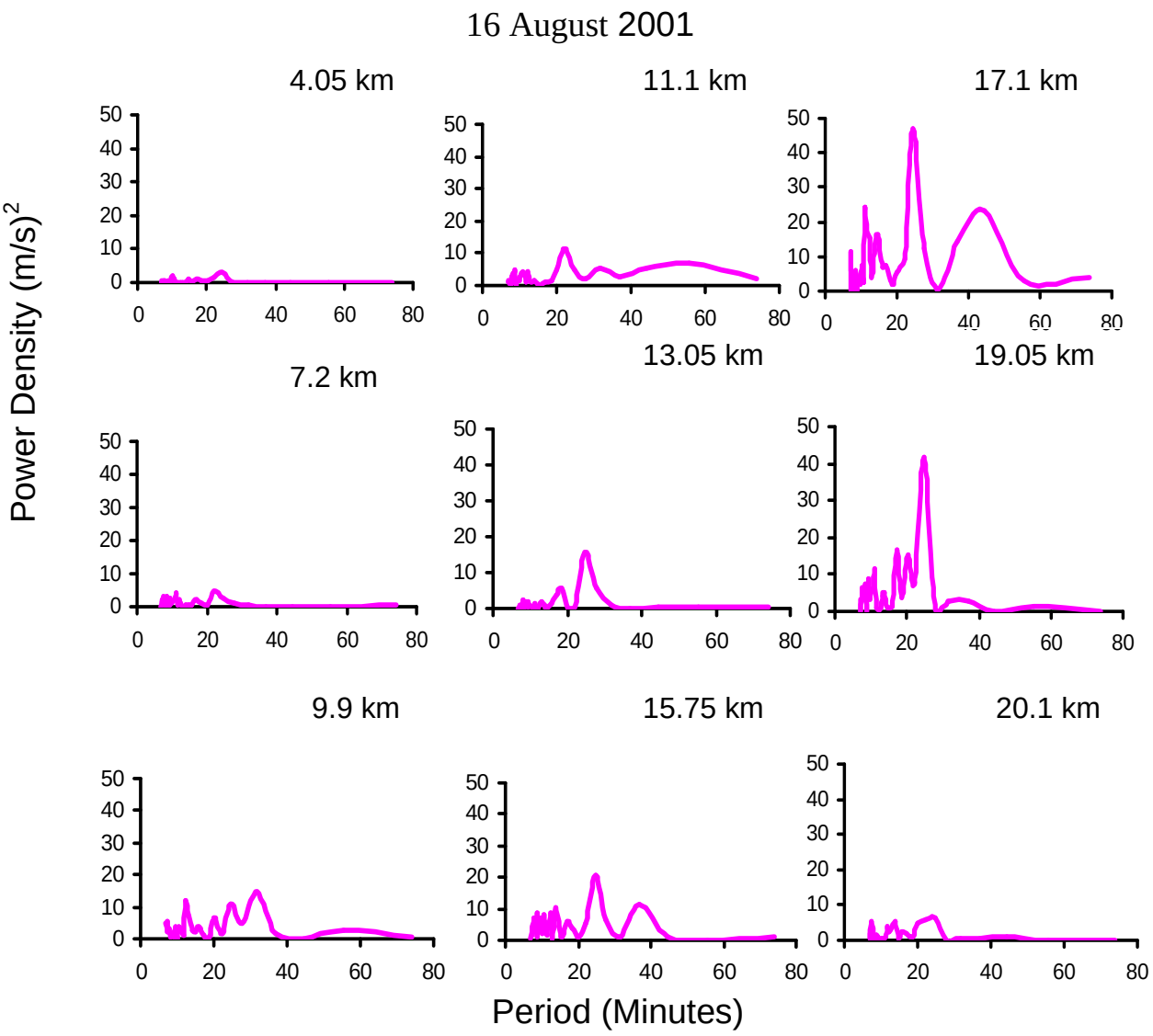

Figure 4.4 (a) Power Spectrum at different heights

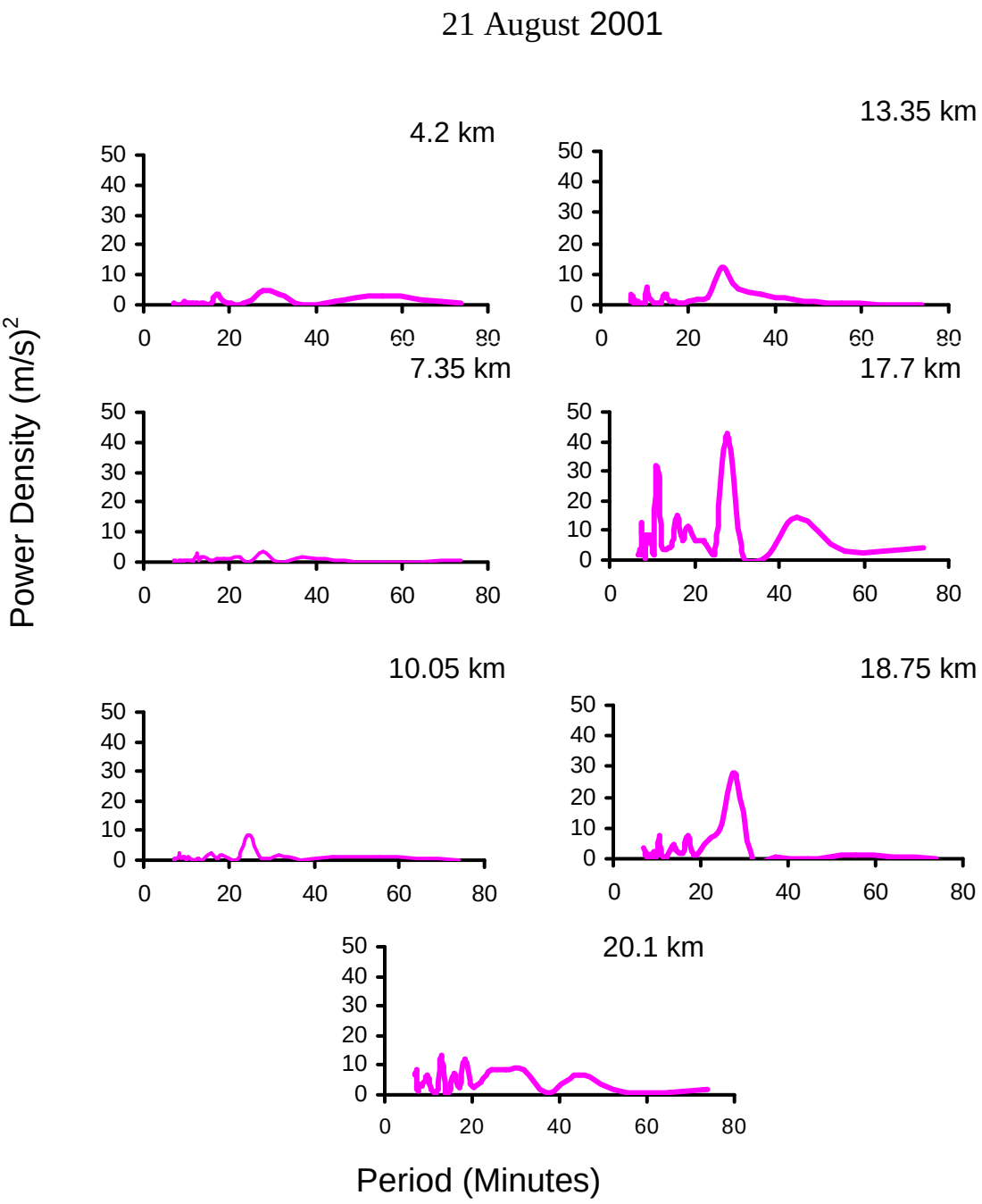

Figure -4.4 (b) Power Spectrum at different heights

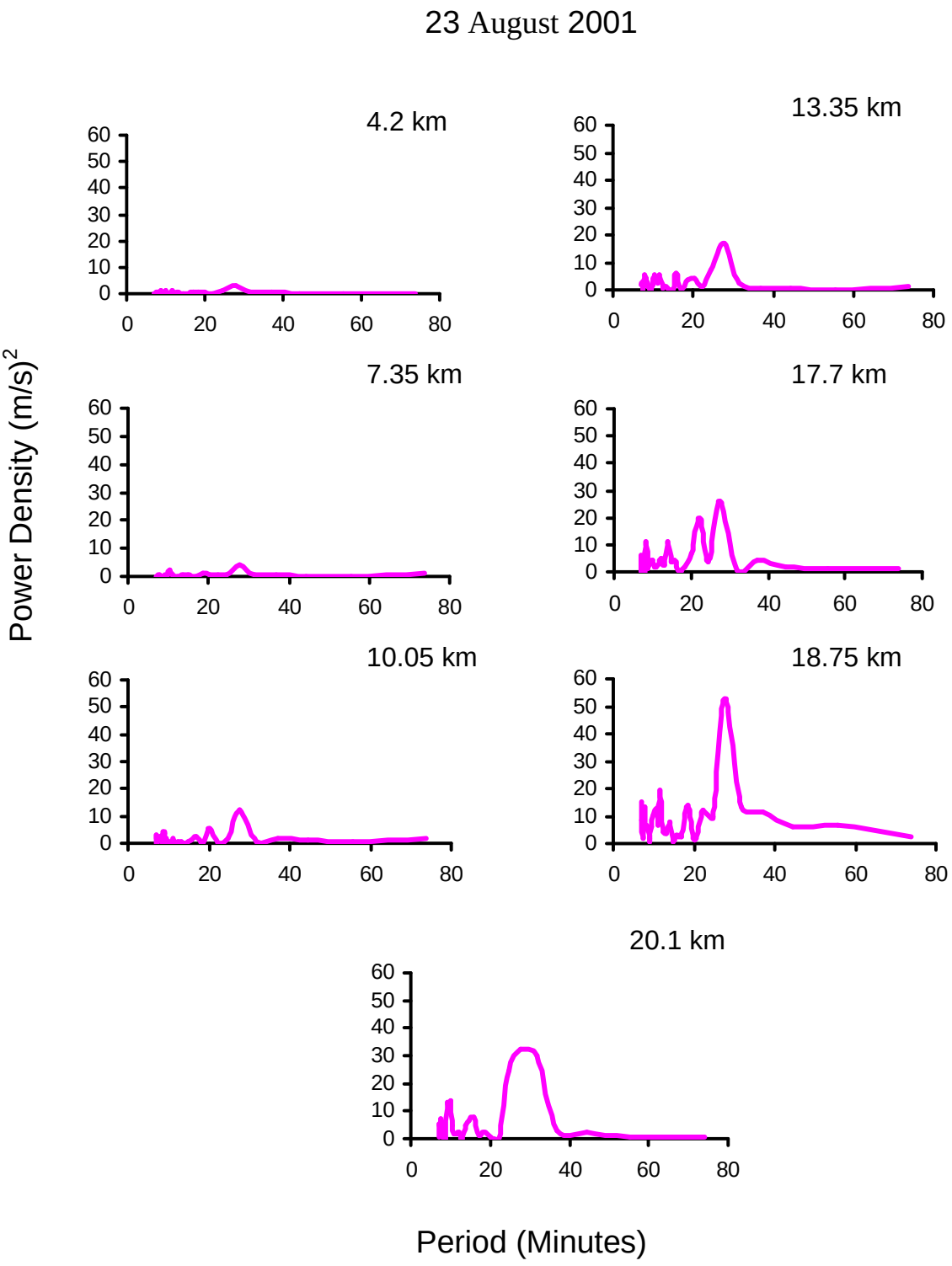

Figure -4.4 (c) Power Spectrum at different heights

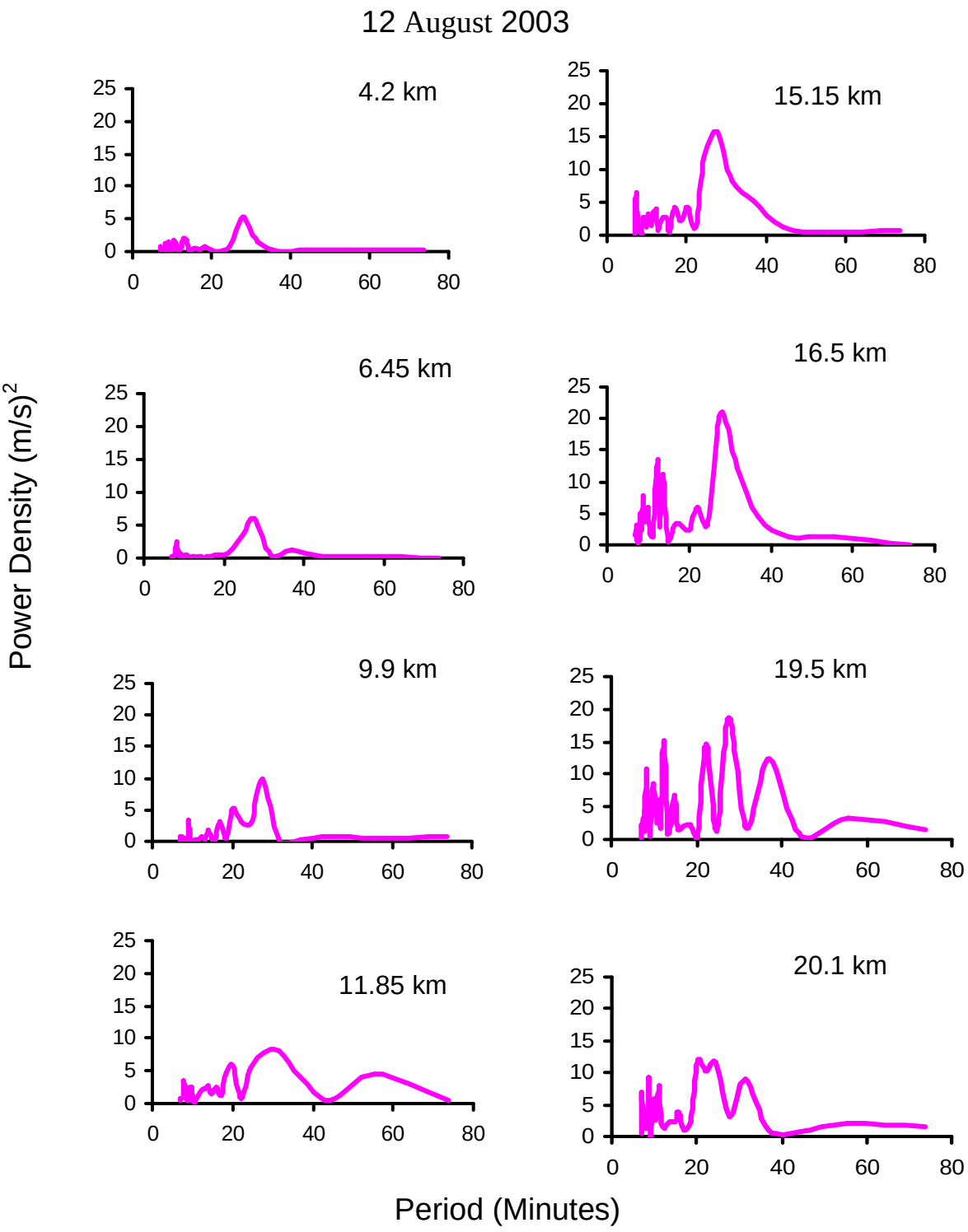

Figure -4.4 (d) Power Spectrum at different heights

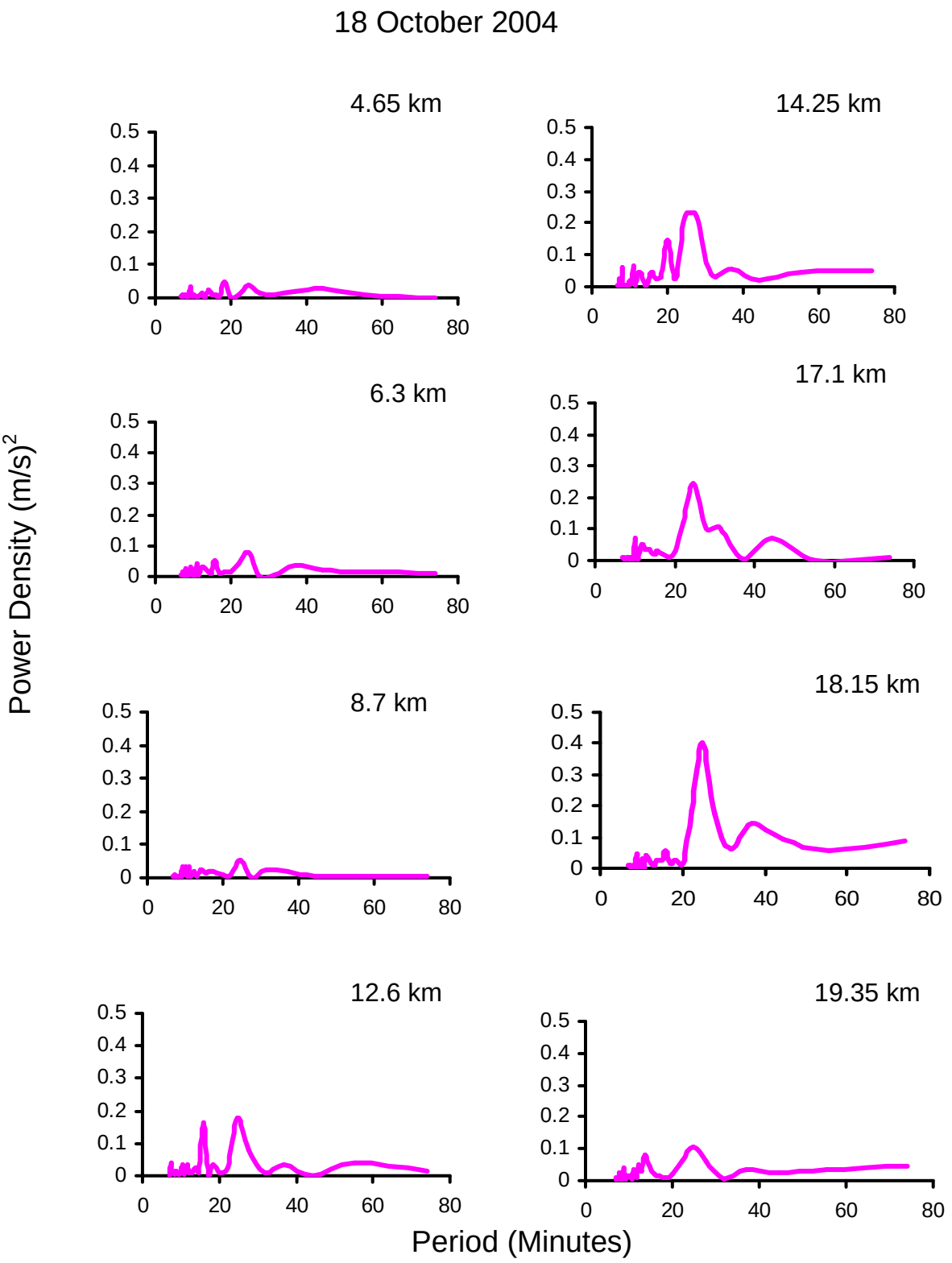

Figure -4.4 (e) Power Spectrum at different heights

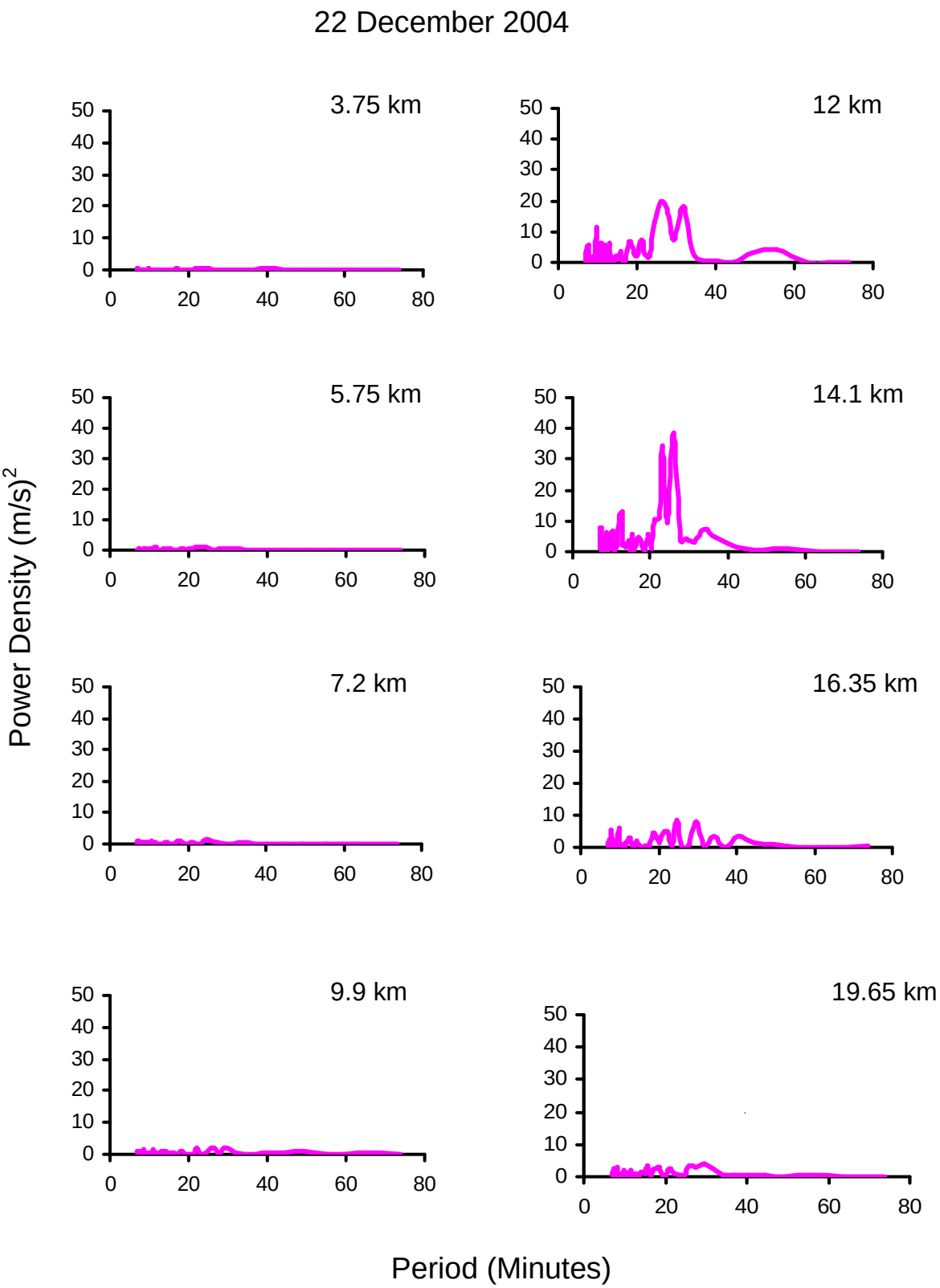

Figure -4.4 (f) Power Spectrum at different heights

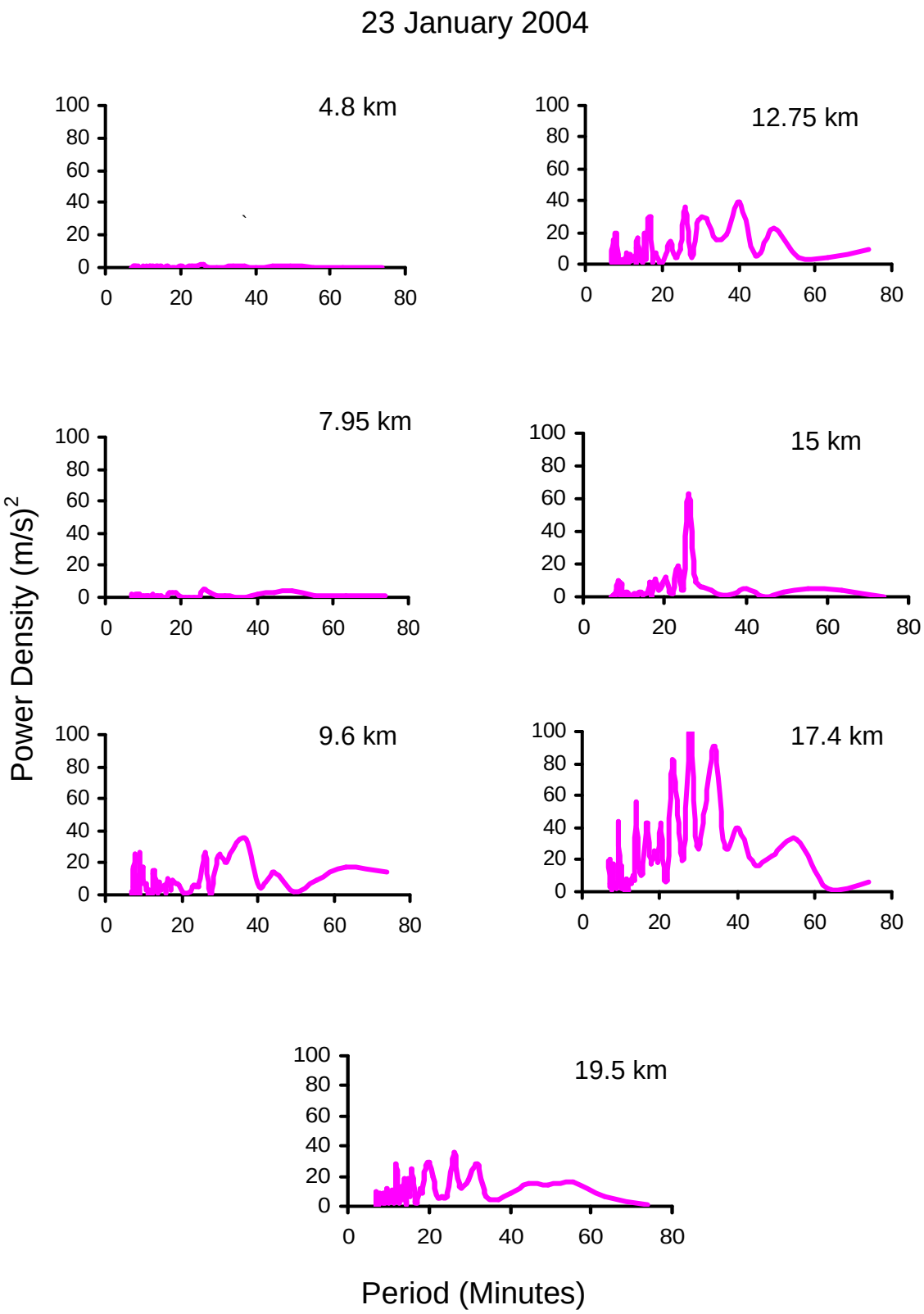

Figure -4.4(g) Power Spectrum at different heights

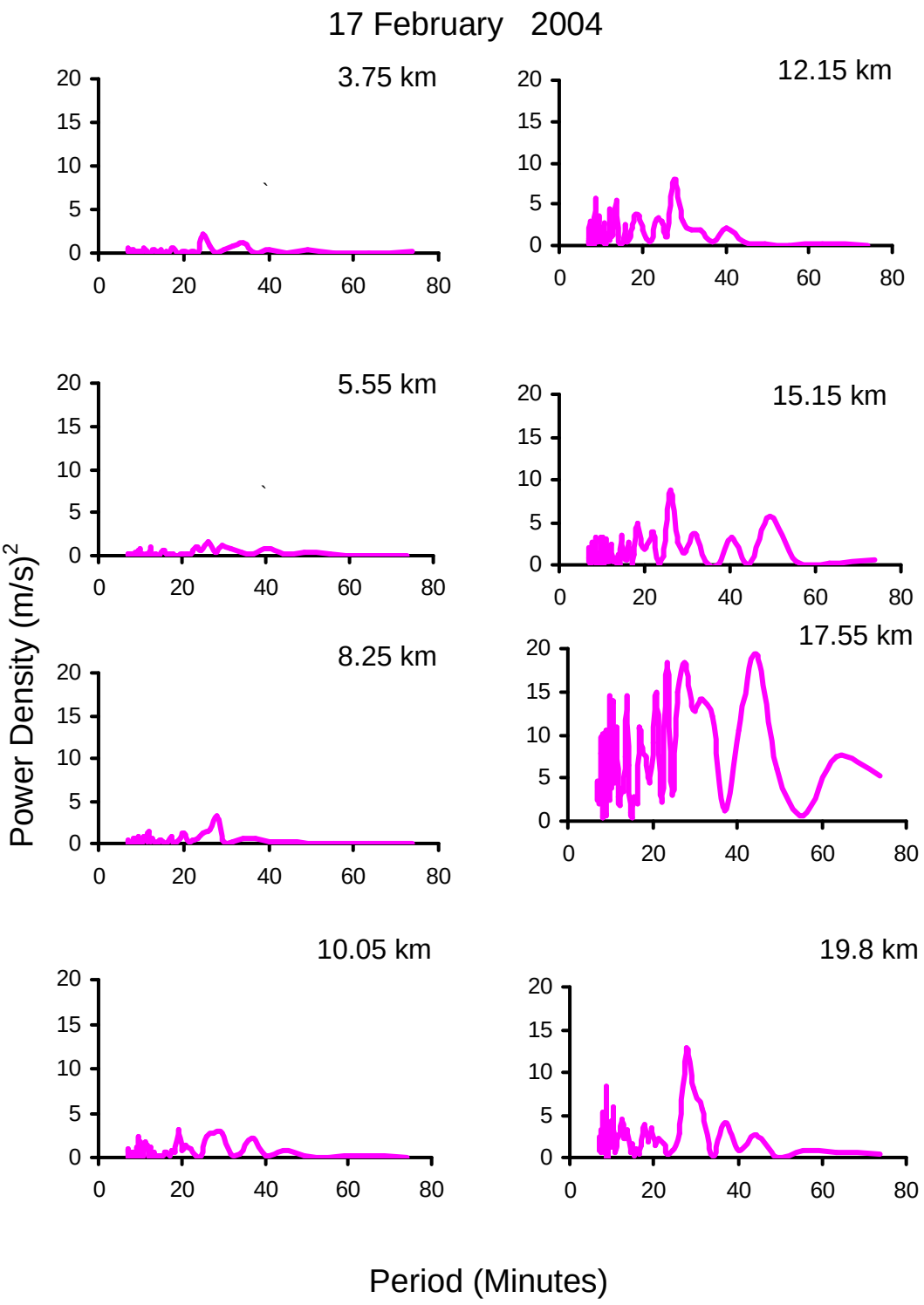

Figure -4.4 (h) Power Spectrum at different heights

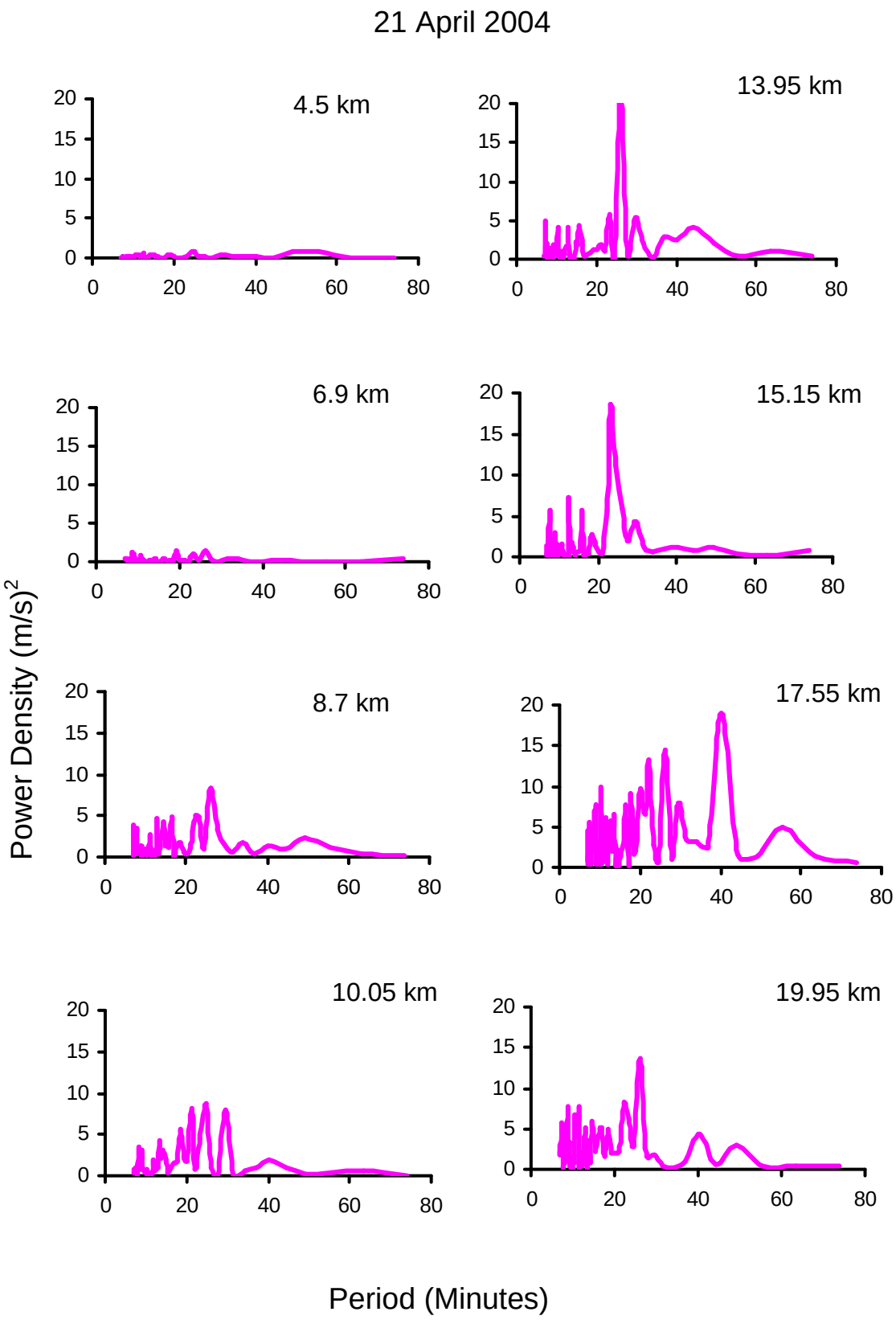

Figure -4.4 (i) Power Spectrum at different heights

one of major sources of the gravity waves Gopa Dutta et al. (1999) have estimated gravity wave variances of periodicity between 2-6 h in the lower atmosphere over Gadanki , India and variance estimated to range between ~0. 2 and 22 m^2 / s^2 . The short period gravity wave variance is found to be 1.5 to 2 times higher compared to long period ones.

Tsuda et al. (1994b) have shown that long period gravity waves with periods of 2-21 h are mainly generated near the ground, probably due to the interaction of the surface winds with topography, while short-period components (5min -2h) seems to be excited near the peak of the jet stream.

(C) Vertical propagation and wavelength from hodograph

We present here the propagation characteristics of dominant gravity waves. To find the vertical wavelength of the gravity waves, hodograph analysis of u', v' components is performed. Clockwise and counterclockwise rotation of the hodograph with altitude indicates the upward and downward phase propagation of a gravity wave respectively. The lengths of major and minor axis of an ellipse u' and v' correspond to wind velocity fluctuation due to a gravity wave. The intrinsic wave frequency ω can be determined from the ratio of the minor and major axes of the ellipse as

$$v'/u' = -i (f / \omega)$$

Where f is the inertial frequency. (Tuda et al.1994) Figure 4.5 (a) represents hodographs for 16 August 2001 for the tropopause at 13 km to 17 km. It clearly shows counterclockwise rotation with altitude which is consistent with the behavior of a gravity wave with downward phase propagation and upward energy propagation. Vertical wavelength of the gravity wave inferred from hodograph is ~5 to 6 km.

Form hodograph for 21 August 2001 we can see that wind vector rotate anticlockwise between 12 to18 km and is indicative of downward phase and upward energy propagation (Figure 4.5 a) . Vertical wavelength of the gravity wave has observed on this day from hodograph is ~5 to 6 km while on 23 August 2001 clockwise rotation with the altitude has been seen which is consistent with the behavior of a gravity wave with upward phase propagation

and downward energy propagation between 12 to 17 km . so the source of the gravity wave should be above 17 km. From Figure 4.5a we observed vertical wavelength of the gravity wave ~5 to 6 km on both the days.

From the hodograph for 12 August 2003 we have seen that wind vector rotate anticlockwise between 10 to14 km and has indicates of downward phase and upward energy propagation (Figure 4.5 a) . Vertical wavelength of the gravity wave has observed on this day from hodograph has ~4 km

In Figure 4.5 b presents hodographs of 23January shows counterclockwise rotation with the altitude which is consistent with the behavior of a gravity wave with downward phase propagation and upward energy propagation. Vertical wavelength of the gravity wave inferred from hodograph is ~4 to 5 km.

From hodograph observed on 17 February 2005 we have seen that wind vector rotates anticlockwise between 14 to 17 km and is indicative of downward phase and upward energy propagation (Figure 4.5 b). Vertical wavelength of the gravity wave is observed on this day from hodograph ~5 to 6 km while on 21 April 2005 anticlockwise rotation with the altitude has been shown which is unswerving with the behavior of a gravity wave with upward phase propagation and downward energy propagation between 10 to 18 km .From figure we had shown vertical wavelength of the gravity wave ~7 to 8 km on this day.

If energy propagates downward from an elevated source then there will be a possibility of mixing of this energy with energy propagating upward from ground level sources and cause a turbulence in structure between the height region about 14 to 17 km and gives a maximum amplitude. Williams and Avery (1996) have suggested a probable source near 14 km where the largest meridional wind amplitude is observed and also suggested the solar radiative heating of cloud tops and cirrus clouds distribution by deep convection in the tropics as a possible source.

Form the hodograph analysis the vertical wavelength observed almost all the cases is ~ 5 to 6 km and upward propagating gravity waves were detected

while on 21 August 2001 the down ward energy propagating waves were observed.

(d) Momentum Fluxes

The surface zonal winds in the tropics are predominantly from east to west. However considerable amount of angular momentum gained by the tropical boundary layer atmosphere is transported vertically upwards in to the middle and upper tropical troposphere. Thus the momentum flux transfer studies lead to the understanding of turbulence and related parameters. These further explain the energy budget of the atmosphere.

The altitude variation of vertical flux of zonal and meridional momentum carried by the wave modes present in the data has been computed using direct method suggested by (**Sasi et al. 1999).** The momentum flux plotted is averaged over a period of about 4-6 hours observation each day for the month of August (2001-2003) and shown in figure **4. 6 a-f.**

The magnitude of zonal momentum (left panel) is less compared to the meridional flux (right panel). The values of zonal momentum flux is in the range of +1 to -1 $(m/s)^2$ while the meridional momentum flux varies from +0.5 to - 0.5 $(m/s)^2$. Both the components of the flux show the signature of appreciable increase after 12 km altitude**.** The positive values of Zonal momentum fluxes indicate transport of eastward momentum and negative values of Zonal momentum fluxes show transport of westward momentum. During the month of August 2002 less value observed compare to other two years (2001 and 2003) of zonal and meridional momentum, it varies from – 0.3 to 0.3 $(m/s)^2$ and -0.2 to +0.3 respectively which is shown in figure 4.6 (c, d).

For the month of the October the variation of zonal momentum flux is in the range of +0.05 to-0.05 $(m/s)^2$ and the meridional momentum flux varies from +0.03 to -0.03 $(m/s)^2$ while during the November the zonal momentum flux is in

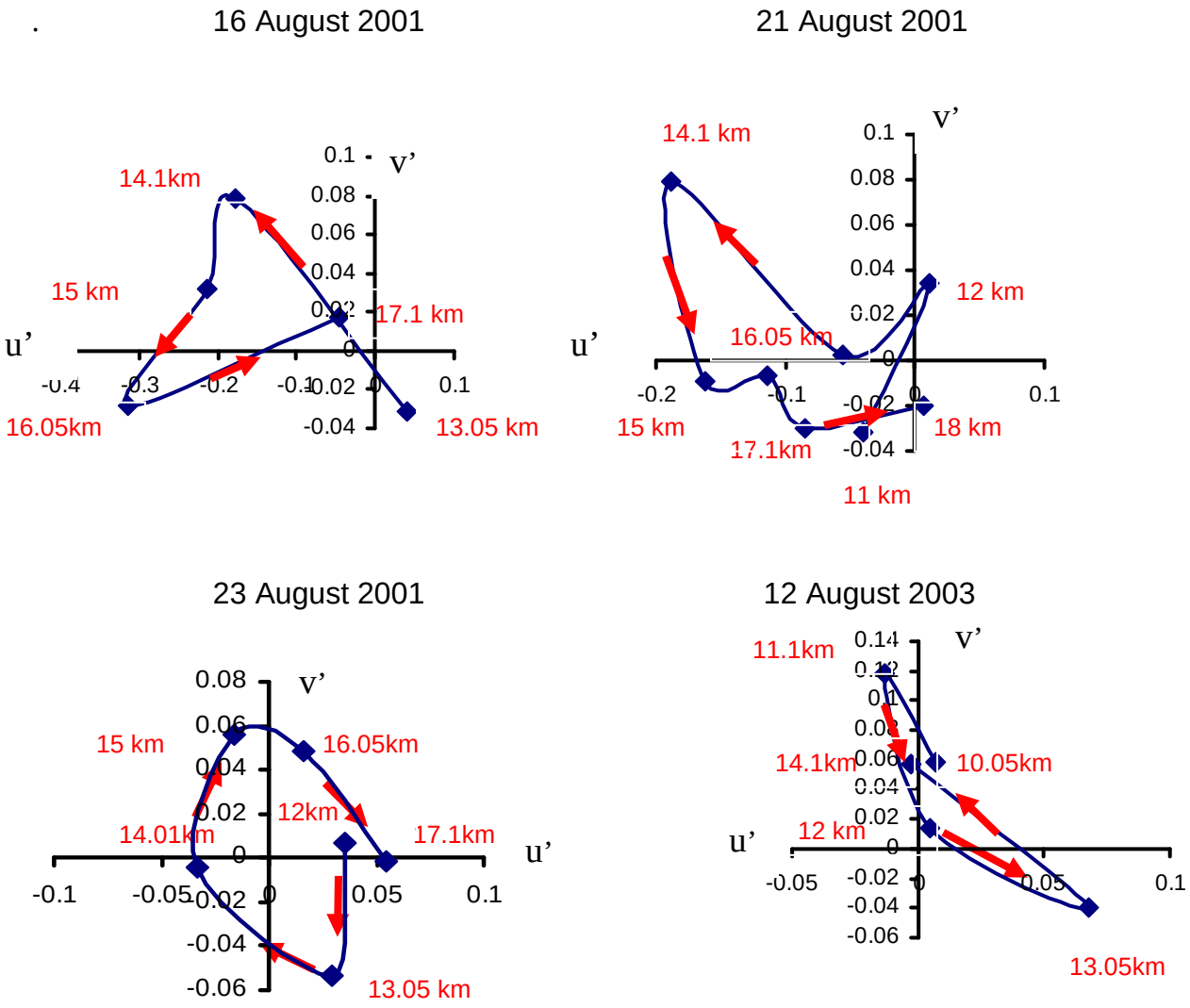

Figure -4.5 (a) Hodograph showing vertical wavelength the direction of rotation with increasing height is shown by arrows;

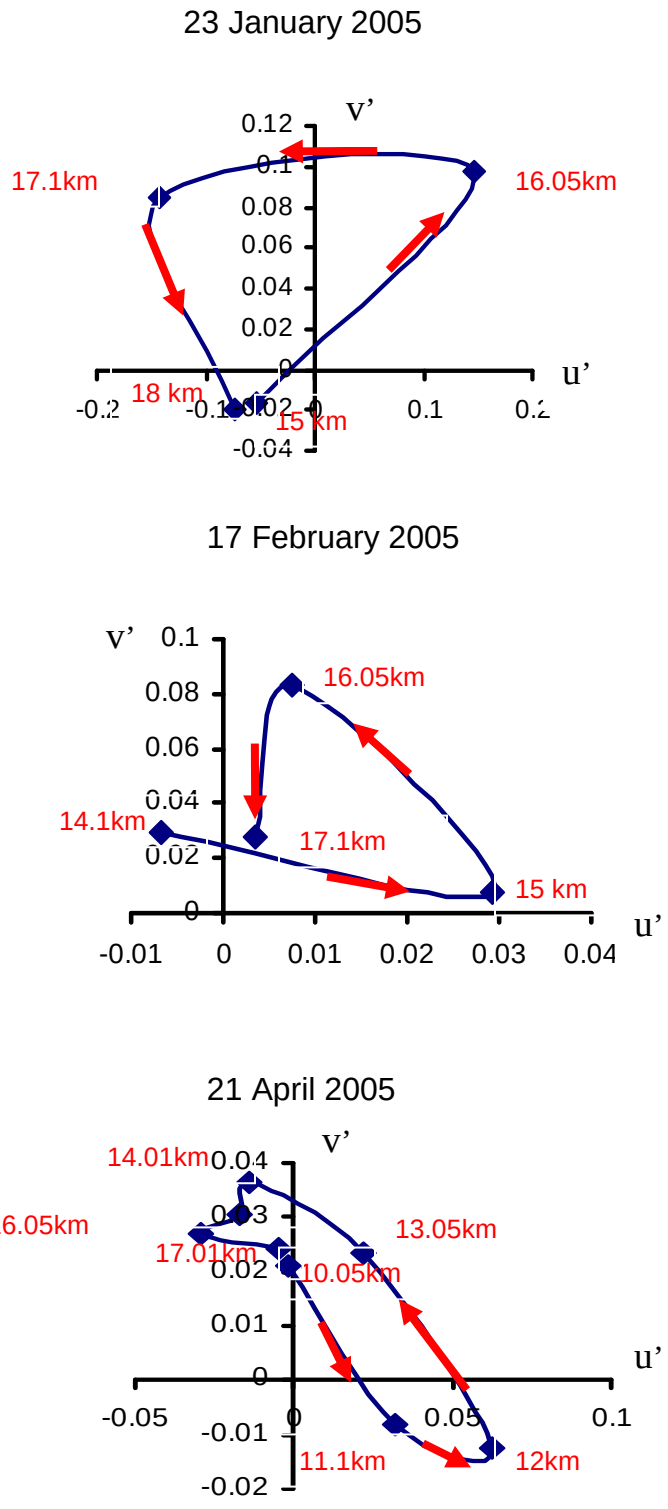

Figure -4.5(b) Hodograph showing vertical wavelength the direction of

the range of +0.5 to -0.5$(m/s)^2$ and the meridional momentum flux varies from +0.2 to -0.2$(m/s)^2$. it is observed in Figure 4.6(g,h,i)

During December 2004, variation is observed in both zonal and meridional momentum fluxes. The magnitude of the zonal and meridional momentum flux varies between +0.3 to -0.3 and +0.02 to -0.8 respectively which is indicate in the figure 4.6 (j)

During the month of the January and February 2005 both zonal and meridional fluxes fluctuate between -0.5 to 0.6 $(m/s)^2$ and +0.6 to -0.5 $(m/s)^2$ in 8 to 18 km altitude respectively. Whereas, for the period of the month February the zonal momentum flux +0.6 to -0.6 $(m/s)^2$ is much more than that of meridional flux -0.05 to 0.05 $(m/s)^2$.which are shown in Figure 4.6 (,k,l,m)

The variation of zonal momentum flux for the results of April 2005 is in the range of +0.5 to -0.3 $(m/s)^2$ while the meridional momentum flux varies from +0.03 to -0.5 observed in Figure 4.6 (n) The momentum flux values are found to be large at heights where velocity variance is large.

The values of the zonal and meridional momentum flux are quit comparable to the values obtained by Fritts et al (1990) using MU radar and Narayan Rao et al., (1997) using Indian MST Radar. Dhaka et al. (2001) have estimated the vertical fluxes of zonal and meridional momentum and found them to be in the range of -0.6 to 1 (m^2/s^2) and -.3 to 0.3 (m^2/s^2) respectively. Vertical flux of Zonal momentum in the troposphere and lower stratosphere have been studied by Prabhakaran Nayar and .Sreeletha (2003) the value of zonal momentum around -1.5 to 0.2 (m^2/s^2) at 16 km altitude.

The pattern of zonal and meridional momentum flux is closely related to the background wind pattern. The zonal momentum flux tends to be large and negative where the mean zonal wind velocity is westward with a negative wave number vector (Sato, 1990).For the meridional wind such a correlation can also be seen. The magnitude of meridional momentum flux is nearly one tenth of the magnitude of the zonal momentum flux. This may be due to the lack of significant anisotropy of meridional wave activity. The present result observed maximum

momentum flux during the August month (Figure 4.6) the magnitude of the zonal and meridional momentum fluxes lies between 1 m^2/s^2 and -.9 m^2 / s^2 and 0.3 and -.3 m^2 / s^2 . Here the magnitude of the zonal momentum flux is small then it is increasing with height this represents that the waves are assumed to be generated in the lower part of the atmosphere and upward propagating waves are dominating.

4.4 Conclusion

Overall, Results seem reasonable and the variance, and momentum flux estimates appears to agree with those of previous studies. Results obtained from the analysis of the data leads to the identification of strong wave activity between 14 to 17 km in the troposphere. Maximum value of the variance has been observed in August 2001 and January 2005 at a height about 14 to 17 km and very less variance observed on October 2004. From the power spectral analysis maximum power density is observed during all the seasons at altitude of ~ 16 to 18 km. No activity has been observed during 18 October 2004. Vertical wavelength is inferred from the hodograph ~5 to 6 km and energy propagated upward during all the days (except 23 August 2001) which is shown in figure 4.5 (a, b) while on 23 August 2001 downward energy propagation is observed. The maximum momentum fluxes is observed during the August month (Figure 4.6) the magnitude of the zonal and meridional momentum lies between 1 m^2/s^2 and -.9 m^2 / s^2 and 0.3 and -.3 m^2 / s^2 and minimum momentum flux is observed during the October 2004 the magnitude of both the zonal and meridional momentum vary between 0.05 to -0.05 and -0.03 and -0.03 m^2/ s^2.

The present results indicate that the values of variance and momentum flux increase with height and reach a maximum around 14 to 17 km. The power spectra also show that the power density increases with height and reaches maximum around 14 to 17 km. This clearly shows that sources of the gravity waves are located in the troposphere and that waves propagate upward, sometimes reaching upto the stratosphere.

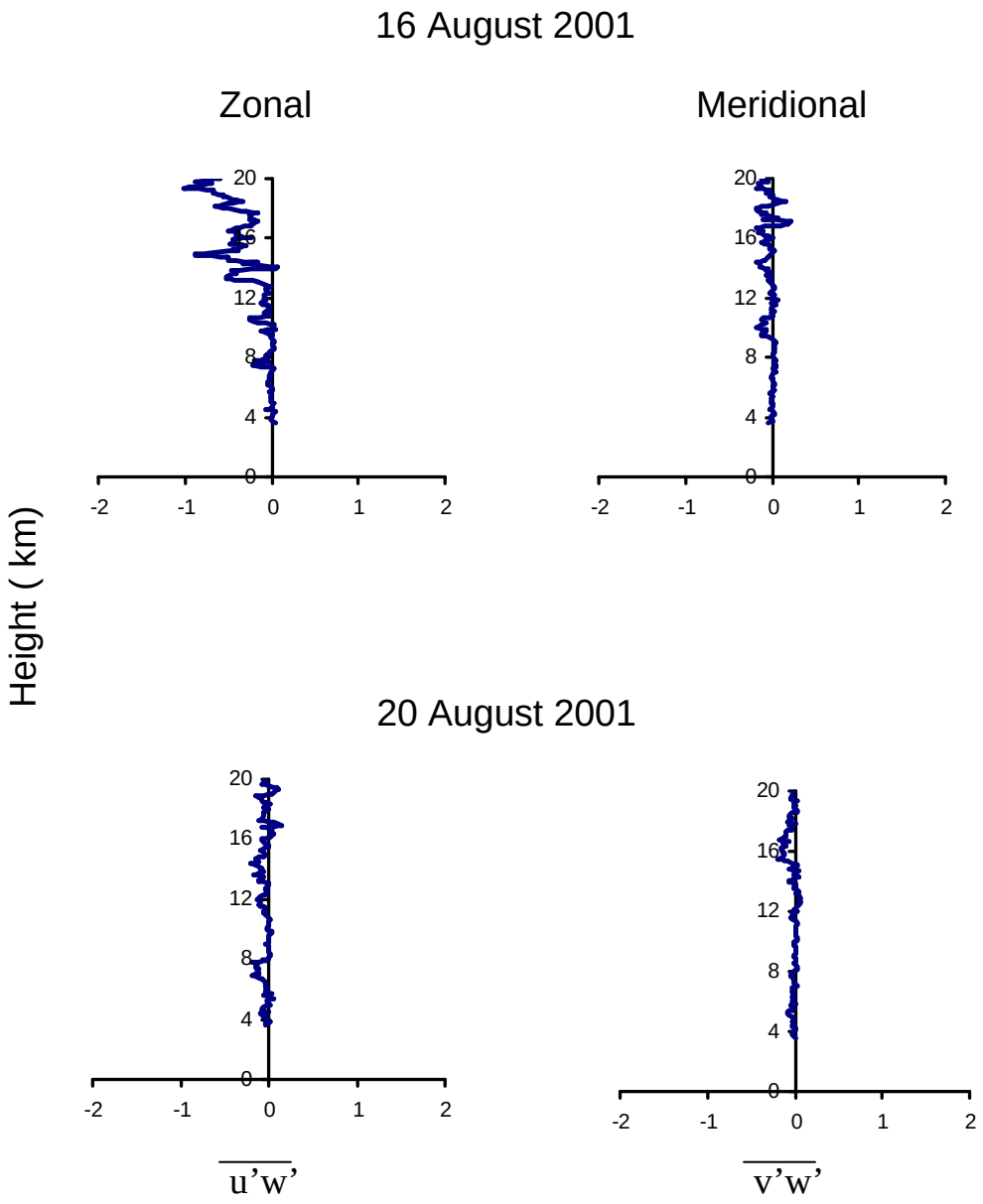

Figure 4.6(a) : Zonal and Meridional momentum flux with height

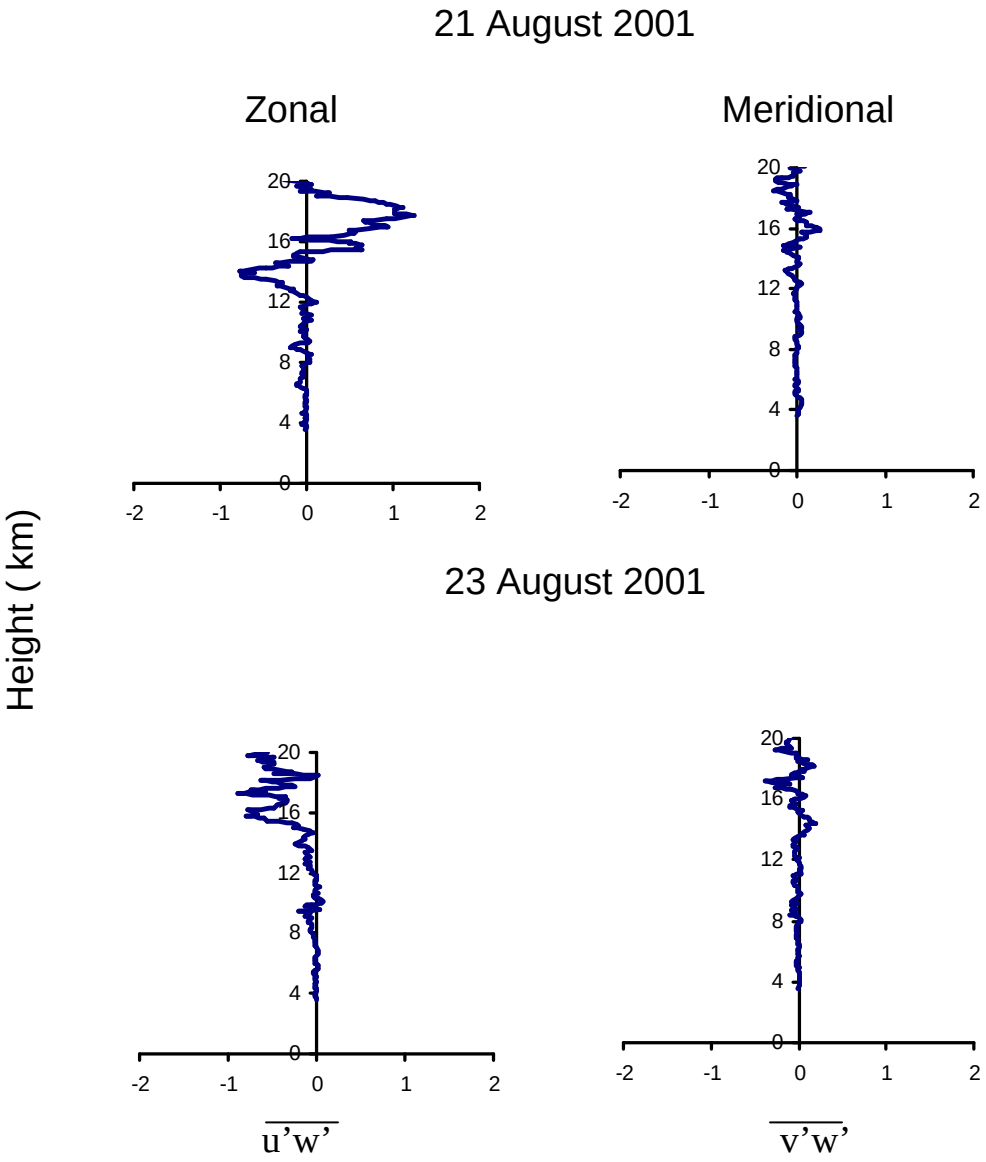

Figure 4.6(b) : Zonal and Meridional momentum flux with height

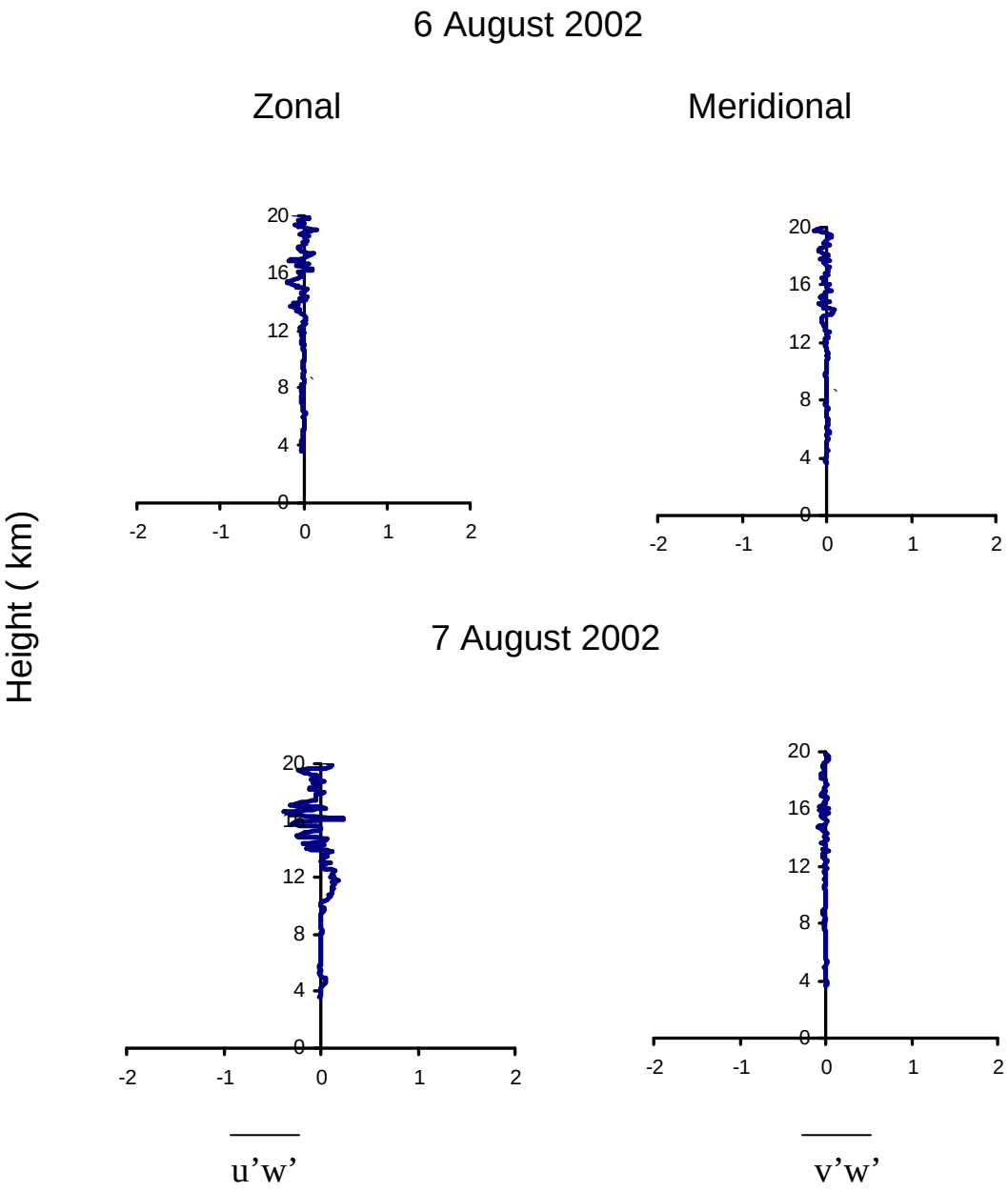

Figure 4.6(c): Zonal and Meridional momentum flux with height

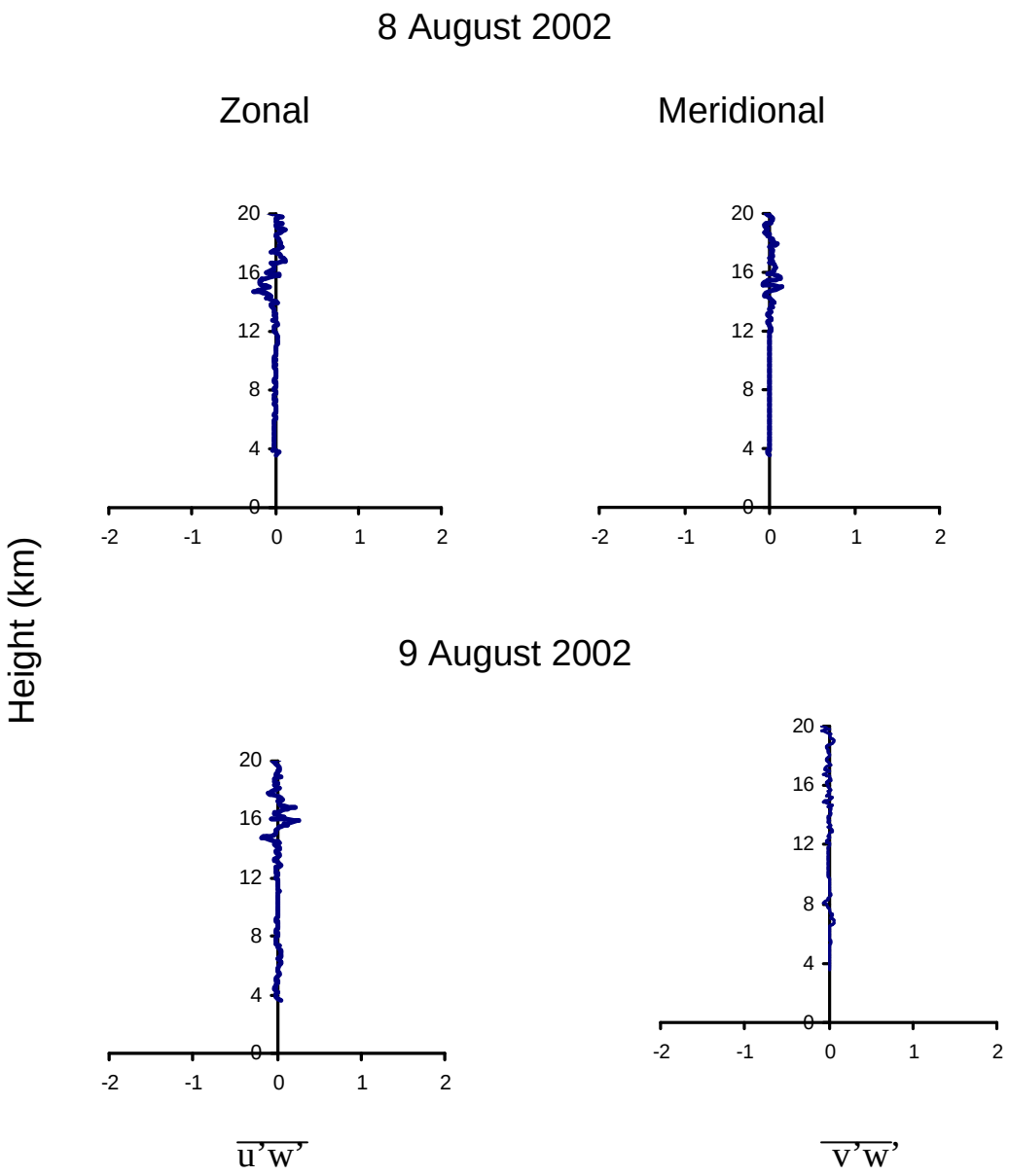

Figure 4.6(d): Zonal and Meridional momentum flux with height

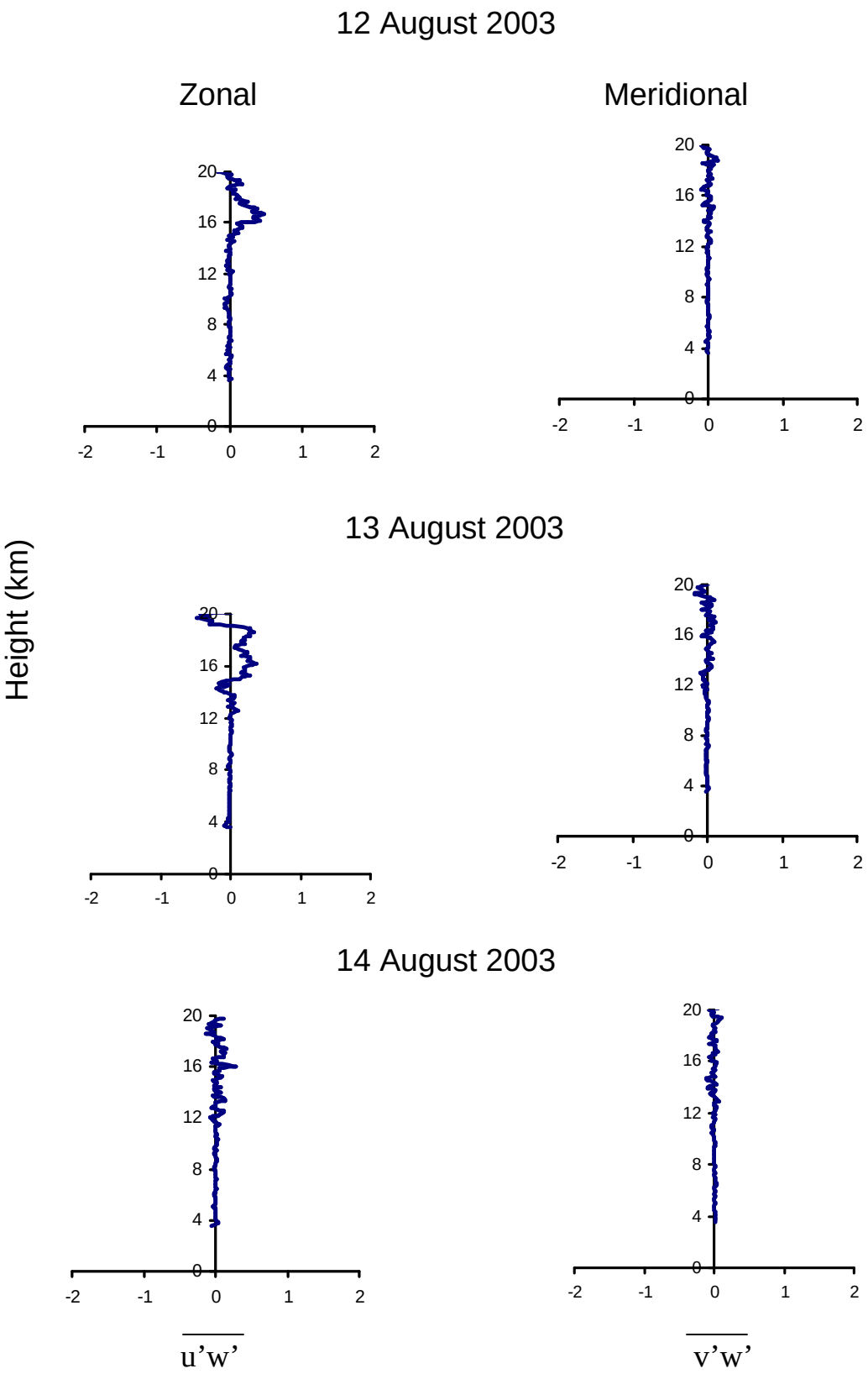

Figure 4.6 (e) : Zonal and Meridional momentum flux with height

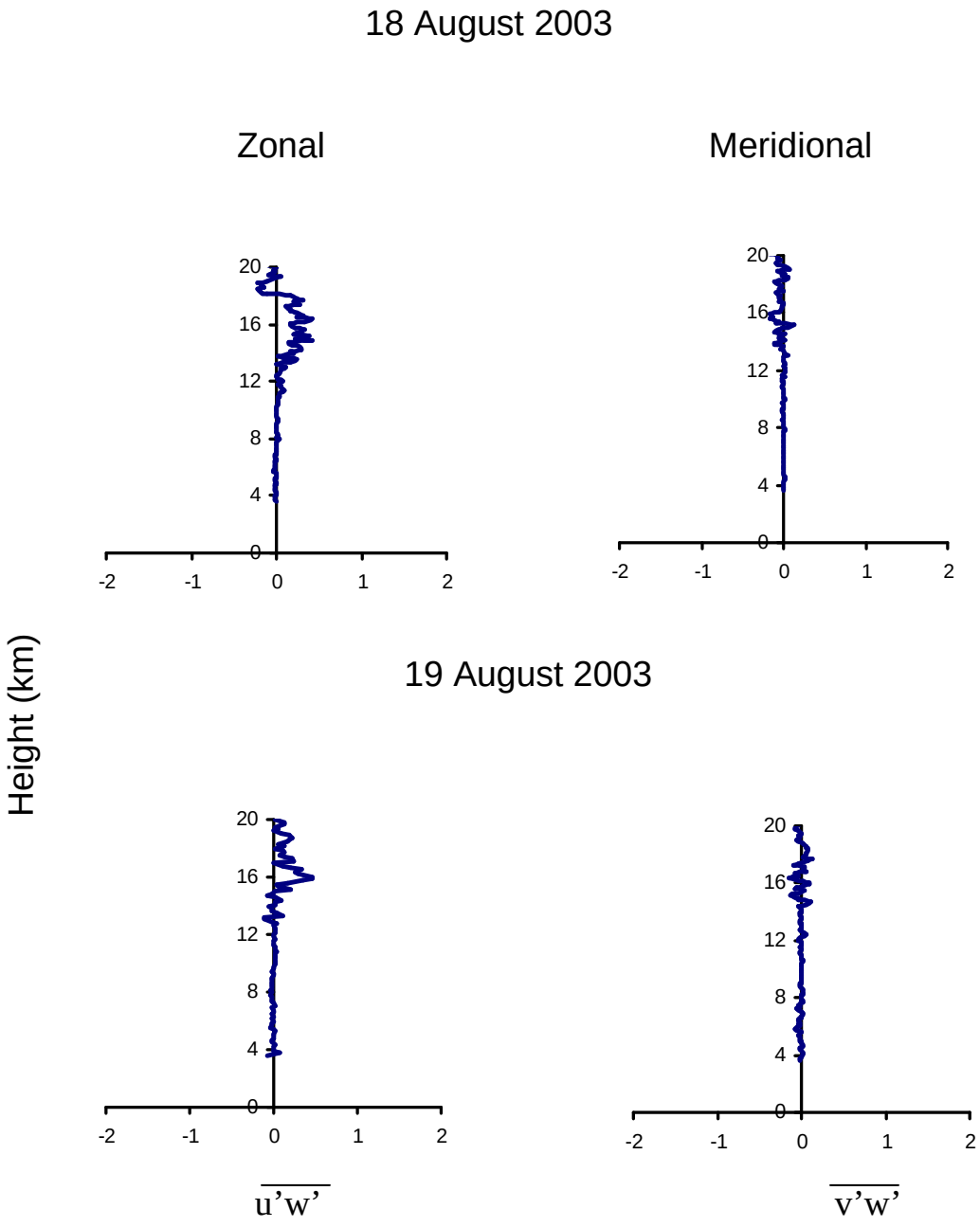

Figure 4.6 (f) : Zonal and Meridional momentum flux with height

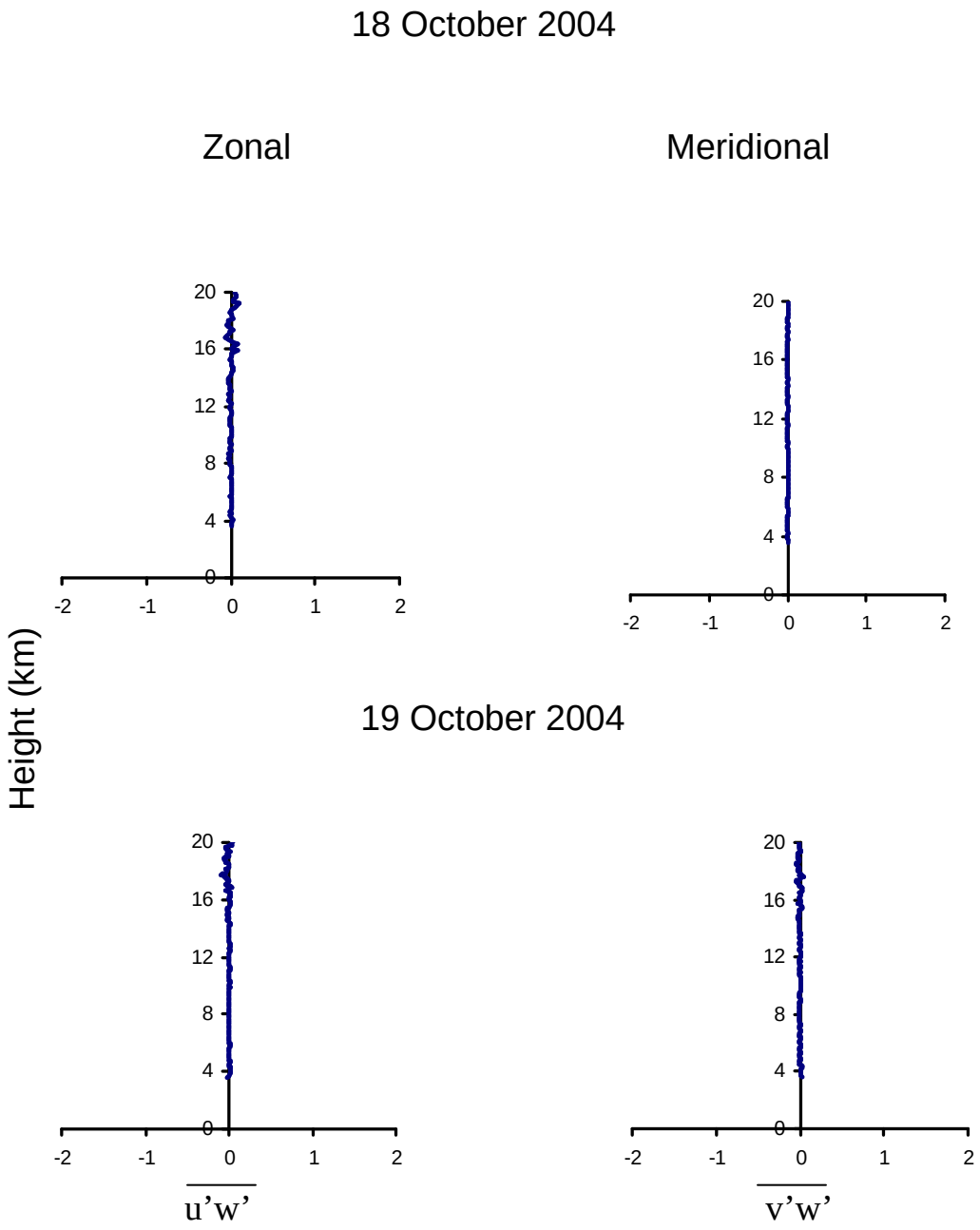

Figure 4.6 (g) Zonal and Meridional momentum flux with height

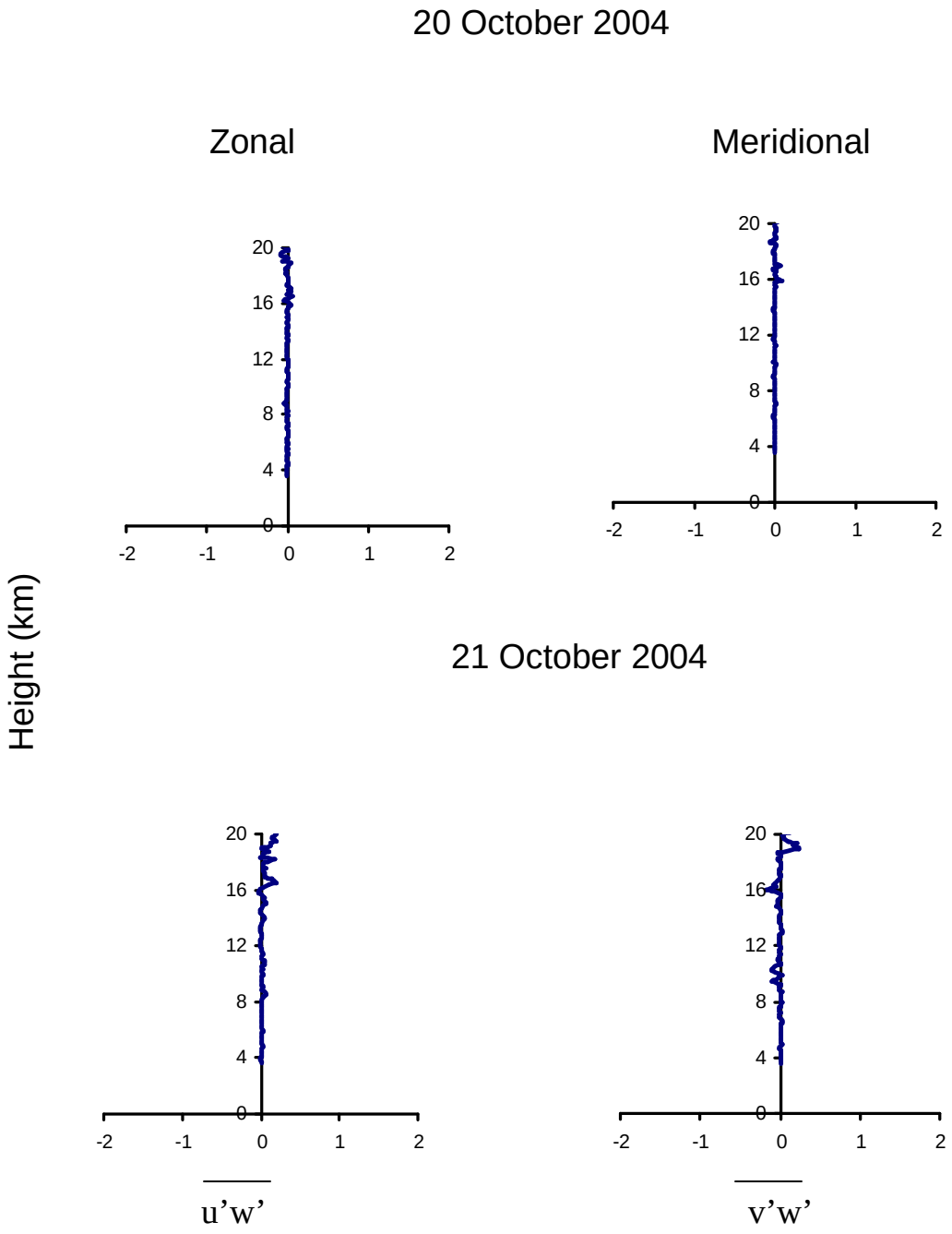

Figure 4.6 (h) Zonal and Meridional momentum flux with height

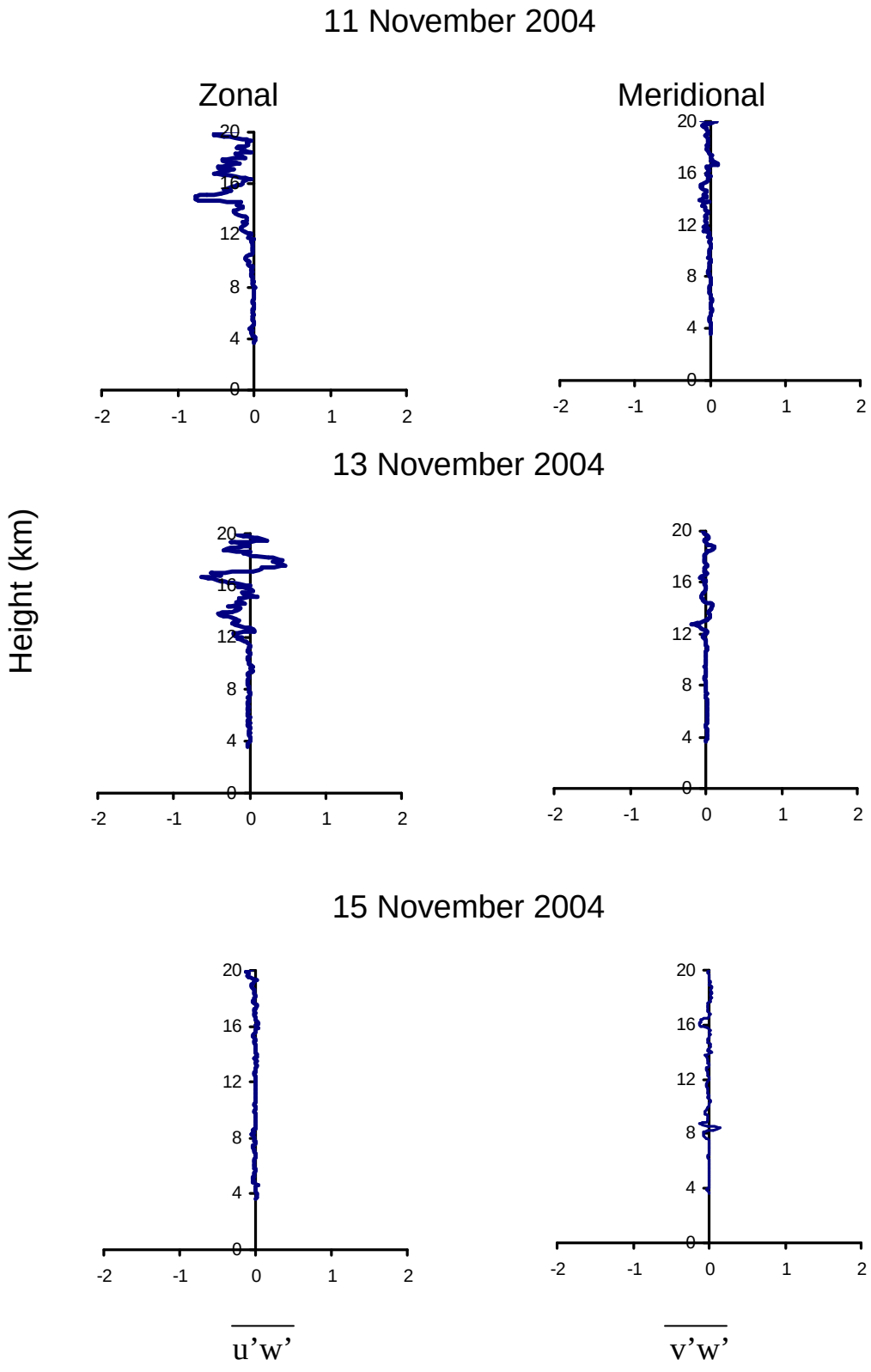

Figure 4.6 (i) Zonal and Meridional momentum flux with height

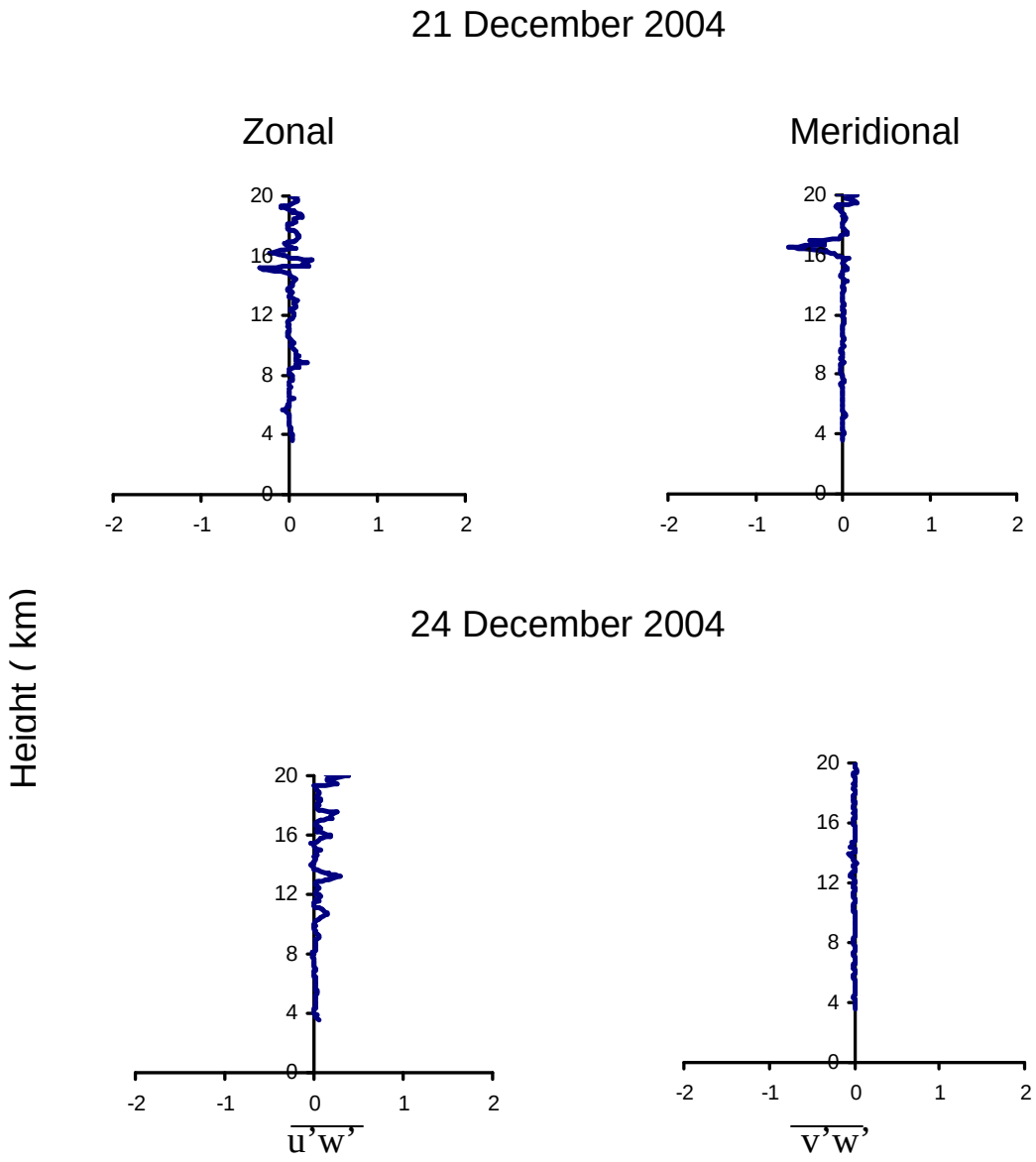

Figure 4.6 (j) Zonal and Meridional momentum flux with height

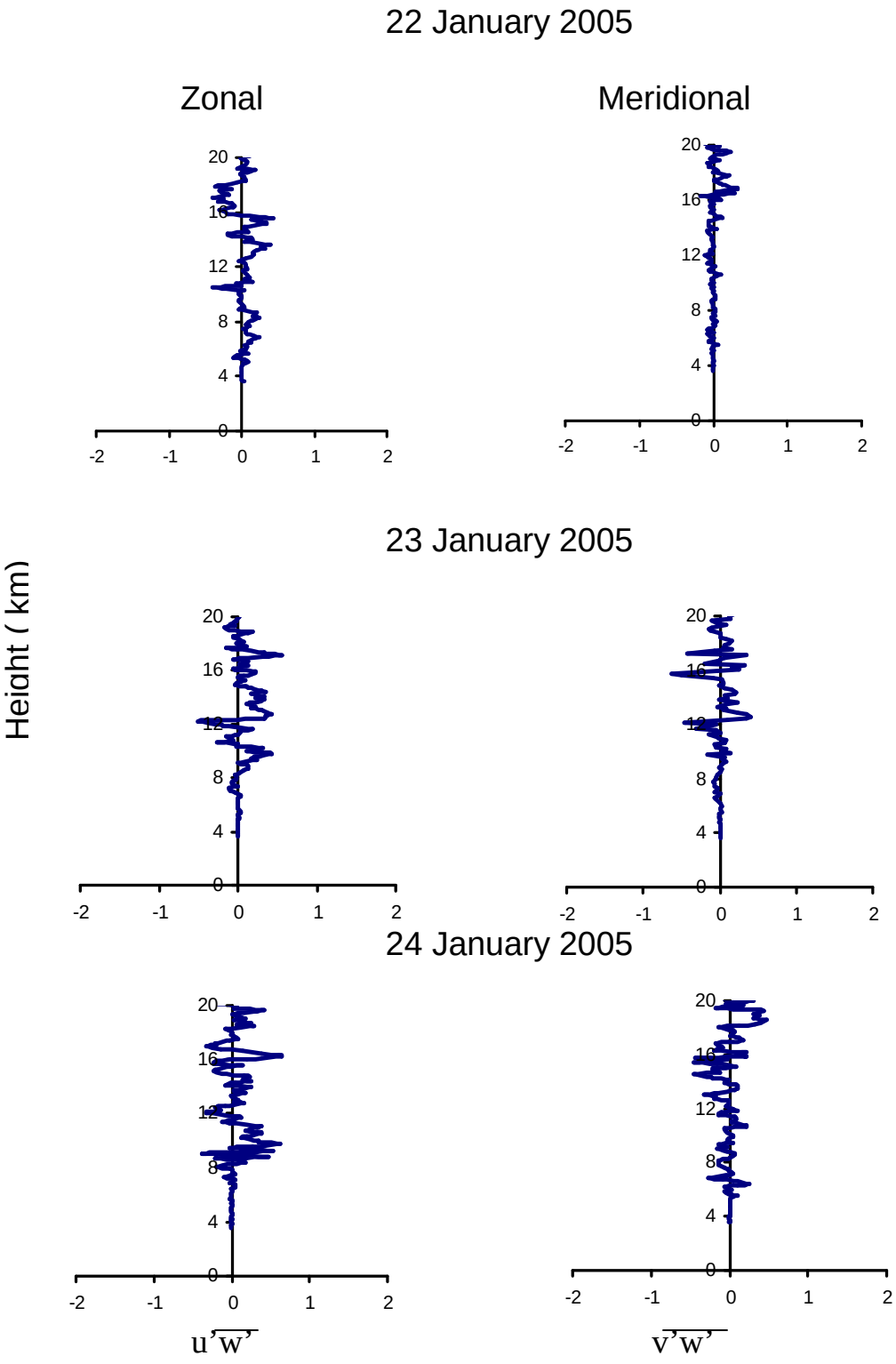

Figure 4.6 (k) Zonal and Meridional momentum flux with height

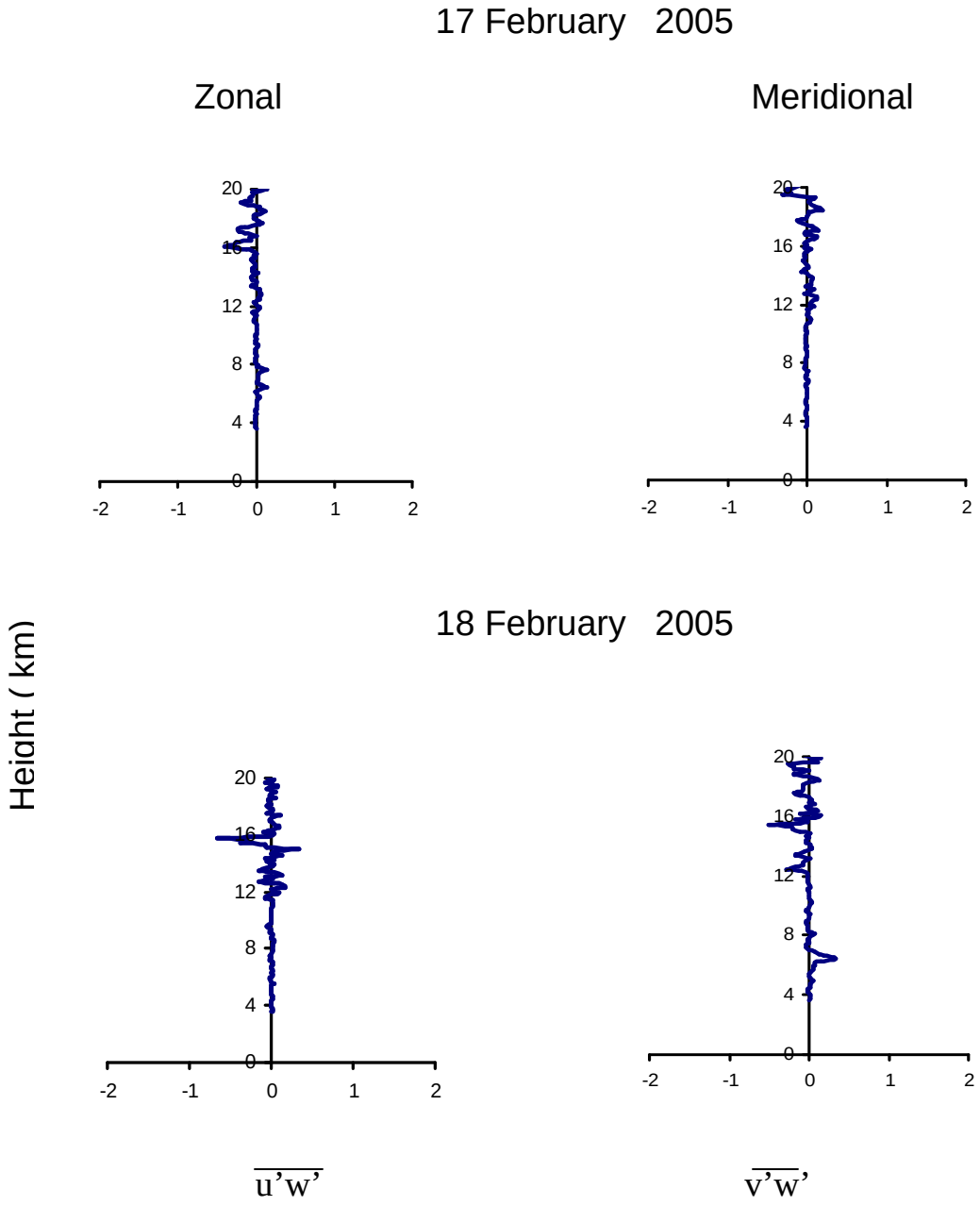

Figure 4.6 (l) Zonal and Meridional momentum flux with height

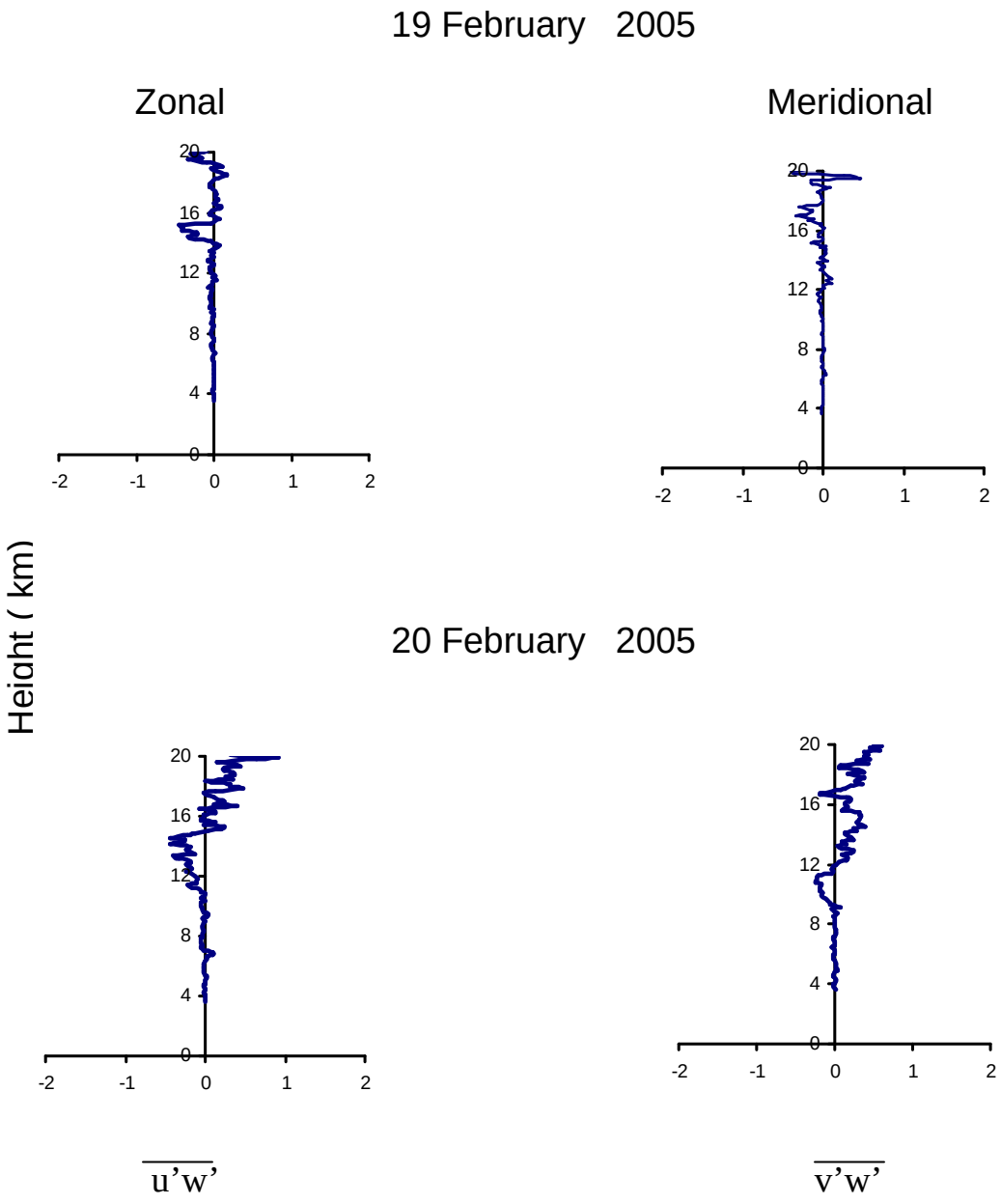

Figure 4.6 (m) Zonal and Meridional momentum flux with height

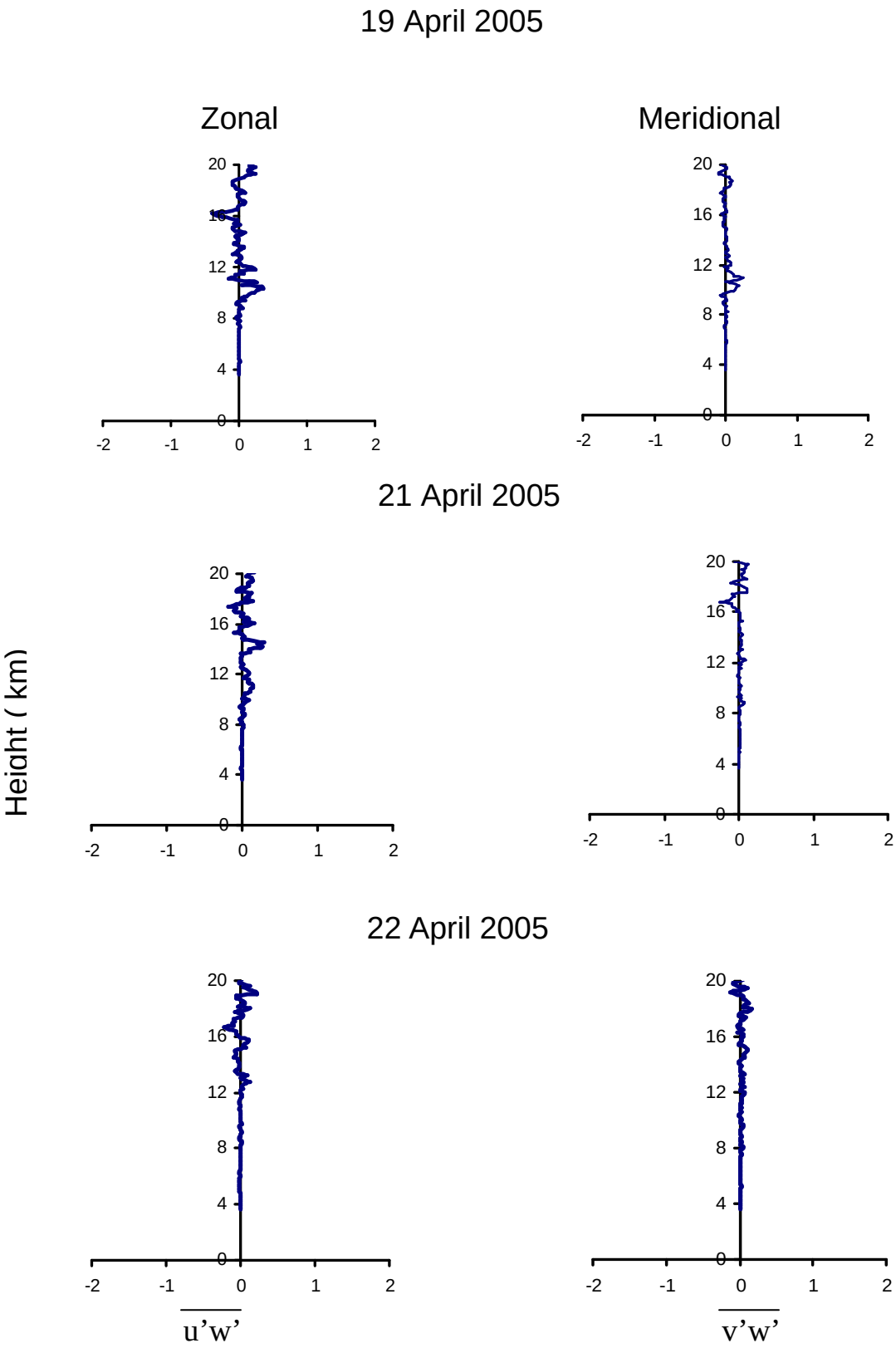
19 April 2005
Zonal
Meridional
21 April 2005
Height (km)
22 April 2005
u'w'
v'w'

Figure 4.6 (n) Zonal and Meridional momentum flux with height

5.1 Summary of the present thesis

The main objective of this thesis is to study atmospheric dynamics in the troposphere and lower stratosphere by using wind observations made with MST Radar at Gadanki (13.5^{o} N 79.1^{o} E), a tropical station.

Wind observations were made at Gadanki (13.5^{o} N 79.1^{o} E) by Indian MST radar for few days in monsoon August (2001-2003), post monsoon (October, November 2004, winter (December 2004, Januray 2005, February-2005) and summer (April 2005). The mean zonal wind is found to be westerly between December to April and easterlies between August to November. The trend is opposite in the lower troposphere. A strong easterly jet (~ 40 m/s^{-1}) is observed during monsoon (August) between 14 to 18 km. Meridional wind velocity ranges between +10 to -10 and is found to be predominantly northerly. Time series of u, v and w are obtained at height intervals of 150 m from these wind profiles. The length of the time series in the present study is 4-6 hrs. A ten point moving height average is subtracted from the observed values of u, v and w to obtain the fluctuations u', v', w'. some signatures of the wave like structures are observed in the vertical profiles of u', v', w'. These are attributed to Gravity wave signatures. The characteristics of the wave like structure observed in the vertical profile in u', v', w' like range of periods, vertical wavelength, height range over which they exist have been determined and give here and concluded that they represent gravity wave signature.

The characteristics of the gravity wave like the variance, periodicity, vertical wavelength and associated momentum flux are describe in chapter IV. The mean variance is plotted as a function of height. A peak in variance is seen between ~ 14 to ~18 km for mostly in all seasons and maximum value observed during monsoon season and winter seasons particularly on 16 ,21 and 23 August 2001 and 23 , 24 January 2005 it reaches maximum value of 60 (m/s)^2 at around 16 to17 km . Similarly from the power spectra the maximum power density (~50 m^2/ s^2) observed during monsoon on 16, 21 and 23 August 2001 and (~100 m^2 /s^2) is observed during winter on 23 January 2005. The range of the period is same ~20-40 minutes in all seasons. The above results show that

convective activity in monsoon season is one of the major sources of the gravity waves. Form the hodograph analysis the vertical wavelength observed in almost all the ~ 5 to 6 km and upward energy propagation was detected while on 21 August 2001 the down ward energy propagation was observed. The present result observed maximum momentum flux observed during the August month. The magnitude of the zonal and meridional momentum lies between 1 m^2/s^2 and -.9 $m^2 / s^{2\ and}$ 0.3 and -.3 m^2 / s^2 . The magnitude of the zonal momentum flux is small at lower heights then it is increasing with height. This indicates that the waves are generated in the lower troposphere and that waves propagate upward and sometime reaching upto the stratosphere.

5.2 Future Work

The study of gravity waves in the present work has been a preliminary assessment of gravity wave activity in the lower atmosphere in the Indian tropical region. The MST radar at Gadanki (13^o N, 79^o E) will provide valuable data to have clearer understanding of such atmospheric process. Further work is planed to the comparison between the amplitude of gravity waves at different periods using wavelet analysis and FFT analysis. Advantage of the wavelet analysis is that, there is no loss of time information compared to FFT and also better spectral resolution at desired interval.

References

Alexander, M J., and L. Pfister	1995	Geophys. Res. Lett ., **22 ,** 2029-2032.
Anandan V.K	1997	Atmospheric Data processor, Technical and user reference manual, National MST Radar Facility.
Asnani, G.C.,	1993	In: Asnani, G,C. (Ed.), Tropical Meteorology, Vol 1 and 2.
Balsley, B.B. and Gage, K.S	1980	J. Pure and Appl.Geophys.,**118,**452
Booker H. G., and W.E. Gordon	1950	Proc IRE (USA), **38,** 401**.**
Bougeault P. et al., (incluant B.Carissimo),	1993	Ann. Geophys., **11,** 395-418.
Brasseur G, A Derudder, G M Keating, M C Pitts	1978	J.Geophys. Res., **92,**903.
Chamberlain, J. W	1978	Int. Geophys. Series,**22, Academic press**
Chang, J. L., Avery, S.K., Riddle, A. C., Palo, S.E., and Gage, K.S.	1997	Radio Sci., **32**, 727-748.
Dhaka, S.K., Devrajan, P.K., Shibagaki, Y., Choudhary, R.K. , Fukao, S.	2001	J. Atmos, Terr, Solar Phys.,**63,** 1631**-** 1642 **.**
Eliassen and., and Palm, E.	1960	Geofysiske Publikas Joner (Oslo) .,**22**, 23.
Evan J. V.	1969	Proc IEEE (USA) **57,** 496.
Farley D. T.,	1966	J. Geophys. Res., **71,** 4091.
Farly D.T.,	1983	MAP Handbook, Ed. S A Bowhill And B Edwards, **9 ,** 71.

Friend A.W.,	1949	Proc IRE, **37**,116.
Fritts D C	1982	J. Atmos Sci., **39**,1936
Fritts D C	1984	Rev. Geophysics., **22** , 275.
Fritts, D.C., T.Tsuda, T.E. VanZandt, S.A. Smith, T.Sato, S. Fukao, and S. Kato	1990	J. Atmos. Sci., **47,** 51-66
Fritts D C and G D Nastrom	1992	J Atmos Sci ,**$9**, 111.
Fukao S., T Sato., S Kato, R. M . Harper, R.F.Woodman., and B. Edwards.,	1978	J. Geophysics. Res., **85,** 4379.
Fukao, S., T. Sato, T. Tsuda, S. Kato, M Inaba, and I. Kimura,	1988a	J. Atmos. Oceanic. Technol., **5,** 57-69.
Gage, K.S and Balsley, B.B.	1980	Radio Sci.,**15**, 243.
Gage K.S., and J.L. Green.	1978	Radio Sci., **13,** 991.
Gossard, E.E.,	1962	J. Geophys. Res., **67,** 745-757.
G . Dutta., B.Bapiraju., P. Balasubrahmanyam., H. Aleem Basha	1999	Ann. Geophy., **17 ,** 1012-1019.
Harper R. M	1978	Geophys.Res.Lett., **5**, 784.
Hines C O	1991	J Atmos Sci **48,** 1360.
Hines, C. O.	1972	Space Res., **12 ,** 1157-1161.
Hitchman, M H., Bywaters, K. W., Fritts, D. C., Coy L. Kudeki, E., Surucu, F., and Woodman , R. F.	1992	J. Atmos. Sci., **49**, 2372.
Hood	1978	J. Geophys. Res., 92,839.
Houghton, J. T.,	1978	Q. J. R Meteorol. Soc **104 ,** 1-29.

Iribarne J. A., and H. R. Cho.,	1980	Atmospheric Physics, D. Reidel pub.
Iyer K.N., R. Pandey, H.P. Joshi, and Jivrajani R. D.	1994	Ind. J. Radio and Space Physics., **23,** 52-58
Jain, A.R., Jaya Rao, Y., Rao, P.B., Anandan, V.K., Damle S. H., Balamusalldhar, P. Kalkarni Anil and Viswarnthan, G.	1995	Radio Sci., **30,**1139.
Krishna Murthy B. V.	1998	Proc INSA ,**64A,** 303.
Krishna Murthy, B. V., Prbhakaran Nayar, S.R. Revathy, K. Mridula, G., Satheesan, K., and Jain.A. R.	2000	Ind. J. Radio and Space Phys. **29**,199.
Lilly, D.K.,	1972	Atm. Meteorol. Soc., **53 ,** 17-23.
Lilly, D. K., and P.J. Kennedy	1973	J . Atmos. Sci., **30,** 1135-1152.
Lindzen, R.S.,	1981	J. Geophys. Res., **86,** 9707-9714.
Mathews J.D.	1984	MAP Handbook, Ed. R.A. Vincent **13,1**34.
McAfee, J.R., B.B. Balsley and K.S. Gage	1989	J. Atmos.Oceanic Technol., **6,**500-508.
Mobbs, S.D., and J. M. Rees,	1989	Antarct. Sci. **1,** 65-75.
Narayana Rao, D., Kishor, P., Narayana Rao,T., Vijaya Bhaskar Rao., Krishna Reddy, K., Yarraih, M, and Hareesh, M.	1997	Radio Sci., **32**, 1375.
Nastrom G D and D C Fritts	1992	J Atmos Sci ,**49,** 101.

Nicolson, I.	1982	The Sun. Rand McNally, New York.
Prabhakaran Nayar, S. R and Sreeletha S.	2003	Ann. Geophy., **21**, 1183-1195.
Prichard, I. T. and L. Thomas,	1993	Ann. Geophys., **11,** 1075-1083.
Rajeev K, K Parmeswaram, M N Sasi, G Ramkumar and B V Krishna Murthy	2003	Adv Space Res. 32(5) , 807-812, DOI 1016/ S2073-1177(03) 00403-4.
Rao, P.B,	1990	Ind. J. Radio and Space Physics., **19,**326.
Rao, P.B., Jain, A.R., Viswanathan,G., and Damle,S.H.	1994	Ind. J. Radio and Space Physics., **23,**1.
Rao,P.B., Jain,A.R., Kishor,P., Balamusalldhar,P., Damle ,S.H., and Viswanathan,G.,	1995	Radio Sci.,**30**,1125.
Reid. I.M., and R.A. Vincent,	1987	J. Atmos. Terr. Phys., **49,** 443-460.
Röttger. J., and C.H. Liu,	1978	Geophys.Res.Lett., **5,** 357.
Röttger J.	1981	J. Atmos.Terr.Phys., **43**, 277.
Röttger J., and M.F.Larsan.,	1990	Radar Meteorology Conference, Ed. Atlas, AMS Chapter 21A, **235**
Sasi, M. N., Lekshmi Vijayan, Deepa, V., and Krishnamurty B.V.	1999	J. Atmos, Terr, Solar Phys.,**61,** 377
Sasi, M.N., G. Ramkumar., V. Deppa and B.V. Krishna Murthy	2000	Geophys.Res.Lett., **27,** 3207.
Sato, K.,	1990	J. Atmos. Sci., **47,** 2803-2817.
Sato, K.,	1993	J. Atmos. Sci., **50,** 518-537.
Sato, T.	1989	MAP Hand Baook, **30,** 19

Smith S. A, D C Fritts and T E Van Zandt, 1987 J. Atmos. Sci., **44**, 1404.

Sutts, G.J., P. Healey, and S.D Mobbs 1994 J.R. Meteorol Soc., **120,** 59-77.

Thomas, L., I.T. Prichard and I. Astin 1992 Ann. Geophys., **10,** 690-697.

Tsuda, T., S. Kato, T. Yokoi, T. Inoue, M. Yamamoto, T.E. VanZandt, S. Fukao, and T.Sato 1990 Radio Sci., **25**, 1005-1018.

Tsuda T., Y.Marayama, H. Wiryosumarto, S.B. Harijno and S. Kato, 1994a J. Geophys. Res., **99,** 10507 – 10516

Tsuda T., Y.Marayama, T. Nakamura, R.A. Vincent, A. H. Manson., C.E. Meek, and R. L Wilson 1994b J. Atmos. Terr. Phys., **54,** 1043-1049.

Van Zandt T. E, 1982 Geophys. Res. Letts., **9,** 575.

Van Zandt T E, 1985 Radio Scu., **20,** 1323

Vincent, R. A., and I.M. Reid, 1983 J. Atmos. Sci., **40,** 1321-1333

Wait J.R, 1962 Electromagnetic waves in stratified Media,(Pergamon press, London), **Ch IV**

Weinstock J J 1990 J. Atmos. Sci. **47**, 2211.

Williams, C. R., and Avery, S. K. 1996 J. Geophys. Res.,101**,**15051.

Wilson R , M L Chanin and A Hauchecorne 1991 J Geophys Res, **96,** 5153.

Yamanaka M D, S Fukao, H Matsumoto, T Sato, T Tsuda and S Kato 1989 Pageoph, **130,** 481.